UNIVERSIDADE DA BEIRA INTERIOR
Ciências da Saúde

New therapeutic approaches for bone regeneration

Ricardo Gil Fradique

Dissertação para obtenção do Grau de Mestre em
Ciências Biomédicas
(2º ciclo de estudos)

Orientador: Professor Doutor Ilídio Correia

Covilhã, Outubro de 2014

UNIVERSIDADE DA BEIRA INTERIOR
Ciências da Saúde

Novas abordagens terapêuticas para regeneração óssea

Ricardo Gil Fradique

Dissertação para obtenção do Grau de Mestre em
Ciências Biomédicas
(2º ciclo de estudos)

Orientador: Professor Doutor Ilídio Correia

Covilhã, Outubro de 2014

List of Publications

- Articles in peer reviewed international journals:

  Diogo G. S., Gaspar V. M., Serra I.R., Fradique R., Correia I.J.; Manufacture of ß-TCP/alginate scaffolds through a Fab@home model for application in bone tissue engineering. Biofabrication, 2014. 6(2):025001. doi:10.1088/1758-5082/6/2/025001

  Torres,A. L., Gaspar, V. M., Serra, I. R., Diogo, G. S., Fradique, R., Silva, A. P., Correia, I. J.; Bioactive Polymeric-Ceramic Hybrid 3D Scaffold for Application in Bone Tissue Regeneration. Materials Science and Engineering: C, Materials for Biological Applications, 2013. 33(7):4460–9. doi:10.1016/j.msec.2013.07.003

- Poster communications:

  Diogo G.S., Gaspar V.M., Serra I.R., Fradique R., Correia I.J.; Bone scaffolds produced by rapid prototyping, IX Annual CICS Symposium, 30 June - 1 July, 2014, Covilhã, Portugal.

  Diogo G.S., Gaspar V.M., Serra I.R., Fradique R., Correia I.J.; Rapid prototyping of composite bone scaffolds for tissue engineering, Biannual encounter of the Technical Divisions of Portuguese Materials Society (SPM), 4th of May, 2014, Covilhã, Portugal.

- Oral presentations:

  Fradique R., Correia I.J.; Design and production of 3D Scaffolds by Rapid prototyping for bone tissue engineering, III National Bioengineering Conferences, 28-29th of May, Covilhã, Portugal

The most exciting phrase to hear in science, the one that heralds new discoveries, is not ’Eureka!’ but ’That’s funny...’

Isaac Asimov

Acknowledgments

I would like to thank my supervisor professor Ilídio Correia, for the opportunity to develop my master's thesis with him. For all the dedication, time, and patience spent in getting here.

To Sónia for all the daily help, and for the acquisition of the scanning electron microscopy images.

To professor Abílio Silva, for the availability and help with the mechanical characterization of the scaffolds.

To all my group colleagues. Thank you for all the help and support. A special thanks to Mariana, with whom I divided the long hours spent in the laboratory. Your help was invaluable throughout this year.

A very special "thank you" to my girlfriend, Cristiana. Thank you for always being by my side, for all your love, and for the infinite patience in my busy lab days.

To my parents and my sister. Without a doubt the most important people in my life, who always helped me unconditionally. I would not be here without them.

Resumo

O envelhecimento da população mundial tem associado o aumento do número de casos de doenças ou defeitos ósseos. Estas situações patológicas, que têm diferentes causas, afetam a mobilidade e a qualidade de vida do indivíduo. Os tratamentos actuais contemplam a utilização de enxertos ósseos, que na sua maioria são autoenxertos. No entanto, estes apresentam algumas limitações, como seja o estado de saúde do paciente que limita a obtenção do enxerto, a extensão da lesão óssea, e ainda a possibilidade de inflingir um maior sofrimento no doente. Este tipo de enxertos nem sempre permitem uma completa recuperação. Neste contexto, surge a Engenharia de Tecidos como área interdisciplinar que utiliza biomateriais e moléculas bioactivas para desenvolver dispositivos que permitam efectuar a reparação ou substituição do tecido ósseo. Uma das abordagens mais utilizadas envolve a produção de "scaffolds", que são matrizes tridimensionais, que tomam papel de molde temporário para a adesão e proliferação celulares, fornecendo suporte mecânico durante a regeneração óssea. Uma abordagem particularmente promissora utiliza a tecnologia de prototipagem rápida para produzir "scaffolds" com estrutura detalhada, utilizado modelos computacionais ou dados provenientes de exames médicos de rotina. O presente estudo descreve a caracterização fisicoquímica, mecânica e biológica de "scaffolds" tridimensionais produzidos com β-Tricalciofosfato/Alginato, utilizando prototipagem rápida. A Espectroscopia de Infravermelho por Transformada de Fourier, Difracção de Raio-X, Ângulo de Contacto e Microscopia Electrónica de Varrimento foram usadas na caracterização da estabilidade mecânica, superfície e porosidade dos "scaffolds" produzidos. O perfil citotóxico dos "scaffolds" foi estudado através de ensaios de MTS *in vitro*, utilizando osteoblastos humanos como células modelo. Os resultados obtidos demonstraram que os "scaffolds" produzidos apresentam óptimas propriedades biológicas e fisicoquímicas, suportando a adesão e proliferação celulares. Os materiais produzidos demonstraram possuir excelente resistência mecânica, igualando ou excedendo as propriedades do osso trabecular, demonstrando o seu potêncial para serem usados na regeneração de tecido ósseo.

Palavras-Chave

"Scaffolds" β-Tricalciofosfato/Alginato, Desenho Assistido por Computador, PVA, Prototipagem Rápida, Engenharia de Tecidos

Resumo alargado

O osso é um tecido altamente dinânimo e vascularizado, e é o principal componente do esqueleto humano. Este tecido é capaz de se auto-regenerar, e é também responsável por muitas outras funções no organismo. A sua estrutura complexa pode ser dividida em matrix orgânica, constituida na sua maioria por colagénio, e matriz inorgânica, maioritariamente hidroxiapatite, assim como os vários tipos de células ósseas, osteoblastos, osteoclastos e osteócitos. Apesar da sua capacidade de regeneração, vários factores como a idade, doenças, ou traumas têm levado a um aumento no número de defeitos ósseos a nível mundial.

As terapias mais utilizadas para a reparação do tecido ósseo envolvem o uso de enxertos ósseos, na sua maioria autoenxertos. No entanto, factores como a disponibilidade limitada, ou a possibilidade de dor crónica, têm limitado a sua utilização.

A Engenharia de Tecidos trata-se de uma área interdisciplinar, que combina o uso de biomateriais com moléculas bioactivas, de forma a estimular a reparação e regeneração do tecido ósseo. Neste campo, as matrizes tridimensionais, ou "scaffolds", têm demonstrado grande potencial para aplicação na regeneração óssea. Estes devem possuir várias propriedades essenciais para permitirem a reparação do tecido: biocompatibilidade, biodegradabilidade, porosidade e resistência mecânica adequadas. Também devem mimetizar a matriz extracelular do local de implantação, de forma a favorecer a adesão e proliferação celulares.

Na produção destas estruturas têm sido utilizados diferentes materiais, nomeadamente metais, polímeros, e cerâmicas, assim como vários métodos de produção. As tecnologias de prototipagem rápida têm facilitado o desenvolvimento de estruturas tridimensionais com arquitectura controlada, através de modelos CAD e de dados provenientes de exames médicos de rotina.

O presente estudo descreve a produção e caracterização das propriedades químicas, mecânicas, e biológicas, de scaffolds 3D produzidos com β-TCP/Alginato. Foram testadas seis formulações diferentes, utilizando três rácios de β-TCP/Alginato (60/40 % (p/p), 70/30 % (p/p), 80/20 % (p/p)), com, e sem PVA na sua composição. Os scaffolds foram produzidos por prototipagem rápida através de uma 3D plotter (Fab@Home).

As propriedades fisicoquímicas dos scaffolds produzidos foram caracterizadas por Espectroscopia de Infravermelho por Transformada de Fourier, Difracção de Raio-X, Ângulo de Contacto, e Microscopia Electrónica de Varrimento. Os resultados mostraram que não existiram alterações na estrutura cristalina dos materiais utilizados, sendo que os "scaffolds" produzidos apresentaram um caracter hidrofílico, o que permitiu a adesão celular. Por outro lado, também se verificou que a superfície dos materiais é irregular e rugosa, o que favorece a adesão celular. Foram ainda avaliadas a porosidade e resistência mecânica dos scaffolds, sendo que a formulação 60/40 demonstrou as melhores propriedades mecânicas, similares às propriedades nativas do osso trabecular. O perfil citotóxico foi avaliado através do ensaio de MTS *in vitro*, utilizando osteoblastos humanos. Os resultados obtidos apresentaram excelentes propriedades biológicas para todas as formulações, suportando e favorecendo a proliferação celular. De forma a avaliar a adesão celular na superfície dos materiais, imagens de microscopia electrónica de varrimento foram adquiridas após incubação com as células, onde foi possível observar as células aderidas e esticadas à superfície dos materiais.

Os resultados obtidos demonstraram que os scaffolds produzidos têm boas propriedades químicas, biológicas e mecânicas, que poderão permitir a aplicação destas estruturas na regeneração de tecido ósseo.

Abstract

The aging of the worldwide population has led to an increase in bone tissue diseases. Wether due to trauma or pathology, if the bone tissue is compromised it constitutes a serious threat to the well being of the individual. Current solutions for bone defects involve the use of bone grafts, particularly autografts. However, these present serious limitations for their use, such as limited availability, or the possibility of chronic pain, and may not allow the patient's full recovery. In this context, Tissue Engineering emerged as a potential solution, since it uses biomaterials and bioactive molecules to develop devices that allow the repair or regeneration of bone tissue. One of the most researched approaches are scaffolds, that are three dimensional matrices, aimed to act as temporary templates for cell adhesion and proliferation, offering mechanical support while the bone tissue regenerates. A particularly promising approach uses rapid prototyping technology to produce 3D scaffolds with highly controlled structure, either from CAD models, or routine exam medical data. The present study describes the physicochemical, mechanical and biological characterization of 3D β-TCP/Alginate scaffold, produced by rapid prototyping. Fourier Transform Infrared Spectroscopy, X-Ray Diffraction, Contact Angle, and Scanning Electron Microscopy were used to characterize the porosity, surface hydrophilic character and chemical composition of the produced scaffolds. In addition, the mechanical stability (Compressive Strength and Young's Modulus) was also evaluated. The biocompatibility of the scaffolds was evaluated by *in vitro* MTS assays, using human osteoblasts as model cells. The results obtained showed that the produced scaffolds present excellent biological and physicochemical properties, allowing for the adhesion and proliferation of human osteoblasts. Moreover, the produced scaffolds presented remarkable mechanical strength, matching or surpassing the properties of native trabecular bone, which is fundamental for their potential use in the regeneration of bone tissue.

Keywords

β-Tricalcium Phosphate/Alginate scaffolds, Computer-Aided Design, PVA, Rapid prototyping, Tissue engineering

Contents

List of Figures

List of Tables

Acronyms

3D	3 dimensional. 7, 8, 10, 12–15, 35
ANK	progressive ankylosis protein. 5
BMP	bone morphogenic protein. 5
BMU	basic multicellular unit. 4
BSA	bovine serum albumin. 15
CAD	computer assisted design. 12, 13
DMEM-F12	Dulbecco's modified Eagle medium: nutrient mixture F12. 15, 18
ECM	extracellular matrix. 3, 8, 10, 21, 23
EDS	Energy Dispersive Spectroscopy. 16, 26
EDTA	ethylenediaminetetraacetic acid. 15, 18
EtOH	ethanol. 15, 17–19
FBS	Fetal bovine serum. 15, 18
FDM	fused deposition modelling. 12
FGF	fibroblast growth factor. 5
FTIR	Fourier Transform Infrared Spectroscopy. 16, 24
HA	hidroxyapatite. 1, 3, 5, 10
IGF-I	insulin like growth factor 1. 4
IL-6	interleukin 6. 4
MCP-1	monocyte chemoattractant protein 1. 4
M-CSF	macrophage colony-stimulating factor. 4
MMP	matrix metallopeptidase. 5
MTS	3-(4,5-dimethylthiazol-2-yl)-5-(3-carboxymethoxyphenyl)-2-(4-sulfophenyl)-2H-tetrazolium. 15, 18, 32
PBS	phosphate buffer saline. 15
PCL	polycaprolactone. 10
PGA	polyglicolic acid. 10
PLA	polylactic acid. 10
PMS	phenazine methosulfate. 18
PTH	pituitary hormone. 4

PVA poly(vinyl) alcohol. 15, 16, 24, 25, 27, 28, 30

RANK receptor activator of nuclear factor κ-B. 4
RANKL receptor activator of nuclear factor κ-B ligand. 4
RGD Arginyl-glycyl-aspartic acid. 5
RT room temperature. 13, 16, 18, 19

SEM Scanning Electron Microscopy. 16, 19, 22, 31
STL Standard Tessellation Language. 13

β-TCP beta tricalcium phosphate. 10, 14–16, 21, 22, 24–28, 30, 33, 35
TGF-β transforming growth factor β. 4, 5
TNF-α tumour necrosis factor α. 4

UV ultraviolet. 18

XRD X-Ray diffraction. 16, 25

Chapter 1

Introduction

1.1 Bone tissue

Bone is a highly dynamic and vascularised tissue, and it is the main component of the human skeleton[1,2]. The principal function of the skeleton is to provide structural support to the body[3], allowing motion by opposing muscular contractions and withstanding functional loads[1,4], while protecting the internal organs, especially the heart, lungs, and spinal cord[5]. It is also involved in different biological functions, namely the production of blood cells through hematopoiesis[3], and ion storage, mainly phosphorous and calcium[2,3].
In spite of a complex structure, bone tissue can be divided in cells and bone matrix. Different types of bone cells are found in bone tissue, each presenting a specific function: osteoblasts, that are known as bone forming cells; osteocytes, involved in bone maintenance; and osteoclasts, that perform bone remodelling[5]. With distinct origins and functions, each cell type is essential for the production and maintenance of the bone matrix.

Bone matrix is composed by an inorganic and organic phase, in a 65/35% ratio[6]. The organic phase is mainly composed of collagen and proteoglicans, while the inorganic phase is composed by calcium phosphate crystals, in the form of HA (hidroxyapatite)[2,3,6].

1.2 Bone anatomy

Bones are exceptionally well suited for the structural demands of the human body, providing high strength and durability while minimizing weight. Moreover, during the lifetime of each individual, the shape, anatomy and mechanical properties may be changed in response to external stimulus[4].
Bones can be classified according to their shape into long, short, flat or irregular[3,6]. Long bones present a cylinder like shape, representing most of the bones of the upper and lower limbs. As hollow tubes, they provide great strength and durability against axial compression forces, while minimizing weight[4]. Short bones resemble a cubic or spheric shape, such as the carpal bones from the wrist, or the tarsal bones, from the ankle[6]. Flat bones, on the other hand, present thin, curved or flat shapes, being the ribs and scapulae examples of this type of bone. Irregular bones have complex shapes that are neither long, short, nor flat, such as the vertebrae and facial bones[3,6]. Bones can also be classified by structure in trabecular, also called cancellous or spongy bone (about 20% of the total skeleton), and cortical or compact bone (about 80% of the total skeleton)[2,3,6].

In addition, the outer surface of the bone is covered by a bi-layered connective tissue membrane, the periosteum. The outer, fibrous layer, is made of irregular collagenous tissue, which contains blood vessels and nerves, while the inner layer is composed by a single layer of bone cells. These facilitate the fixation of tendons or ligaments to the bone.

The endosteum is a connective tissue membrane that covers the internal surfaces of all bone cavities, and it is composed by a single layer of cells[6,7].

Each growing long bone can be further characterized by three different sections: the diaphysis that composes the bulk of the bone, the epiphysis, located at the ends of the bone, and the epiphyseal plate, located where new bone is formed during growing[6-8].

An important structure within the long bones is present in the diaphysis, that can contain the medullary cavity. This cavity, together with the cavities in cancellous bone, is filled with marrow. Blood cell formation occurs in the red marrow, while yellow marrow is mainly adipose tissue, with adults presenting mostly the former, except for a few particular bones[6,7]. This yellow marrow can act as a localized energy reservoir in emergency situations, like bone fractures[9].

Flat, short and irregular bones usually present a cancellous interior surrounded by two layers of compact bone, with the cancellous centre filled with marrow[6,8].

On a smaller scale, bone can be also classified as woven or lamellar, according to the fibres organization[3,4,6]. Woven bone presents randomly oriented collagen fibres, and usually occurs during growing stages, such as foetal development or fracture repair. It is typically remodelled to form lamellar bone[3,4].
Lamellar bone is a layered type of bone, composed of 3-7 μm lamellae, with collagen fibres lying parallel to each other[4,6].

A brief schematic of the internal structure and organization of bone tissue is presented on figure 1.1.

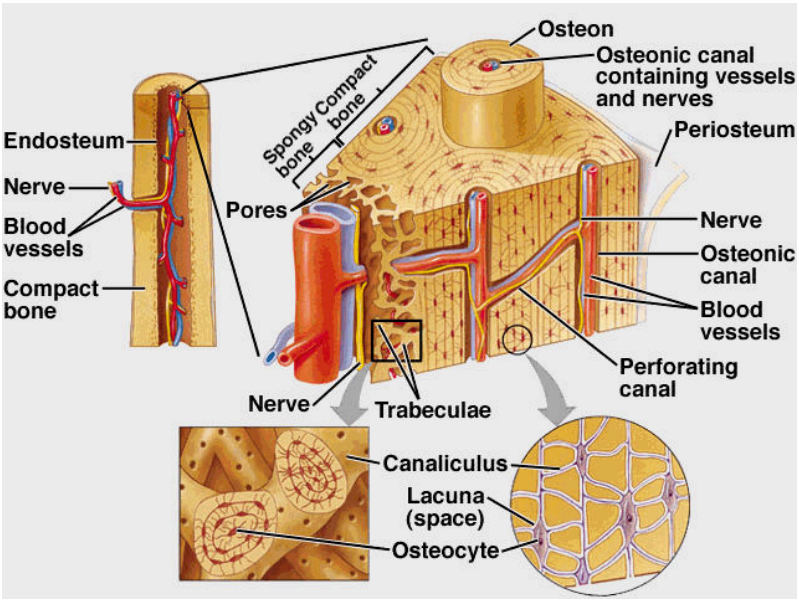

Figure 1.1: Schematic view of bone tissue structure and organization. Adapted from Booth[10]

1.3 Bone histology

1.3.1 Bone matrix

As previously described, bone matrix is a composite of organic and inorganic materials, in a 35/65% ratio[6]. The organic phase is mainly constituted by collagen and proteoglycans, and the inorganic by calcium phosphate crystals. These components are in a delicate balance, if the mineral is diminished, the bone becomes more flexible, due to increased collagen. If, on the other hand, the collagen is removed, the bone becomes mainly composed of mineral, and thus very brittle[6,11].
The bone matrix composition also changes with age, with the decreasing bone turnover causing an increase in the mineralization degree, thus leading to a decrease in bone collagen content[12,13].

1.3.2 Bone cells

Osteoblasts are mononuclear and basophilic cells with a large spherical nucleus, and highly developed rough endoplasmic reticulum and Golgi apparatus[14]. In addition, these cells present secretory behaviour, producing collagen and proteoglycans and releasing them to the surrounding environment[6,15]. They also release matrix vesicles, on which Ca^{2+} and PO_4^{3-} are concentrated to form HA crystals. These will then act like seeds for mineralization of the matrix. In this way, osteoblasts create new ECM (extracellular matrix) and regulate its mineralization. These cuboid shaped cells can live up to 8 weeks, depositing 0.5-1.5 µm of osteoid per day[4,6]. On the other hand, osteoblasts also act as bone lining cells during the quiescence phase of bone[16].

Osteocytes are osteoblasts that have become surrounded by bone matrix, but are morphologically and functionally different[16,17]. These types of cells account for 90/95% of all cells in the bone. They are relatively inactive, but can still produce the components needed to maintain the bone matrix[6,17].
Currently, it is believed that these cells may actually modulate the spatial and temporal formation and resorption of bone tissue, through the high number of dendritic processes that interconnect the osteocytes and the bone lining cells[4,6,17]. It was also proposed that these cells can act like mechanosensor cells, transducing mechanical stress and guiding bone remodelling[16,17]. Nitric oxide, Wnt and cadherin-mediated signalling have been suggested as transduncing mechanisms, being activated following mechanical strain. However, the precise mechanical stimulus and response remain unclear[17-19].

Osteoclasts are responsible for bone reabsorption[15,20], mobilizing Ca^{2+} and phosphate ions from the bone matrix, resorbing the bone in a multiple stage process[4,21]. These are highly specialized giant cells, multi-nucleated and highly migratory[4,15,20], derived from the red bone marrow monocyte/macrophage lineage[6,14]. Capable of absorbing up to 200 000 μm^3/day of bone matrix[4], they also present numerous mitochondria, a well developed Golgi apparatus around the nuclei, endoplasmic reticulum, vacuoles and lysosomes. This cellular organization is the result of their great involvement in protein synthesis, in particular lysosomal enzymes[15].

1.3.3 Bone remodelling

Bone is a dynamic tissue, constantly being remodelled. In this process, represented in figure 1.2, old bone matrix is replaced by new matrix, whether due to bone growth or repair, adjustments to stress, or calcium regulation[22,23]. Osteoblasts and osteoclasts gather in a temporary assembly called BMU (basic multicellular unit)[17,22-24], regulated by mechanical forces, bone cell turnover, hormones (PTH (pituitary hormone), growth hormones, etc), cytokines and local factors[17].
The bone remodelling process can be divided into four main phases: activation, resorption, reversal, and formation[4,20,22,23,25] and the full process can take 3-6 months to be completed[4].

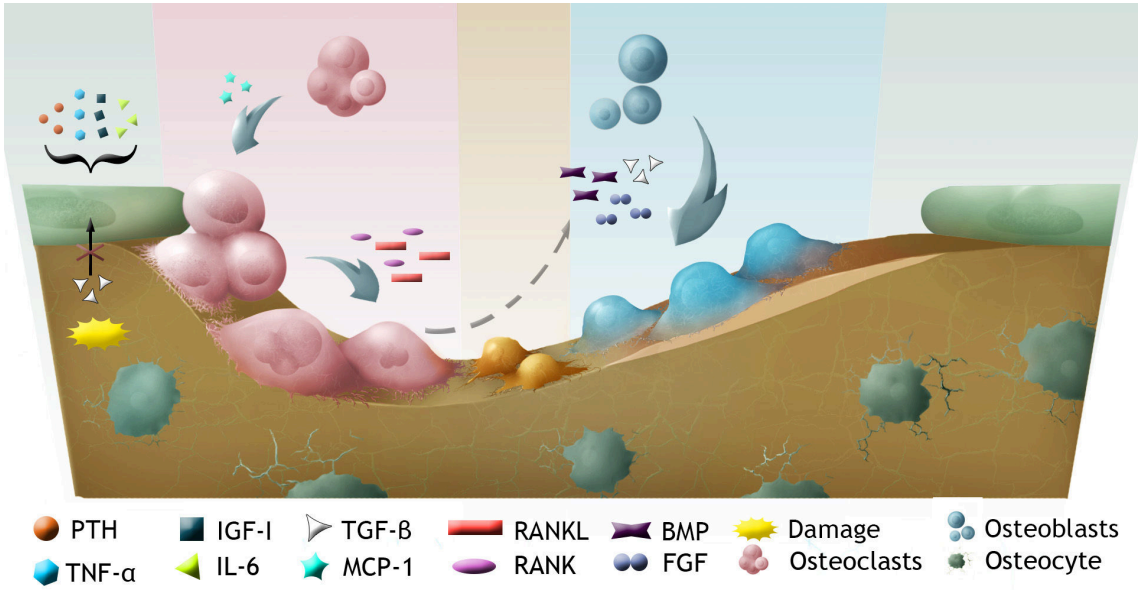

Figure 1.2: Schematic view of bone tissue cells and bone remodelling.

Activation phase

This stage involves the detection of an initiation signal, that can be a mechanical strain, damage, or factors released on the bone microenvironment[20,22,25]. In response to either the direct endocrine signals, or signals produced by osteocytes, osteoblasts react by recruiting osteoclast precursors to the remodelling site, through the release of a chemoattractant, MCP-1 (monocyte chemoattractant protein 1)[20].
In particular, IGF-I (insulin like growth factor 1), TNF-α (tumour necrosis factor α), IL-6 (interleukin 6), and PTH, activate bone lining osteoblasts, causing an increase in the surface expression of the RANKL (receptor activator of nuclear factor κ-B ligand) by these cells. On the other hand, responding to osteoclastogenic stimulus, osteoblastic cells present in the bone marrow secrete M-CSF (macrophage colony-stimulating factor). This induces the expression of RANK (receptor activator of nuclear factor κ-B) in pre-osteoclastic cells. The RANKL/RANK interaction leads to pre-osteoclast differentiation into multinucleated osteoclasts[22,23].
In addition, damage to the bone or immobilization can result in osteocyte apoptosis, leading to increased osteoclastogenesis. This is due to a decrease in the levels of TGF-β (transforming growth factor β), which is an osteoclastogenesis inhibitor secreted by osteocytes in basal conditions[20].
Another osteoclast activation signal can be induced by hormones. PTH is an endocrine remodelling signal used to maintain calcium homoeostasis. This hormone is secreted by the parathyroid

glands in response to low calcium levels in the serum[20], and can stimulate both bone formation when secreted intermittently, and bone resorption when secreted continuously[24].
In the bone, it activates a transmembrane G-protein-coupled receptor on the surface of osteoblasts, that activates protein kinase A, protein kinase C and intracellular calcium signalling pathways. This osteoblast activation causes a wave of transcriptional responses that modulate the secretion of molecules responsible for the recruitment, differentiation, and activation of osteoclasts, establishing bone resorption[20].

Resorption phase

During this stage, osteoclasts adhere to the bone surface and start to dissolve the bone[20,22]. Cell anchorage is done via $\alpha_v\beta_3$ integrin molecules, creating an isolated microenvironment underneath the cell[20,25].
The organic and inorganic components of the bone are degraded through different processes. The inorganic component is mostly dissolved by decreasing the pH[22], which is performed by pumping hydrogen ions into the sealed zone[20,25]. The organic components are degraded by lysosomal enzimes, MMP (matrix metallopeptidase) and cathepsin K, released by osteoclasts, that degrade the unmineralized osteoid lining at bone surface[20,22]. This exposes RGD (Arginyl-glycyl-aspartic acid) adhesion sites that facilitate further osteoclast attachment, enhancing bone resorption[20]. To avoid excessive bone resorption, osteoclasts suffer apoptosis after this stage.

Reversal phase

This stage marks the transition from osteoclast to osteoblast activity, with osteoblast precursors being recruited and differentiating[25,26]. In this phase, bone lining cells prepare the bone surface for the subsequent bone deposition by osteoblasts, cleaning it from bone matrix leftovers[20,24,25].They are also believed to be responsible for the signals that allow the transition from bone resorption to bone formation[20,24].

Formation phase

Throughout the formation phase osteoblasts lay down bone until they have replaced the resorbed bone completely[24]. The resorption phase releases a variety of growth factors stored in the bone matrix, such as BMP (bone morphogenic protein), FGF (fibroblast growth factor), and TGF-β, that are responsible for the recruitment of osteoblasts into the absorbed area[22,25].
Once osteoblasts are on site, and fully differentiated, both the organic and inorganic components are deposited, like collagen type I, which is the main organic component of the bone matrix, proteoglycans, osteonectin, bone sialoprotein and osteocalcin[20,25]. The precise mechanism of bone mineralization is still unclear, although it is believed that alkaline phosphatase, nucleotide pyrophosphatase phosphodiesterase, and ANK (progressive ankylosis protein) take part in creating the optimum concentration of extracellular inorganic phosphate to allow for HA formation[20].

The remodelling cycle is concluded when all reabsorbed bone is replaced. At the end of the cycle, osteoblasts either enter apoptosis, revert back to bone lining phenotype, or differentiate into osteocytes within the matrix[20]. Even though the bone remodelling process is one of the most reliable in the body, there are circumstances where it fails[19]. In fact, the pathologies inherent

in bone disorders are almost always related to this cycle, influencing either bone formation or resorption[4].

1.4 Bone disorders

Bone disorders can be due to a variety of factors. Abnormal growth can cause gigantism or dwarfism, while abnormal collagen contents can lead to osteogenesis imperfecta. Mineral and vitamin deficiencies cause rickets, and bacterial infections can cause bone destruction, as is the case of osteomyelitis. Osteomalacia and osteoporosis are also responsible for bone damage, through decalcification[6].
As already described, bone disorders arise primarily from derails in the bone remodelling process. Many of these metabolic diseases, with the exception of osteoporosis, present increased bone turnover, and are often associated with increased bone resorption due to high levels of serum PTH[27]. The most common metabolic bone diseases are acquired[25], that is, derived from a disease or endocrine dysfunction, and include osteoporosis, renal osteodystrophy (the skeletal changes of hyperparathyroidism and chronic renal failure), as well as Paget's disease[25,28].

Osteoporosis

Osteoporosis is the most common metabolic bone disease[28], with an estimated 27.5 million people affected in the European Union[29]. Osteoporosis is characterized by low bone mass and structural bone deterioration, causing increased bone fragility and vulnerability to fractures[25,27,28]. It is most commonly due to an imbalance between bone resorption and bone formation. While both are heightened, they are altered with different intensities, resulting in higher bone resorption than bone formation, and leading to a loss in bone mass[28]. This disorder is more common in older populations, especially in women, due to the hormonal changes that they suffer with age. Nevertheless, excluding the hormonal effects of menopause, the disease has the same rate of progress in both genders[28].

Renal osteodystrophy

Renal osteodystrophy includes a heterogeneous group of metabolic bone diseases derived from chronic kidney disease[25,28]. Among these are included osteomalacia[25], deriving from vitamin D deficiency with profound defects in mineralization[27]; osteitis fibrosa[25], a loss of bone mass derived from overproduction of PTH; osteopenia[25], when the bone density is lower than normal, a pathological situation that can precede osteoporosis; and osteosclerosis[25], a localized increase in bone density, that is associated with osteopetrosis. This type of disorders clearly reflect the importance of PTH and vitamin D on bone metabolism[25,28], since most of bone related diseases derive from abnormalities in the metabolism of either or both of these components[30].

Paget's disease

Paget's disease is a disorder of the bone remodelling process, involving the abnormal destruction of needed bone, and construction of unneeded bone[25], leading to the production of structurally

abnormal tissue[27,28]. Although the causes are not entirely understood, it is believed that it can be caused by a viral infection during childhood, and several genetic mutations have also been identified on patients with the disease[25,28].

It is clear that there is a need for new therapies to treat bone defects, either caused by disease or trauma.

1.5 Bone grafts

As already described, bone presents self-regeneration and remodelling. However, this is a limited ability. There are certain traumas that the organism is unable to heal without surgical intervention, called critically sized osseous defects[31]. In such cases, bone grafts are usually used for enhancing the formation of new bone. The capacity of bone grafts to regenerate tissue is measured according to their osteogenic, osteoconductive and osteoinductive potential[32]. An osteogenic graft is capable of inducing the maturation of osteoprogenitor cells into osteoblasts, facilitating the formation of bone tissue. Osteoconduction is related with the formation of bone on a surface, in particular, the ability of the graft to support the bone growth in a 3D (3 dimensional) defect. Finally, osteoinduction refers to the recruitment and maturation of osteoprogenitor cells into the defect site[31].
These bone grafts are divided into three main categories: autografts, allografts and xenografts[32].

Autografts

Autografts are considered the gold-standard of bone grafting[33,34], and are the basis to which all of the other methods are compared. They consist of transplanting bone tissue from a donor to the lesion site, within the same patient[31,32]. They usually present high success rates[31], with excellent biological properties: the collected bone is rich in osteogenic cells, osteoconductive bone matrix and growth factors[32,33,35]. In addition, there is no risk of rejection or disease transmission, since only tissue from the patient's own body is used[35].
However, the harvesting of bone from a different site can cause pain[32,33], infection, scarring[32], blood loss, and donor site morbidity[32–34]. Since the graft is being taken from the patient, there is also limited tissue availability[33]. In addition, there is no guaranty that the cellular components survive transplantation[33], and questions have been raised about the osteoinductivity of these grafts, since the uncertain quantities of certain growth factors on autografts can cause insufficient tissue regeneration[35].

Allografts

Allografts are used as an alternative to autografts, and are obtained from human donors or cadavers[31,34]. Even though these types of bone grafts eliminate the need for a donor site, and the supply limitations, they lack the osteoinductive capacity of autografts[31,33]. They also present the risk of viral disease transmission and immunogenicity[31–34]. The processing techniques used to lower these risks also decrease the mechanical resistance of the grafts, and usually eliminate the cellular phase of the bone tissue[33].

Xenografts

Also worth mentioning are xenografts, bone grafts obtained from other species. Since the potential for immune rejection and disease transmission is much higher from animal bone than from human bone, these types of bone grafts are processed through more intensive treatments,[34], which further limits the biologic and mechanical properties of these materials.

Due to all the aforementioned limitations, bone graft substitutes have been the focus of intense research in the area of Bone Tissue Engineering, with has as main objective to create bone scaffolds that mimick the microenvironment of the bone[32].

1.6 Tissue engineering

Tissue engineering emerges as "an interdisciplinary field that applies the principles of engineering and the life sciences toward the development of biological substitutes that restore, maintain, or improve tissue function"[2]. In particular, bone tissue engineering tries to create grafts with the capacity to induce the restoration of bone structure and functions[34,36], favouring regeneration over replacement[2], and are usually composed of an ECM-mimicking structure (scaffold), cells, and growth factors[3,34,37].
The ideal tissue engineered construct should be able to completely replace autologous bone grafts[3]. However, even when the constructs cannot fully replace these grafts, they can be added to the autologous graft to increase its volume, diminishing the amount of bone needed[3].
Bone tissue engineering tries to recreate the appropriate environment for the regeneration through the extensive use of 3D scaffolds[38]. Nonetheless, the scaffolds currently generated are limited by the current manufacturing techniques, and are based on a randomly distribution of cells, matrix, and bioactive molecules[37]. As such, the mimicking of both functional and biological complexity is seen as the current challenge to achieve full tissue regeneration[37].

1.6.1 3D scaffolds

Fundamentally, scaffolds are templates for tissue regeneration[38], capable of delivering cells and growth factors to a damaged tissue, while providing mechanical support during the regeneration phase[37]. Scaffolds have been created through a variety of techniques using different biomaterials that present certain key qualities for a successful regeneration[38]: biocompatibility[3,36,38,39], biodegradability[3,36,38-40], osteoconductivity[3,36,39], osteoinductivity[3,36,39], appropriate mechanical properties[3,36,38,39], adequate structure[3,36,38,39], and ease of manufacture[38,41].

- Biocompatibility
  This is considered to be one of the most important properties of bone scaffolds[3]. Neither the scaffold, nor any of its components and by-products, can be toxic or cause any adverse response in the host[3]. In addition, it must allow for normal cell adhesion, functioning, and proliferation[38].

- Biodegradability
  A bone scaffold is designed to serve as a temporary matrix, and eventually be replaced with bone tissue. As such, it must degrade within the body at the same rate of new tissue formation[40]. To accomplish this, a controlled inflammatory response must occur, with an affluence of cells such as macrophages[38]. It follows that this property must be adjusted

not only to the local of implantation of the scaffold[39], but also taking into account the age of the patient who receives it[38].

- Osteoconductivity
  For a scaffold to be able to improve the regeneration of a damaged bone tissue, cells must be able to migrate, adhere, proliferate, and deposit new bone matrix[3,39].

- Osteoinductivity
  The scaffold should also be able to induce the formation of new bone, as well as cell differentiation[36]. While this characteristic is usually connected to growth factors, recent studies have shown that bone induction can derive from the physical structure of the scaffold as well[3].

- Appropriate mechanical properties
  In order to provide adequate mechanical support, a bone scaffold must have mechanic properties similar to the host bone[36,38,39]. The Young's Module of bone ranges from 0.1-0.2GPa of cancellous bone, to 15-20GPa in cortical bone. The compressive strength also presents very different ranges: 2-20MPa for cancellous bone, and 100-200MPa for cortical bone[39]. Since these properties vary largely according to the bone type and location, scaffolds must be tailored to their specific application, taking into account the loads they will have to bear once implanted.

- Adequate structure
  The structure of the scaffold is closely connected to its mechanical properties, and structural modifications can drastically affect the mechanical resistance. However, it also has profound effects on the biological properties. The porosity of a scaffold increases the available area for cell growth and attachment[3,38]. In addition, interconnected porosity allows the diffusion of essential nutrients and oxygen[3,38,39], as well as waste products[38]. To facilitate bone ingrowth, scaffolds must possess pores with a minimum of $100\,\mu m$ in diameter[39], with the ideal range between 200 to $300\,\mu m$[39]. Recent studies have shown that a combination of micro and macro porosities can perform better than macro-porous scaffolds[39]. The presence of micropores on a structure greatly increases the surface area for cell adhesion, and can also contribute for a greater concentration of calcium and phosphate ions, by providing a sheltered environment within the scaffolds, thus improving bone regeneration[42].

- Acceptable manufacturing technology
  Ultimately, for a scaffold to be able to have any clinical impact and viability, it must be cost effective and its production scalable[38,41]. Whether the scaffold needs *in-vitro* culture before implantation, how easy it is to handle, its storage needs, as well as the sterilization methods, are all factors that can affect the clinical viability of a scaffold[38].

1.6.1.1 Biomaterials for scaffold production

Biomaterial is currently defined by the European Society for Biomaterials as a "material intended to interact with biological systems to evaluate, treat, augment or replace any tissue, organ or function of the body"[38]. These types of materials have suffered a great evolution since their inception, spanning already four generations[43].
The first biomaterials were biologically inert, and the main goal was simply to replicate the physical properties of the native tissue with minimal toxic effects[43,44]. When the properties of

these materials proved to be insufficient, and in conjunction with a better understanding of the foreign body response, the research focus changed towards the creation of a biological response, with bioactive materials. This marked the rising of the second generation of biomaterials, that elicited not only a biological response, but also presented a controllable resorption within the body[43,44]. Osteoconductive implants became routine, with the use of synthetic HA and bioactive glasses on porous implants and coatings. Also, the creation of structures that facilitated tissue ingrowth and 3D interlocking with the surrounding tissue contributed to the formation of a mechanically strong interface[43]. The advances in scientific knowledge, mainly in molecular biology and proteomics, allowed the design of biomaterials capable of creating specific cellular responses, giving origin to the third generation of biomaterials[43]. Moreover, these materials are being modified with biological components obtained from the ECM, that are specifically recognized by cells seeded on them[44]. Finally, the fourth generation of biomaterials combines the properties of all previous generations, while trying to mimic the native tissue: biomimetic materials. These materials try to recreate the complexity of the physiological environments[43,44], with some of them being already capable of modulating genetic activation and expression after implantation[44], as well as respond to variations in temperature, pH and ionic force[45–47].

It is thus clear that the choice of materials used in the production of scaffolds for bone regeneration is a key aspect in their performance. A variety of biomaterials is used for bone scaffold manufacturing, although they usually fall within four main categories: ceramic, polymeric, metallic, or composite scaffolds[32,39].

Ceramics

The ceramics used in bone tissue engineering are commonly composed of calcium and phosphate[3]. Ceramic scaffolds can be divided into bioinert or bioactive scaffolds, with the latter further divided into resorbable and non-resorbable scaffolds[32]. Bioactivity refers to the ability of the scaffold to modify its surface structure and establish connections with the surrounding bone when implanted[41].
The most used ceramics are HA and β-TCP (beta tricalcium phosphate), which closely resemble the mineral phase of the bone, and are therefore highly biocompatible, bioactive and osteoconductive[38,41,48]. However, these materials are different when it comes to their degradation rates. While β-TCP presents an almost ideal biodegradability *in vivo*, HA shows almost no biodegradation[3,41,49]. In addition, the ability of β-TCP to bond directly to tissue, and regenerate bone without intermediate tissue, as well as proper bio-resorption rate, have made it one of the most used ceramics in tissue engineering[3,32,39,43,49].
Also, in spite of its great compressive strength, which is usually equal or greater than the native bone tissue[31], ceramics tend to present a hard and brittle nature[31,38,40,43]. In addition, it can be difficult to process them into highly porous structures, which further limits their use in scaffold production[40]. The mechanical properties of native bone results from the combination of both its organic and inorganic phases. When ceramics are used alone they have limited properties for load-bearing applications[41].

Polymers

Polymers can either have a natural origin, such as collagen[36,50], starch[34], silk[34], or alginate[34], or they can be synthesized[31,41], as PLA (polylactic acid)[36,38,39], PCL (polycaprolactone)[39,51], or

PGA (polyglicolic acid)[36,38,39].
Since some natural polymers actually are structural constituents of tissues, these materials present greater biocompatibility and biodegradability[50]. However, they usually present lower mechanical resistance and faster degradation rates, which limits their use in tissue engineering[50]. Synthetic polymers are highly versatile[31,50], with controlled properties, although they have a lack of bioactivity. Furthermore, the degradation products of these polymers can sometimes present negative effects on the regeneration process[31].
Alginate, which was the polymer used in this study for scaffolds production, is a natural polysaccharid derived from brown seaweeds[43,52]. Composed of 1,4-linked β-D-mannuronic acid (M) and α-L-guluronic acid (G) residues, this polymer can form stable hydrogels cross-linked with divalent cations[52,53]. This cross-linking happens between two G blocks of adjacent polymer chains, through interaction with the carboxylic groups and, as a consequence, the stiffness of the gel produced is directly related to the M/G ratio of the polymer and quantity of free divalent cations in solution[53,54].

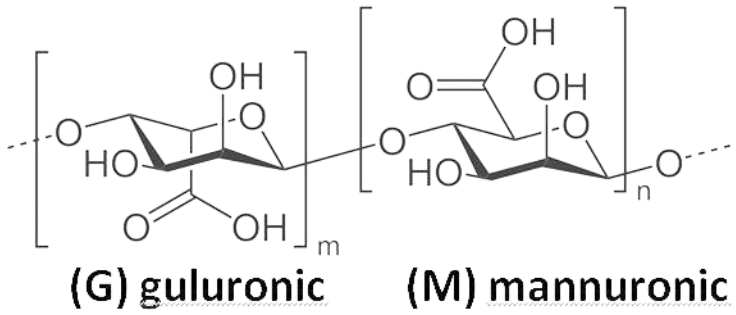

Figure 1.3: Sodium alginate chemical structure. (Adapted from Narayanan et al.[55])

Alginate is extremely versatile, easily forming gels, fibers, foams, and nanoparticles, at physiological conditions[53], while being biocompatible, and non-immunogenic[54]. Still, the dissolution rates of ionically cross-linked alginates cannot be perfectly controlled, and it presents slow degradation kinetics *in vivo*.

Metals

Titanium and tantalum feature among the most common used metals for scaffold production. While these materials have great compressive strength and fatigue resistance, they are not biodegradable. In addition, they do not allow the incorporation of biomolecules[39], requiring coatings and surface treatments to immobilize biologically active peptides[56]. The release of toxic metallic ions is also a concern[32,39].

Composites

Composite materials have in their constitution two or more distinct materials, for example ceramics and polymers[39,57]. These combinations try to overcome the drawbacks of the brittleness of ceramic scaffolds by adding a polymer, thats is inherently more flexible[50].

1.6.2 Rapid prototyping techniques for 3D scaffold production

The current challenge in tissue engineering is to mimic the natural structure of living tissue[38]. Until now, the most used methods of scaffold production included solvent casting[58,59], phase inversion[60,61], fiber bonding[62,63], melting[64,65] and freeze drying[66,67]. However, these methods present severe disadvantages, such as the use of toxic solvents, the inability to create large structures with suitable mechanical properties or lack of structure and porosity control[1].

The advances in computer technology allowed the development of rapid prototyping techniques for tissue engineering applications. These enable the manufacturing of highly reproducible 3D scaffolds[68], with increased complexity and control, from a CAD (computer assisted design) model[57]. In addition, the model used for scaffold production can be derived from medical data, and thus be tailored specifically for a particular damaged tissue with high anatomic accuracy[57,69,70].

The most common rapid prototyping techniques in use are 3D printing, FDM (fused deposition modelling) and 3D plotting[1,71].

3D printing uses a liquid binder dispensed onto thin layers of powder, following the objects profile, creating a final structure in a layer-by-layer assembly[1,72]. This approach is limited by the binder used, since many of the available binders are toxic, and the structures cannot have closed surfaces, otherwise unbounded powder would accumulate inside[73].

FDM employs the deposition of a thermoplastic filament on a platform, by melting extrusion, also in a layer-by-layer fashion, the stacking of layers creating the final structure[1]. Given the temperatures used for the polymer extrusion this technique does not allow for the incorporation of cells nor biomolecules on the interior of the material used[74].

Finally, in 3D plotting a hydrogel is dispensed through a syringe onto a platform[1]. This deposition can be achieved by pneumatic action, screw-driven, or piston action, with the latter providing the best flow control. This robotic deposition has resolutions in the order of 200 µm, with high fabrication speeds, and is one of the most promising technologies[37].

In this work a Fab@Home 3D plotter was used for scaffold production (figure 1.4). This model was developed by Malone and Lipson[75], and was previously used for tissue engineering applications[76,77].

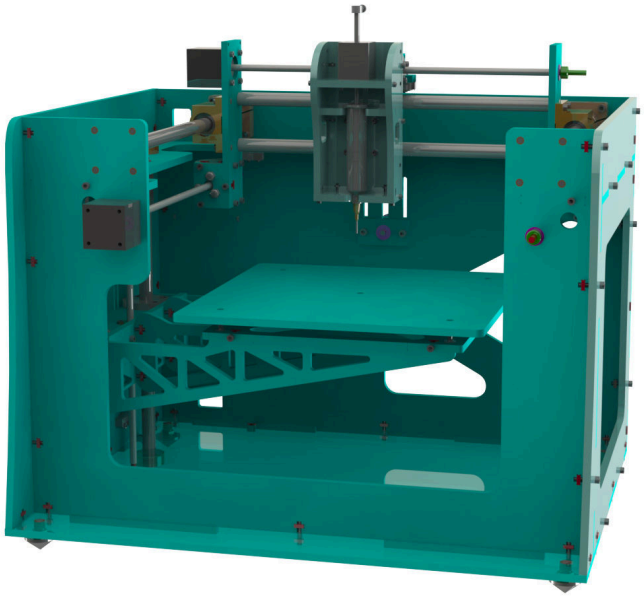

Figure 1.4: Image of a Fab@Home plotter used to produce the scaffolds used in this study

1.6.2.1 Fab@Home 3D plotter for scaffold production

As described above, the 3D plotting technology has great advantages over other methods, mainly the possibility of using viscous solutions for scaffold production at RT (room temperature). The viscosity of the solution used has a great effect on the accuracy and resolution of the equipment. In addition, several settings should be taken into account before a scaffold can be produced. The dispensing pressure, the nozzle diameter, the depositon rate, and the printspeed, depend on the solution used, as well as the CAD model, and must be adjusted accordingly[78].
In brief, the CAD model is designed or scanned, and converted to STL (Standard Tessellation Language) format. This is then loaded onto the Fab@Home software, that slices the model into several layers. With the syringe loaded with the solution and the equipment properly configured, the scaffold is deposited layer-by-layer onto the plotter platform[75,78].

1.7 Aims

Additive manufacturing of β-TCP/Alginate composite scaffolds for bone tissue engineering

- Optimization of the design of the 3D structure
- Optimization of the viscosity of the solution
- Study the influence of β-TCP content on the scaffolds properties
- Study the influence of a β-TCP binding agent on the scaffolds properties
- Evaluate the mechanical, physicochemical and biological properties of the produced scaffolds

Chapter 2

Materials and Methods

2.1 Materials

Amphotericin B, BSA (bovine serum albumin), cacodylate buffer (Mw=214.03 g/mol), calcium chloride (Mw=110.98 g/mol), DMEM-F12 (Dulbecco's modified Eagle medium: nutrient mixture F12), EtOH (ethanol), EDTA (ethylenediaminetetraacetic acid), 25% (v/v) glutaraldehyde, L-glutamine, penicillin G, PBS (phosphate buffer saline), PVA (poly(vinyl) alcohol) (Mw=31 000 g/mol), sodium alginate (Mw=120 kDa to 190 kDa), streptomycin, trypan blue and trypsin were purchased from Sigma-Aldrich (Sintra, Portugal). β-TCP powder (Mw=310.20 g/mol) was obtained from Pancreac® (Barcelona, Spain). Sodium hydroxide was acquired from Pronalab (Barcelona, Spain).
MTS (3-(4,5-dimethylthiazol-2-yl)-5-(3-carboxymethoxyphenyl)-2-(4-sulfophenyl)-2H-tetrazolium) reagent, inner salt was purchased from Promega (Madison, USA). FBS (Fetal bovine serum) was purchased from Biochrom AG (Berlin, Germany). Human osteoblast cells (CRL-11372) were obtained from American Type Culture Collection (VA, USA). 96-well plates were acquired from Orange Scientific (Braine LÁlleud, Belgium). Tris Base was obtained from Fischer Scientific (Portugal).

2.2 Methods

2.2.1 Rapid Prototyping of beta tricalcium phosphate/Alginate composite scaffolds

To produce the scaffolds herein described an additive manufacturing method was used. In particular, a Fab@Home plotter was used, for the creation of well defined, highly reproducible 3D structures[75]. This type of system deposits a highly viscous solution in a controlled manner, in this case a β-TCP/alginate composite.
For this study, six types of scaffolds were produced, using different ratios of β-TCP/alginate, and PVA.
Briefly, a 1% (w/v) PVA solution was prepared by dissolving the polymer in double deionized and filtered water (obtained using a Milli-Q Advantage A10 ultrapure Water Purification System; resistivity=18.2MΩ/cm at 25 °C), with overnight agitation. Then, a 15% (w/v) alginate solution was prepared, dissolving the alginate in either water or in the PVA solution. This solution was then homogenized in a X10/25 ultraturrax (Ystral, Germany) for 30 minutes. Finally, β-TCP powder was added to the solution according to the specific ratios studied (table 2.1), and the solution was again homogenized.

Following, a 5% $CaCl_2$ solution was added to the composite solution, following a 0.14:1 (% v/v) ratio of $CaCl_2$ to alginate. In this step, alginate goes through a ionic crosslinking process, which allows for the increased viscosity of the solution through the formation of a hydrogel[53]. This

Table 2.1: Chemical composition of the produced scaffolds

Scaffolds	β-TCP	Alginate	PVA
60/40	60	40	No
70/30	70	30	No
80/20	80	20	No
60/40/PVA	60	40	Yes
70/30/PVA	70	30	Yes
80/20/PVA	80	20	Yes

increase in the viscosity is essential for the later deposition process.
The Fab@Home model reproduces a computer designed 3D model, in a layer-by-layer process. As such, the model of the scaffold was produced in OpenSCAD software (version 2014.3, ©2009-2014 Marius Kintel and Clifford Wolf), and then exported to STL format. Afterwards, the solution was filled into a 10 cm^3 disposable syringe barrel, and the scaffolds plotted through a 22G polypropylene tapered nozzle. Following, the scaffolds were maintained in a 5% $CaCl_2$ bath for 24 hours, for full crosslinking, after which they were left to dry at RT for 24 hours. Finally, the scaffolds were freeze-dried for 24 hours.

2.2.2 Physicochemical and morphological characterization of the scaffolds

2.2.2.1 Scanning Electron Microscopy analysis

SEM (Scanning Electron Microscopy) micrographs were acquired in order to characterize the morphology, porosity and surface of the scaffolds. The samples were mounted onto aluminium stubs with Araldite glue, and sputter-coated with gold using a Quorum Q150R ES sputter coater. The SEM images where then captured with variable magnifications, at an acceleration voltage of $20\,kV$, using a Hitachi S-3400N Scanning Electron Microscope.

2.2.2.2 Fourier Transform Infrared Spectroscopy analysis

To measure the physicochemical characteristics of the scaffolds, FTIR (Fourier Transform Infrared Spectroscopy) was used. The FTIR spectra obtained for the samples are the average of 128 scans, between 400 and $4000\,cm^{-1}$, with a spectral resolution of $4\,cm^{-1}$. All the samples were crushed to a powder, mounted on a diamond window, and the spectra recorded with a Nicolet iS10 FTIR spectrophotometer (Thermo Scientific, Waltham, MA, USA). All the components of the scaffold were also analysed in pure state for comparison with the samples[79].

2.2.2.3 X-Ray Diffraction analysis

XRD (X-Ray diffraction) measurements were performed in order to evaluate the phases and crystallinity of the ceramic component of the scaffolds after their production.
All samples were mounted in silica supports, and the data recorded over a range of 5° to $90^\circ 2\theta$ degrees, with continuous scans of 1°/min, using a copper ray tube operated at $30\,kV$ and $20\,mA$[70,77].

2.2.2.4 Energy Dispersive Spectroscopic analysis

EDS (Energy Dispersive Spectroscopy) was used for elemental characterization of the various scaffolds. The samples were placed on aluminium stubs, air-dried at RT, and analysed in a

XFlash Detector 5010(Bruker Nano).

2.2.3 Mechanical characterization of the scaffolds

Compression assays were performed in order to evaluate the mechanical behaviour of the scaffolds. The dimensions of the final scaffolds were measured and introduced into a Zwick® 1435 Material Püfung (Ulm, Germany). The assays were performed using a crosshead speed of 3 mm/min and a load cell of 5 kN. Five specimens of each sample were used for each assay. The compressive strength of each scaffold was calculated according to equation (2.1)[80].

$$Cs = \frac{F}{w * l} \quad (2.1)$$

Where F is the load at the time of fracture, and *w* and *l* represent the width and length of the scaffold, respectively.
The Young Modulus was calculated using the values from the equation (2.1), and applying equation 2.2.

$$YM = \frac{Cs}{Hd} \quad (2.2)$$

Where *Hd* stands for the height deformation at maximum load, and *Cs* is the scaffold tensile strength. Average values and standard deviations (s.d.) were determined for each sample (n=5).

2.2.4 Swelling studies

The swelling capacity of the scaffolds was determined following a method adapted from Valente et al.[52]. Samples from each scaffold were placed in eppendorfs containing 5 mL of Tris buffer (pH=7,4), at 37 °C. The samples were then retrieved from the solution at predetermined intervals, and weighted, after removing the excess of Tris with filter paper. After this process, the samples were re-immersed in buffer solution. Three samples of each scaffold were used and the swelling ratio was evaluated using equation (2.3).

$$\text{Swelling ratio (\%)} = \frac{W_t - W_0}{W_0} * 100 \quad (2.3)$$

Where W_t is the final weight of the scaffolds, and W_0 their initial weight.

2.2.5 Porosity evaluation

To determine the microporosity of the different scaffolds a liquid displacement method was adapted from Torres et al.[80]. In brief, scaffolds were weighted, immersed in absolute EtOH for 48 hours, and weighted again. EtOH was chosen for its ability to penetrate throughout the scaffolds without shrinking nor swelling the matrix[81]. The porosity was then calculated by the amount of EtOH absorbed, through equation (2.4):

$$\text{Porosity (\%)} = \frac{W_w - W_d}{D_{ethanol} * V_{scaffold}} * 100 \quad (2.4)$$

Where W_w and W_d are the wet and dry weights of the scaffolds, respectively, $D_{ethanol}$ represents the density of EtOH at RT and $V_{scaffold}$ the volume of the wet scaffold.

2.2.6 Characterization of the degradation profile of the scaffolds

The degradation of the composite scaffolds was investigated through a method adapted from Jeong et al.[82] and Freed et al.[83]. In brief, scaffolds were placed in 24 well plates, fully immersed in DMEM-F12, at $37\,^{\circ}$C. At predetermined intervals the samples were removed, completely dried and weighted. The degradation percentage at each point was calculated through equation (2.5):

$$\text{Weight Loss (\%)} = (1 - \frac{W_i - W_t}{W_i}) * 100 \quad (2.5)$$

Where W_i corresponds to the initial weight of the sample and W_t to the weight of the sample at time t.

2.2.7 Contact Angle Measurements

Contact angle measurements were performed using the sessile drop technique, adapted from Diogo et al.[77], using water as reference fluid. Drops were placed at different points on the surface of the scaffolds, and the data was acquired usind a *Data Physics Contact Angle System OCAH 200*, operated in static mode at RT.

2.2.8 Biological characterization of the scaffolds

2.2.8.1 Cell culture in the presence of the scaffolds

Human osteoblasts (CRL-11372) were cultured in DMEM-F12, supplemented with 10% heat inactivated FBS, streptomycin (100 µg/mL) and gentamicin (100 µg/mL) in 75 cm^2 T-flasks. Cells were maintained in a humidified environment at $37\,^{\circ}$C, with 5% CO_2, until confluence was attained. Subsequently, cells were trypsinized with 0.18% trypsin (1:250), and 5 mM EDTA, centrifuged at 300 RCF, for 5 min, and the pellet resuspended in 5 mL of complete culture medium. Cellular density was then determined using a Neubauer chamber and trypan blue.
Prior to cell seeding, the scaffolds were cut into pieces with appropriate sizes and placed into 96-well plates for sterilization (n=5). This was achieved by subjecting the scaffolds to UV (ultraviolet) light for 30 min. Subsequently, cells were seeded at a density of $10x10^3$ cells per well, for cell viability and proliferation evaluation. The culture medium was replaced every two days until the end of the assay.

2.2.8.2 Evaluation of cell viability and proliferation in the presence of the scaffolds

Cell viability was determined using an MTS assay, at 4 and 7 days after seeding. The metabolic activity of the cells was assessed by quantifying the metabolic conversion of MTS to formazan. Briefly, the medium in each well was replaced with a mixture of 100 µL of fresh culture medium

containing 20 µL of MTS/PMS (phenazine methosulfate) reagent solution. The cells were then incubated for 4 hours at 37 °C. Following the incubation period, 80 µL of the supernatant were transfered into a 96-well microplate and the fluorescence intensity measured at 492 nm using a microplate reader (Anthos 2020, Biochrom). Cells cultured without materials were used as negative control (K^-) and cells cultured with EtOH (96%) were used as positive control (K^+).

2.2.8.3 Scanning Electron Microscopy analysis

In order to evaluate the morphology and topography of the scaffolds as well as the cellular behaviour in their presence, SEM was performed according to the method adapted from Lee and Chow[84]. Briefly, the samples were washed at RT with cacodylate buffer solution, then fixed for 30 minutes in 2.5%(v/v) glutaraldehyde in 0.1M sodium cacodylate solution. The samples were then frozen in liquid nitrogen for 2 min and then freeze-dried for 2 hours.
For SEM analysis, the samples were mounted onto aluminium stubs with Araldite glue, and sputter-coated with gold using a Quorum Q150R ES sputter coater. The SEM images were captured at variable magnifications, with an acceleration voltage of 20 kV, using a Hitachi S-3400N Scanning Electron Microscope.

2.2.9 Statistical Analysis

Statistical analysis of the obtained results for the different groups of scaffolds, and the various conditions, was performed by using one-way analysis of variance (ANOVA), with the Newman-Keuls post hoc test. The statistical test was used for comparison of the mean and the differences between groups. A *p* value less than 0.05 ($p<0.05$) was considered statistically significant.

Chapter 3

Results and Discussion

3.1 Morphological characterization of the scaffolds

As previously described, biodegradable scaffolds for bone tissue regeneration must fulfill certain requirements, such as good biocompatibility and suitable structure. They must also provide mechanical support during the regeneration phase, as well as adequate physicochemical environment for cell proliferation.
Since most types of materials present certain disadvantages when used alone, in this work composite materials were used for scaffold development. In particular, a polymer and ceramic composite was chosen, mimicking the natural bone matrix. Thus, this study describes the development, optimization and production of scaffolds aimed for bone tissue regeneration, composed of β-TCP and alginate. Figure 3.1 presents the CAD model used, as well as the printed scaffold by rapid prototyping. The designed model is a 13 mm x 13 mm x 13 mm cube, with porous structure.

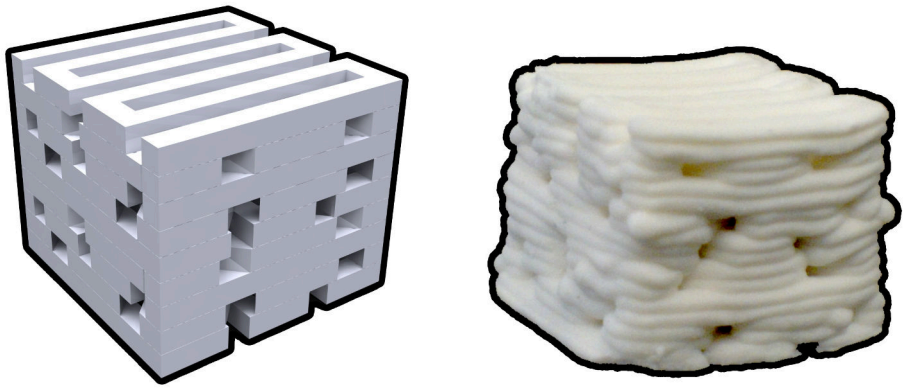

Figure 3.1: Images of the CAD model used (left) and of the final printed model (right)

Herein, alginate was chosen for its biocompatibility, and ability to act as temporary ECM. In addition, the ability to control the degradation rate of this polymer is a great advantage for the tailoring of the properties of the scaffold[53,54]. On the other hand, β-TCP was chosen for its resemblance with the natural ceramic component of bone tissue, and consequently, its increased biocompatibility and osteoconductivity[38,41,48], allied to its enhanced mechanical resistance. Furthermore, the combination of these materials has already been shown to improve cell adhesion and proliferation, with the potential to support cell growth and differentiation before implantation[77,85].

Macroscopic images of the produced scaffolds were acquired, to assess their morphology (figure 3.2).

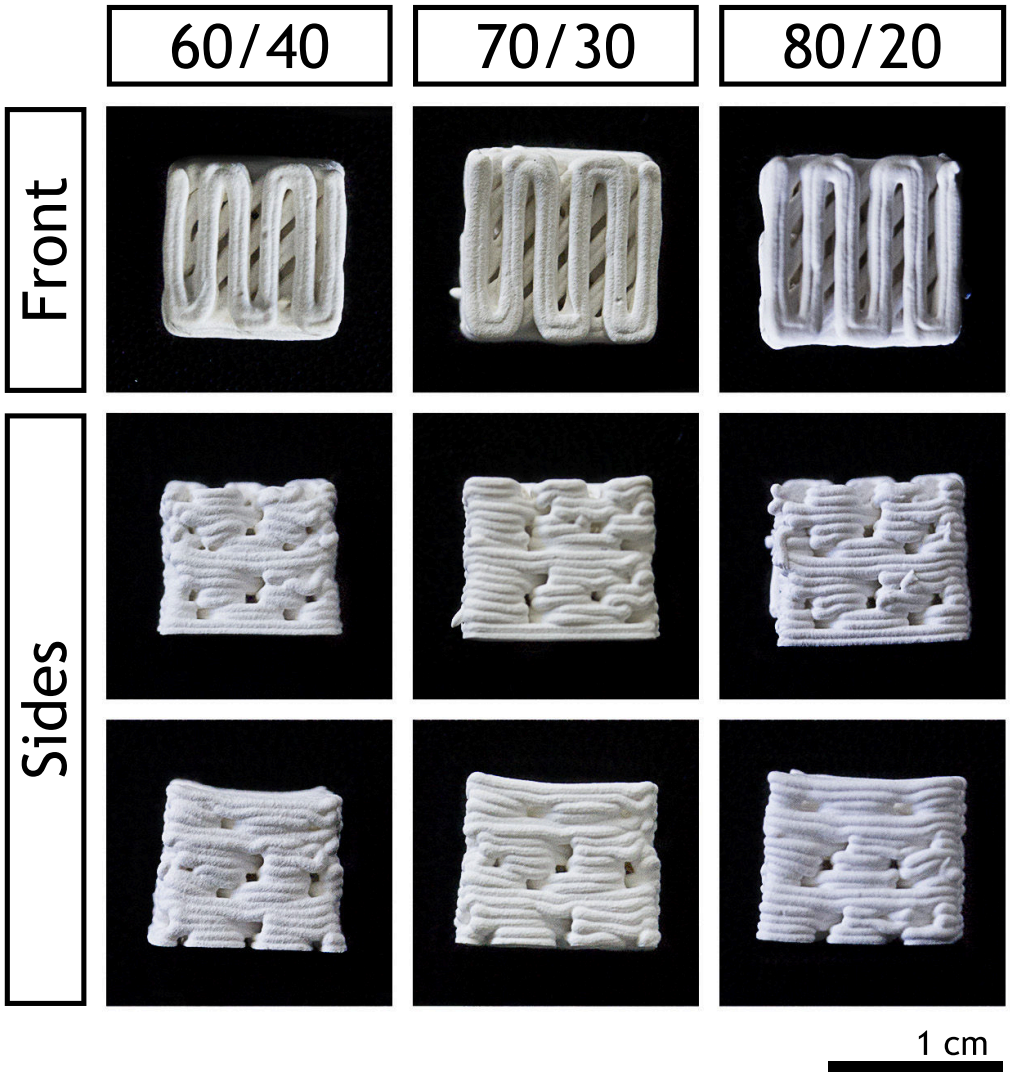

Figure 3.2: Macroscopic images of the different produced scaffolds

It is possible to observe that the β-TCP content had a direct effect on the scaffolds structure, namely on the scaffolds dimensions. It was previously described that alginate gels and scaffolds present shrinkage during air drying[86]. Rassis et al.[87] have related that the presence of solid fillers in an alginate solution has a direct effect on the volume loss after drying. The compression of the polymeric matrix leads to the compression of the β-TCP particles against each other. In effect, the scaffolds containing the highest percentage of β-TCP were capable of maintaining their dimensions showing a lower amount of shrinkage, since the amount of incompressible ceramic particles limits the shrinking that the scaffolds can suffer. Nonetheless, all the formulations maintained their shape, with a well defined structure and design.

Following, SEM images were acquired, to characterize the scaffolds surface morphology (Figure 3.3).

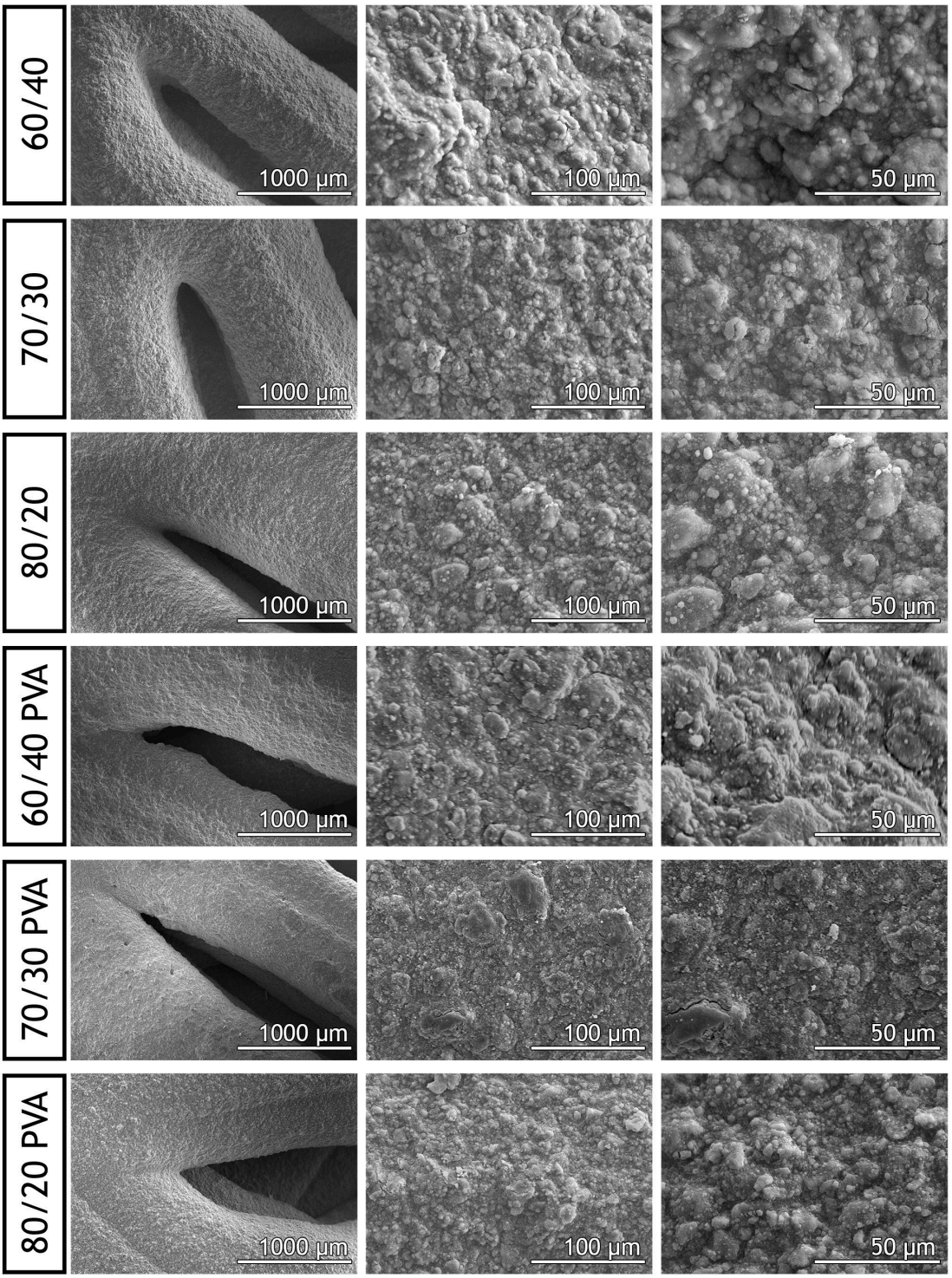

Figure 3.3: SEM images showing the morphology of the scaffolds at different magnifications

In figure 3.3 it is possible to observe that all the scaffolds presented similar surface characteristics, with high roughness and irregularities. It has been previously described that the cellular morphology, adhesion and proliferation are directly affected by the scaffolds surface characteristics. In particular, human osteoblasts present increased metabolism, and ECM production, when in contact with rough surfaces. This effect is caused by an increased contact surface, directly related to the increased adhesion points on irregular surfaces[88].

3.2 Physicochemical characterization of the scaffolds

3.2.1 Fourier Transform Infrared Spectroscopic analysis

The FTIR spectra of the raw materials and of the produced scaffolds, are present in figure 3.4.

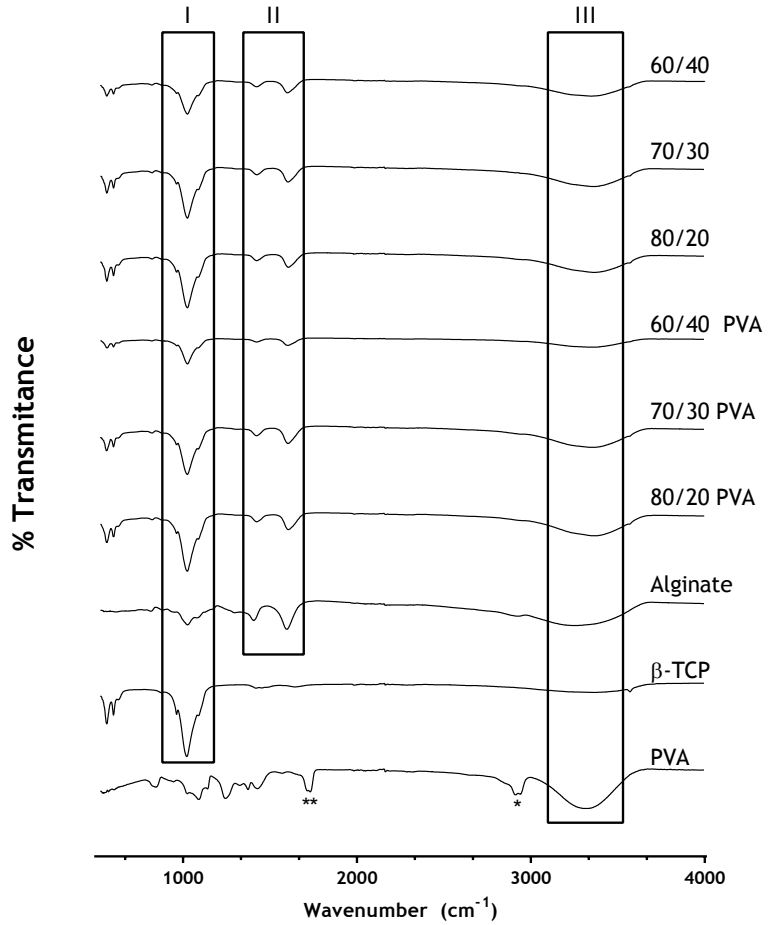

Figure 3.4: FTIR analysis of the powders and 3D scaffolds.

The β-TCP spectrum presents a major peak at $1020\,cm^{-1}$ (I), characteristic of a P=O stretch vibration, revealing the presence of the inorganic phosphate components of β-TCP[70]. This peak is also present on the spectra of the produced scaffolds, with an intensity that is proportional to the ceramic content.

The FTIR spectrum of sodium alginate powder presented two major peaks at 1400 and $1600\,cm^{-1}$ (II), corresponding to the C=O stretching of the carboxylate group[89]. In addition, a stretching vibration correspondent to the O—H bonds of alginate appeared in the range $3000-3600\,cm^{-1}$ (III)[90]. These peaks were also present in the spectra of the different scaffolds, without perceptible variations among the different formulations.

In the PVA spectrum, all major peaks are related to the hydroxyl and acetate groups. In particular, a large band is present between 3550 and $3200\,cm^{-1}$, representative of a O—H stretching from hydrogen bonds (III), and a vibrational band between 2840 and $3000\,cm^{-1}$ (*), that belongs to a C—H stretching from alkyl groups. In addition, the peaks at $1735-1750\,cm^{-1}$ (**) are

relative to a C=O and C—O stretches, from the acetate group of PVA[91]. However, the characteristic peaks of PVA are not observed in the other spectra since low concentrations were used for scaffold's production[77].

3.2.2 X-ray diffraction analysis

To confirm the crystalline phases of β-TCP an XRD analysis was performed. The XRD patterns of both the β-TCP powder and the produced scaffolds, are present in figure 3.5.
It can be observed that the β-TCP spectra presents two intense peaks located at 2θ=25°-32°, characteristic of this material[49]. These peaks demonstrate the successful incorporation of the ceramic component in the scaffolds, and the lack of any amorphous phases show that the crystalline structure was not affected during the production steps[70].

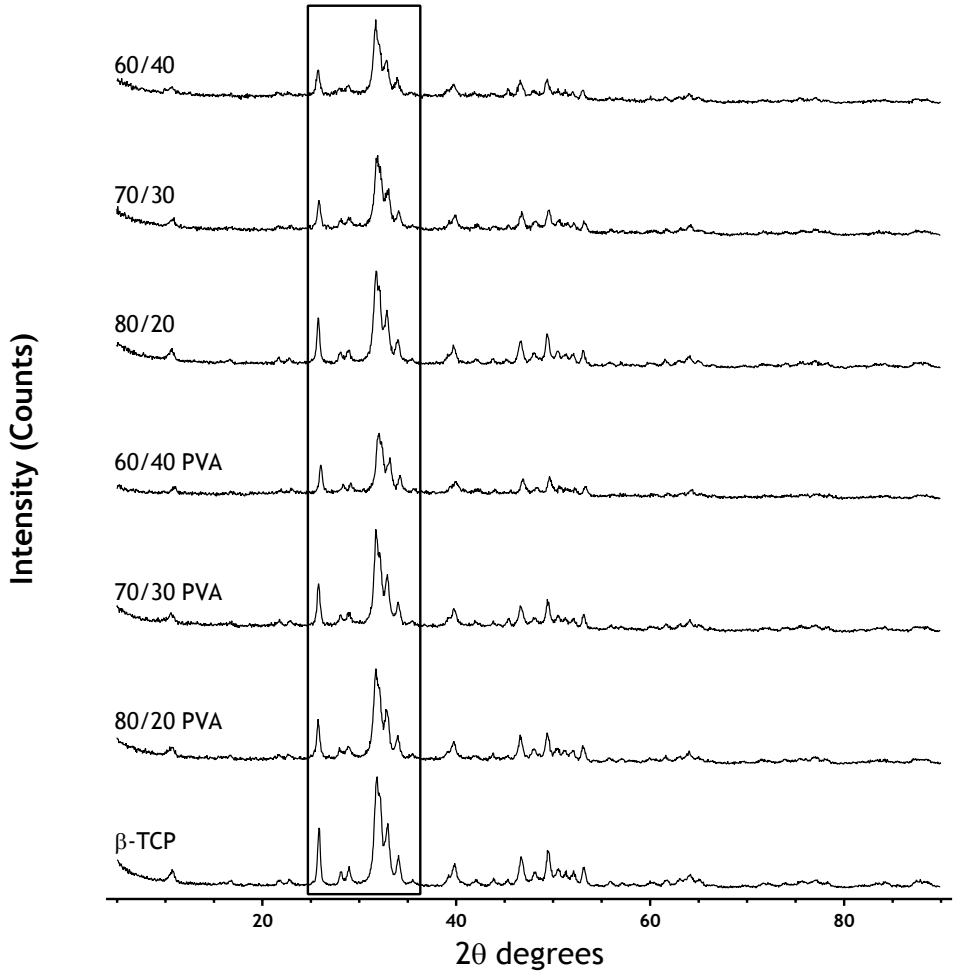

Figure 3.5: XRD spectra of β-TCP and of the produced scaffolds

3.2.3 Energy dispersive spectroscopic analysis

An elemental analysis of the scaffolds was performed to characterize the chemical composition of the scaffolds. In figure 3.6 it is possible to observe that all the scaffolds have a high percentage of carbon and oxygen, derived mainly from the alginate. In fact, the carbon content of the scaffolds rises with the increasing amount of alginate.

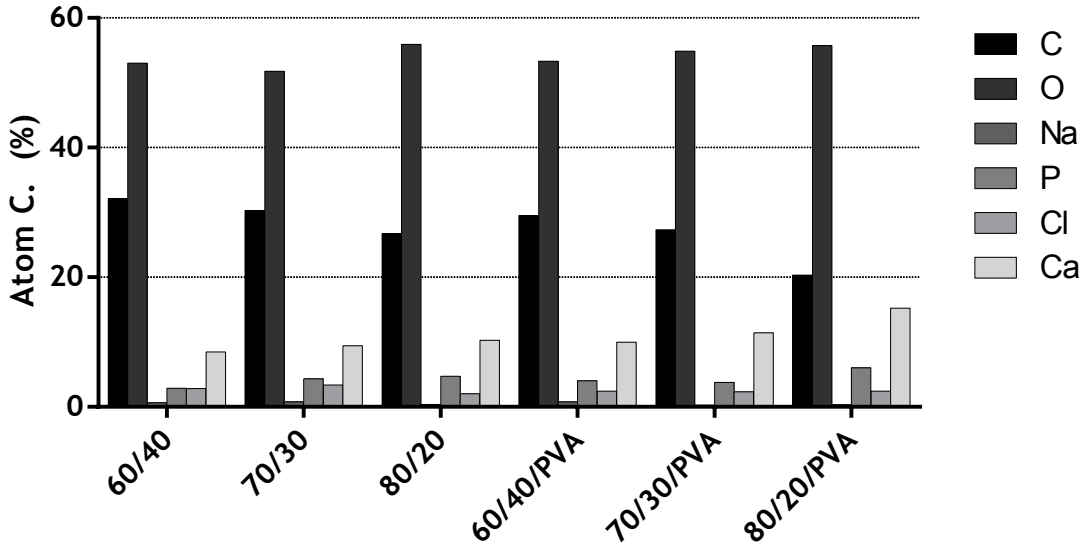

Figure 3.6: EDS analysis of the produced scaffolds

The results of this analysis show an increase in phosphate and calcium ions, with increasing ceramic content of the scaffold. Such results were expected, since these are the main components of β-TCP. As such, the EDS analysis is in agreement with the scaffolds composition.

3.2.4 Mechanical characterization of the scaffolds

The mechanical behaviour of the scaffolds was analysed through the resistance to compression and Young's modulus, present in figure 3.7.

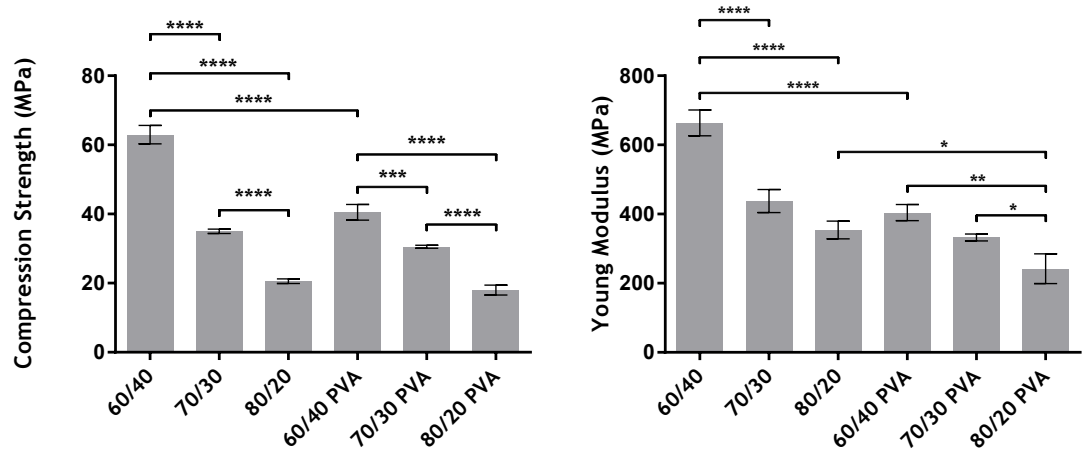

Figure 3.7: Mechanical characterisation of the scaffolds

From figure 3.7 it is possible to observe that the 60/40 scaffolds presented the highest compression strength when compared to the other scaffolds. It was previously described that an increased ceramic content leads to lower mechanical resistance[92,93], as was observed. Furthermore, in a biphasic solution, the polymeric component acts as a binder for the ceramic

particles. In the particular case of hydrogels, the gelation process creates a three-dimensional matrix, yielding a bone like structure by trapping the ceramic particles[94]. The composition of the 60/40 scaffolds closely resembles the native bone composition, mimicking the fine balance of strength and elasticity present in bone tissue. The high β-TCP content in the 70/30 and 80/20 scaffolds lead to an increased brittleness and fragility, characteristic of pure ceramic scaffolds[93].

Comparing with the natural bone, the scaffolds with the lowest mechanical resistance, 80/20, presented a compressive strength similar to that of cortical bone, at about $20\,\text{MPa}$. Furthermore, the 60/40 scaffolds showed more than half the resistance of cortical bone, proving that this type of scaffolds can achieve more than adequate mechanical stability for non load bearing sites.

We can also note that the addition of PVA to the scaffolds compositions lowered their mechanical resistance, in particular for the 60/40 scaffolds. Islam and Karim[95] have previously reported that alginate presents better mechanical properties than PVA, as was also confirmed here.

The Young modulus analysis showed that the scaffolds with lowest ceramic content present the highest modulus. In addition, it was also shown that PVA has a negative effect on the scaffolds mechanical properties, decreasing the Young modulus. Comparing with the natural bone, all the scaffolds surpassed the Young Modulus of cancellous bone. However, they are still one order of magnitude lower than the modulus for cortical bone, demonstrating the difficulty of perfectly mimicking the mechanical structure of such a complex tissue.

In short, the scaffolds with the 60/40 formulation presented the best mechanical properties, both for compression strength, and for Young Modulus, surpassing the mechanical properties of trabecular bone.

3.2.5 Swelling studies

The swellings profiles obtained for the scaffolds are presented in figure 3.8. It is possible to observe that all the scaffolds presented a rapid swelling in the first minutes and stabilized after about 10 hours of immersion.

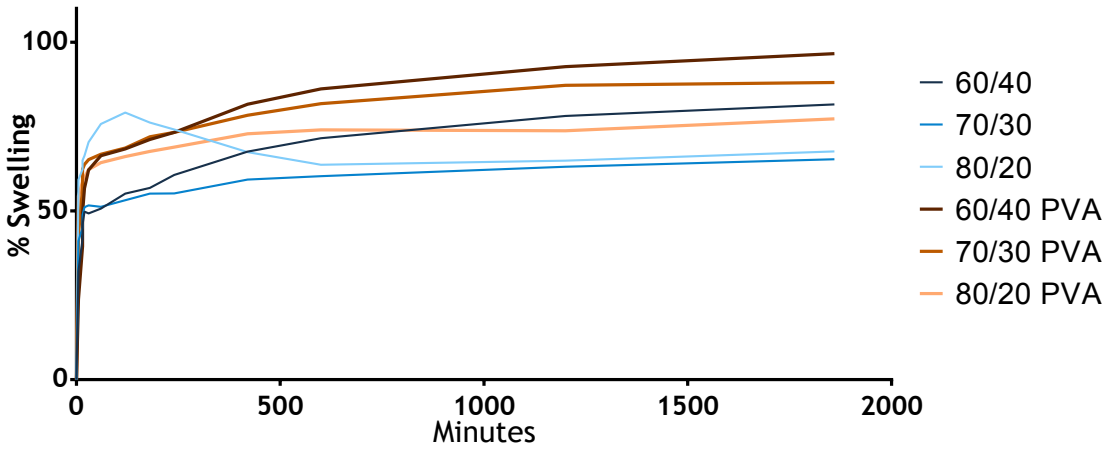

Figure 3.8: Swelling profile of the scaffolds

Valente et al. have previously reported that the polymer network of alginate is capable of absorbing large quantities of water, filling its void regions[52]. This effect was confirmed in the

results obtained in this study, where the scaffolds containing higher amounts of β-TCP, and thus less void regions, presented a lower swelling ratio.
The results also show that the scaffolds containing PVA present a slightly higher swelling behaviour. This is due to the ability of PVA to absorb water, increasing the swelling capacity of the scaffold[96].

3.2.6 Porosity evaluation

Figure 3.9 shows that the scaffolds with highest β-TCP content present the highest porosity values (> 10% porosity). During the drying process the scaffolds suffer shrinking, which is responsible for the compression of the polymer matrix. In this stage, the scaffolds with high ceramic content present more incompressible particles, thus limiting the amount of shrinkage that they can suffer, and consequently showing increased porosity[70,77].
In addition, the presence of PVA on the scaffold's composition can hinder the compaction effect of alginate, leading to a decrease in scaffold's density, and thus increased their porosity.
These results are in agreement with the mechanical resistance data. Porosity and density are inversely proportional. Density is closely related to the mechanical resistance of a scaffold. Therefore, the most resistant scaffolds should also be the denser, as can be observed in figure 3.9.

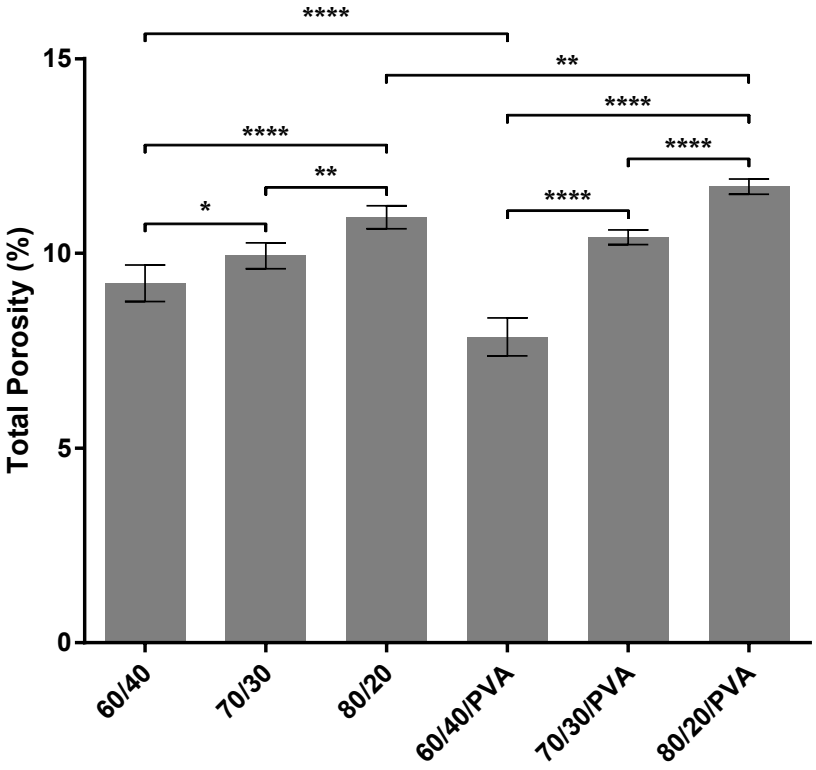

Figure 3.9: Porosity evaluation of the scaffolds

Nevertheless, the obtained scaffolds present microporosities that are far from being ideal for a good cell migration, as well as nutrients and oxygen flow. However, this lack of microporosity is balanced by a regular and sufficient macroporosity, as can be seen in figure 3.3.

3.2.7 Characterization of the degradation profile of the produced scaffolds

The degradation profile of the produced scaffolds is presented in figure 3.10.

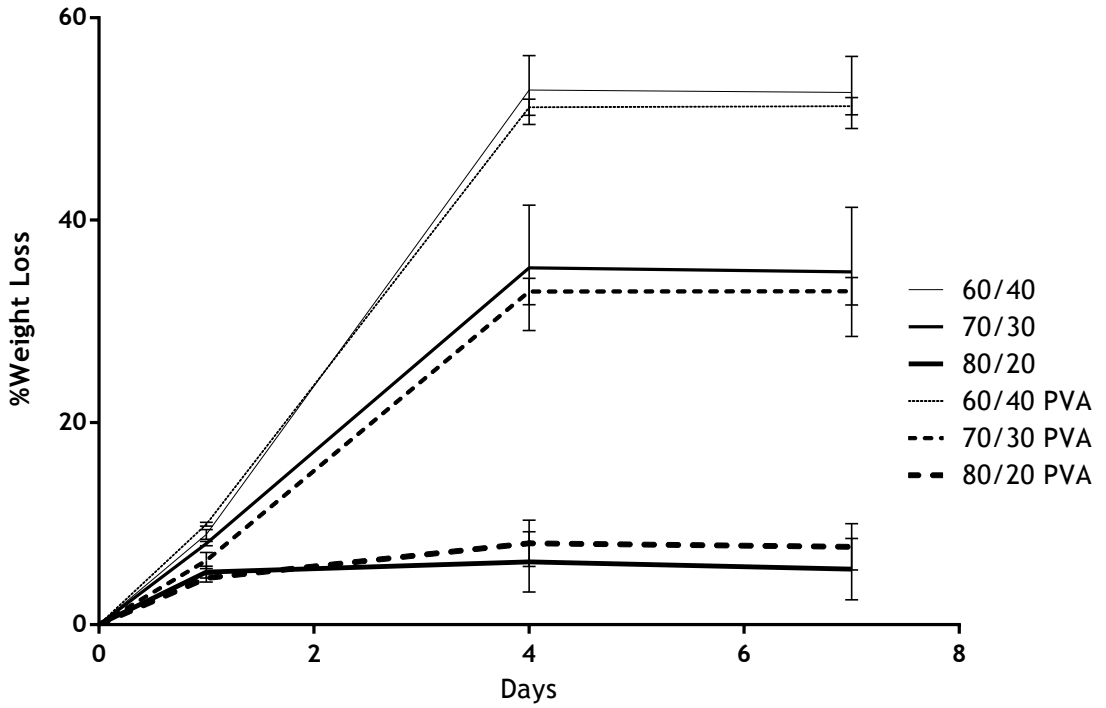

Figure 3.10: Degradation profile of the scaffolds

In vivo, alginate only depolymerises by spontaneous alkaline β-elimination of its glycosidic linkages, due to a lack of enzymes capable of degrading this compound in humans. However, it can suffer disintegration by gradual exchange of calcium ions with sodium, reversing the gelling process[53]. The results obtained revealed that the scaffolds have a degradation profile dependent on the relative alginate content of the scaffolds, with the scaffolds containing a higher percentage of the polymer enduring a greater loss of mass. Nonetheless, none of the scaffolds lost more than 45% of its mass, and all stabilized after 4 days. In addition, Weinand et al. have previously reported that cells can disperse throughout the structure of similar scaffolds within 7 days, and deposit new bone tissue[97]. These results show that the produced scaffolds present a degradation rate suitable for bone tissue regeneration.

3.2.8 Contact angle measurements

The contact angle results are represented in figure 3.11.

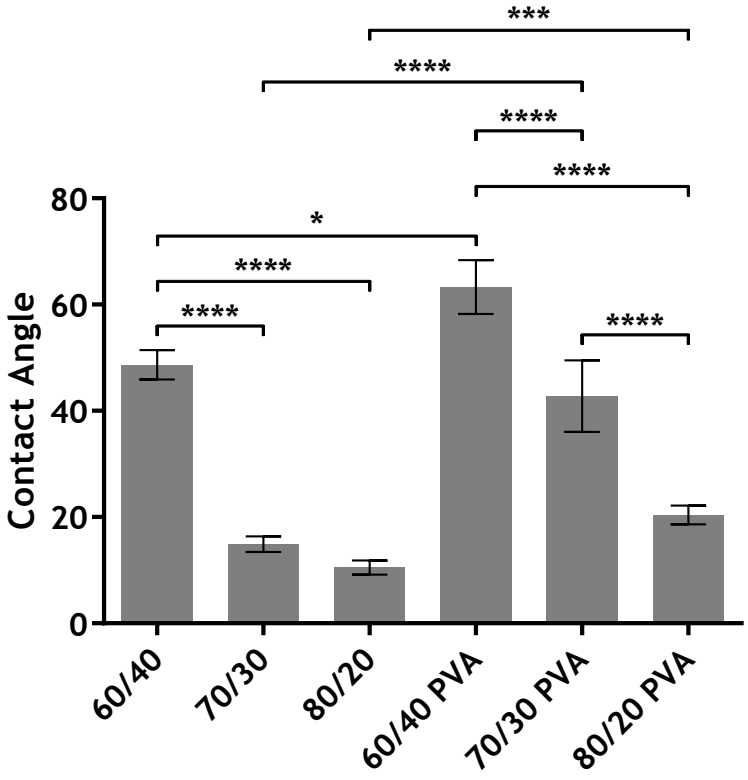

Figure 3.11: Contact angle of the produced scaffolds

It is possible to observe that all the scaffolds present a moderate to highly hydrophilic surface, with contact angles below 70. Furthermore, they present a clear increase in the hydrophilic character when the β-TCP content of the scaffolds is higher, as previously described by Diogo et al. and Hu et al., benefiting cell attachment and growth[77,98]. In addition, PVA also decreased the hydrophilicity of the scaffolds, increasing the contact angle of all compositions.

3.2.9 Analysis of the scaffolds biological properties

3.2.9.1 Characterization of the cytotoxic profile of the scaffolds

In vitro studies where performed to elucidate about the cytotoxicity of the scaffolds. Human osteoblastic cells were cultured in contact with the scaffolds for up to 7 days, and their viability assessed at 4, and 7 days. The optical images acquired at the mentioned time points after cell seeding demonstrated that they were able to adhere and proliferate in the presence of the composite scaffolds (Figure 3.12), in a comparable rate to that of the negative control. In the positive control it is possible to observe the cells in their typical spherical shape which is characteristic of dead cells.

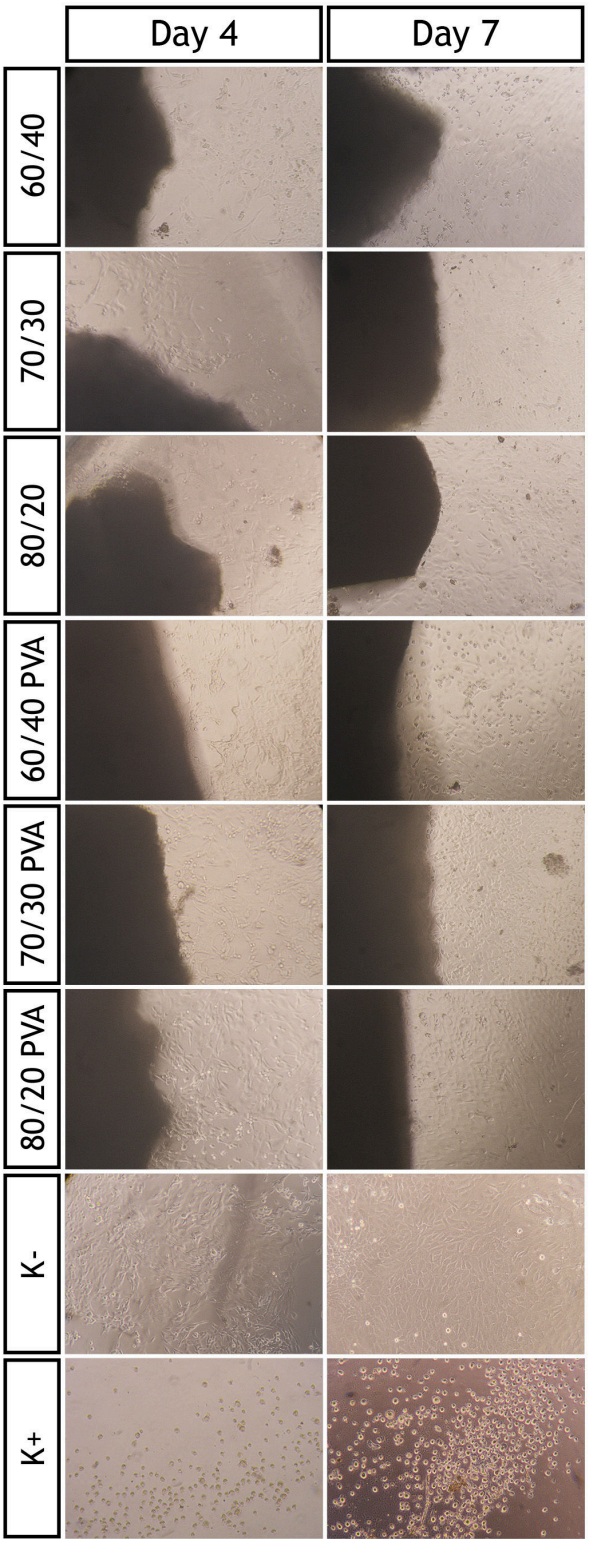

Figure 3.12: Macroscopic images of human osteoblasts in the presence of the scaffolds

To further characterize the cytotoxic profile of the scaffolds, and to evaluate the cellular adhesion on their surface, SEM images were acquired (figure 3.13).
Figure 3.3 demonstrated that the scaffolds presented high roughness and irregularities, creating possible attachment points for the cells. In fact, it is possible to observe that the cells were able to adhere to the surface of the material after 24 h of being seeded. Moreover, after 7 days,

most cells had spread throughout the entire scaffold's surface, creating a cell layer around the scaffold, demonstrating that all the scaffolds presented a suitable surface for cell adhesion and proliferation.

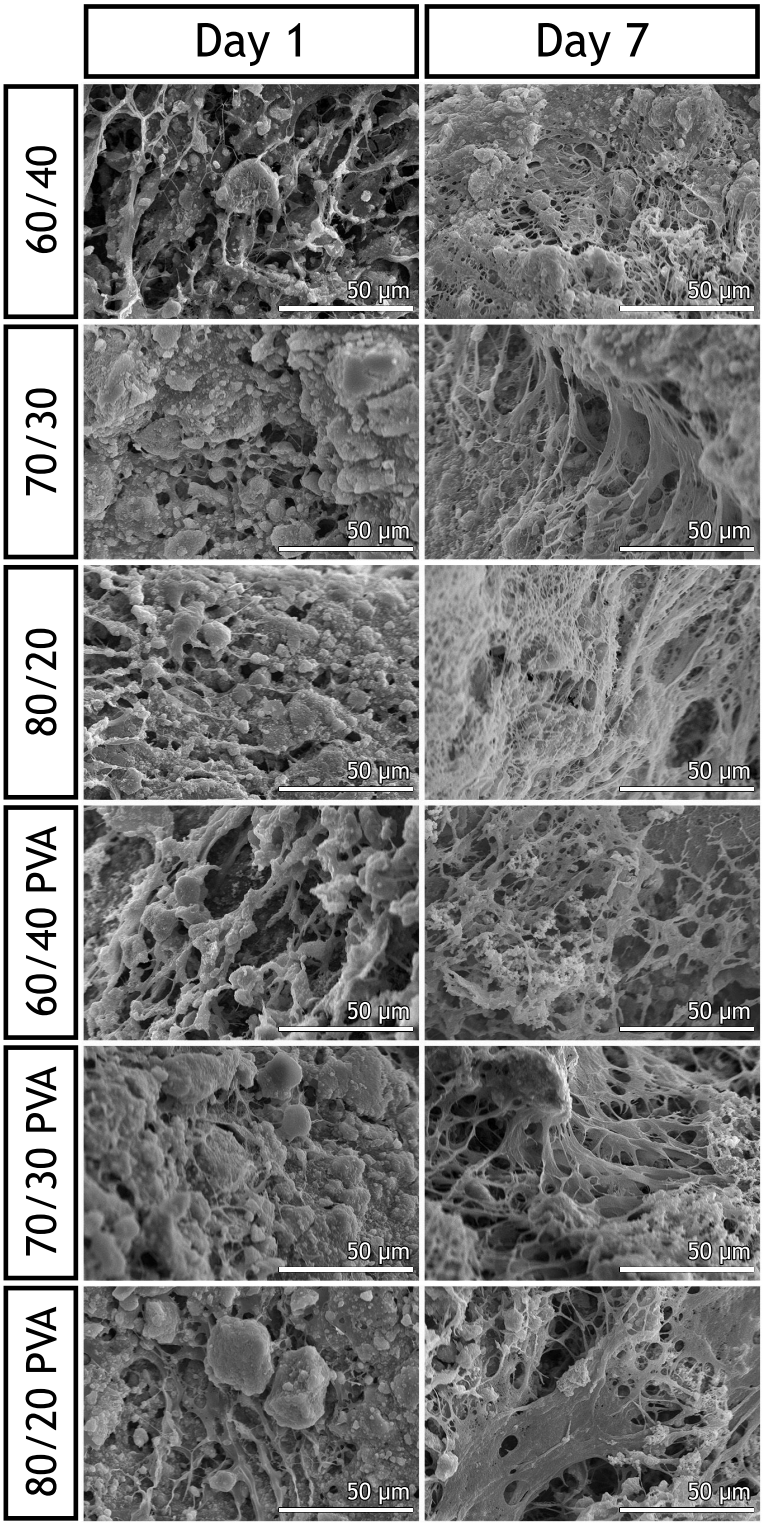

Figure 3.13: SEM images of osteoblasts morphology in the presence of the scaffolds

In figure 3.14 it is presented the results obtained in the MTS assay.

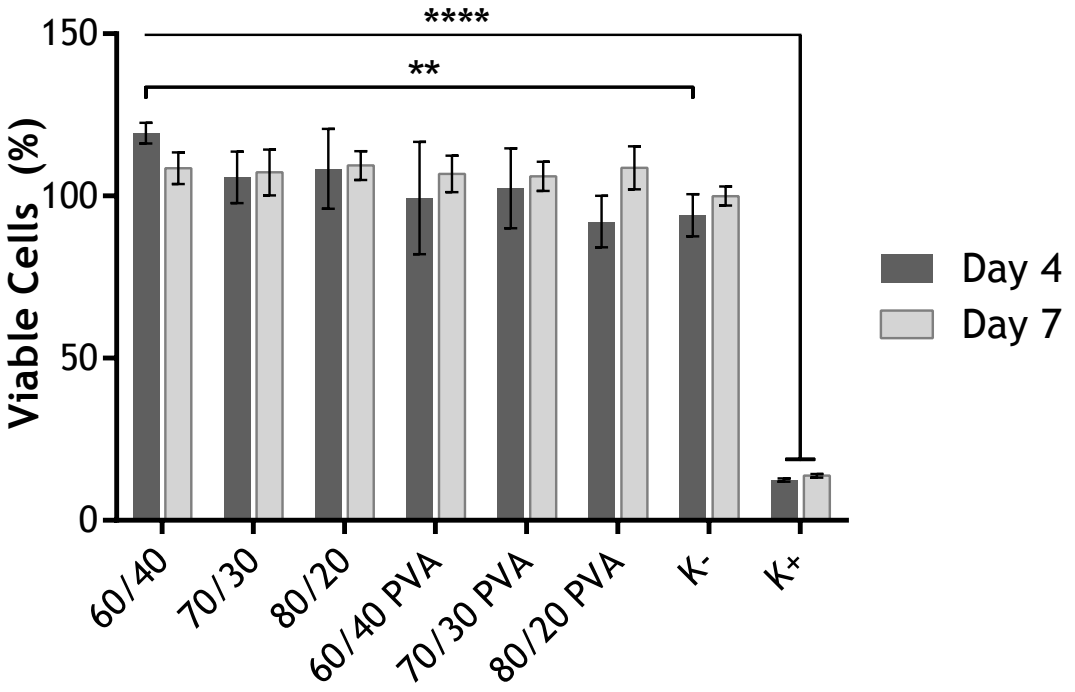

Figure 3.14: Evaluation of human osteoblast cell viability cultured in contact with the different scaffolds. Each result is the mean ± standard error of the mean of at least three independent experiments. Statistical analysis was performed using one-way ANOVA with Dunnet's post hoc test (* $p<0.05$)

The results obtained show that cells remained viable after 4 and 7 days in the presence of the scaffolds. The 60/40 formulation presented the highest cell viability. In fact, all the tested scaffolds presented excellent viability after 7 days of incubation, indicating that these scaffolds provide an appropriate environment for cell proliferation. These results can be attributed to the osteogenic potential of β-TCP, capable of creating a layer similar to apatite on the surface of the material[99], thus inducing the proliferation of osteoblast cells.

Chapter 4

Conclusions and Future Perspectives

The aging of the world population has brought an increase in the number of patients suffering bone defects and diseases. The current technologies available on point of care are limited, especially when dealing with large bone defects. With this in mind, temporary and biodegradable scaffolds are an excellent alternative to overcome this problem. A variety of materials and techniques have been used for the production of scaffolds. Rapid prototyping technologies are emerging as one of the most promising tools that allows the production of 3D constructs with highly controlled structure, and even recreating the shape and dimensions of the natural tissue to replace, based on medical data. The Fab@Home model used in this work allowed the production of scaffolds with the different ratios of β-TCP and Alginate, and may also allow for the encapsulation of cells or bioactive molecules.

Herein, composite scaffolds with a controlled and uniform structure were produced with six different formulations. The physicochemical assays performed demonstrated that the final scaffolds maintained the crystalline structure of the ceramic component, as well as its composition. In addition, the hydrophilic character of the produced scaffolds allowed cellular adhesion and proliferation, with the surface roughness providing adequate cell anchorage. The *in vitro* assays suggest an adequate biocompatibility, especially for the 60/40 scaffolds. This formulation also presented the best mechanical properties, presenting mechanical characteristics better than those of trabecular bone. In addition, this scaffold presents a constitution similar to that of bone tissue, favouring osteointegration and bone regeneration.

However, the porosity of all of the produced scaffolds was far from ideal, possibly hindering the bone regeneration process, being a possible improvement in further studies. In addition, it would also be interesting to perform *in vivo* studies to fully characterize the scaffold's potential for clinical application, since the *in vitro* assays performed cannot fully emulate a systemic regenerative response. Moreover, the current generation of biomaterials is mimicking and manipulating the signaling machinery inside an organism. Thus, the possible incorporation of biomolecules such as BMP's could also greatly improve the regenerative potential of these materials. Finally, the application of rapid prototyping technologies enables the delivery of personalized care, with the design of the scaffolds mimicking the exact structure of the bone defect to fill, leading to shorter healing times.

Bibliography

[1] Salgado, A.J., Coutinho, O.P., and Reis, R.L. Bone tissue engineering: state of the art and future trends. *Macromolecular Bioscience*, 2004. **4**(8):743–65. doi:10.1002/mabi.200400026. 1, 12

[2] Kneser, U., Schaefer, D.J., Polykandriotis, E., and Horch, R.E. Tissue engineering of bone: the reconstructive surgeon's point of view. *Journal Of Cellular And Molecular Medicine*, 2006. **10**:7–19. doi:10.1111/j.1582-4934.2006.tb00287.x. 1, 8

[3] Gaalen, S.v., Kruyt, M., Meijer, G., Mistry, A., Mikos, A., Beucken, J.v.d., Jansen, J., Groot, K.d., Cancedda, R., Olivo, C., Yaszemski, M., and Dhert, W. *Tissue engineering*, chapter 19 - Tissue engineering of bone, pp. 559–610. Academic Press, Burlington. ISBN 978-0-12-370869-4, 2008. doi:10.1016/B978-0-12-370869-4.00019-7. 1, 2, 8, 9, 10

[4] Sommerfeldt, D.W. and Rubin, C.T. Biology of bone and how it orchestrates the form and function of the skeleton. *European Spine Journal*, 2001. **10 Suppl 2**:S86–95. doi:10.1007/s005860100283. 1, 2, 3, 4, 6

[5] Shapiro, I.M., Layfield, R., Lotz, M., Settembre, C., and Whitehouse, C. Boning up on autophagy: The role of autophagy in skeletal biology. *Autophagy*, 2014. **10**(1):7–19. doi:10.4161/auto.26679. 1

[6] VanPutte, C., Regan, J., Russo, A., Tate, P., Stephens, T., and Seeley, R. *Seeley's Anatomy & Physiology*. McGraw-Hill Science/Engineering/Math, 2013. ISBN 0073403636. 1, 2, 3, 6

[7] Clarke, B. Normal bone anatomy and physiology. *Clinical Journal of the American Society of Nephrology*, 2008. **3 Suppl 3**:S131–9. doi:10.2215/CJN.04151206. 2

[8] Ralston, S.H. Structure and metabolism of bone. *Medicine*, 2005. **33**(12):58. doi:10.1383/medc.2005.33.12.58. 2

[9] Krings, A., Rahman, S., Huang, S., Lu, Y., Czernik, P.J., and Lecka-Czernik, B. Bone marrow fat has brown adipose tissue characteristics, which are attenuated with aging and diabetes. *Bone*, 2012. **50**(2):546–52. doi:10.1016/j.bone.2011.06.016. 2

[10] Booth, K. *Medical assisting : administrative and clinical procedures including anatomy and physiology*. McGraw-Hill, New York, 2011. ISBN 0073374547. 2

[11] Meng Bao, C.L., Y.Teo, E., S.K. Chong, M., Liu, Y., Choolani, M., and K.Y.Chan, J. *Advances in Bone Tissue Engineering*, 2013. doi:10.5772/55916. 3

[12] Bailey, A.J., Sims, T.J., Ebbesen, E.N., Mansell, J.P., Thomsen, J.S., and Mosekilde, L. Age-related changes in the biochemical properties of human cancellous bone collagen: Relationship to bone strength. *Calcified Tissue International*, 1999. **65**(3):203–210. doi:10.1007/s002239900683. 3

[13] Grynpas, M. Age and disease-related changes in the mineral of bone. *Calcified Tissue International*, 1993. **53**(1):–57. doi:10.1007/BF01673403. 3

[14] Jayakumar, P. and Di Silvio, L. Osteoblasts in bone tissue engineering. *Proceedings Of The Institution Of Mechanical Engineers Part H-Journal Of Engineering In Medicine*, 2010. **224**(12):1415–1440. doi:10.1243/09544119JEIM821. 3

[15] Nakamura, H. Morphology, function, and differentiation of bone cells. *Journal of hard tissue biology*, 2007. **16**(1):15–22. 3

[16] Meyer, U., Wiesmann, H.P., Handschel, J., and Kübler, N.R. *Fundamentals of Tissue Engineering and Regenerative Medicine*, chapter Bone Tissue Engineering, pp. 211–232. ISBN 978-3-540-77755-7, 2009. doi:10.1007/978-3-540-77755-7_17. 3

[17] Datta, H.K., Ng, W.F., Walker, J.A., Tuck, S.P., and Varanasi, S.S. The cell biology of bone metabolism. *Journal Of Clinical Pathology*, 2008. **61**(5):577–87. doi:10.1136/jcp.2007.048868. 3, 4

[18] Crockett, J.C., Rogers, M.J., Coxon, F.P., Hocking, L.J., and Helfrich, M.H. Bone remodelling at a glance. *Journal Of Cell Science*, 2011. **124**(Pt 7):991–8. doi:10.1242/jcs.063032.

[19] Ehrlich, P.J. and Lanyon, L.E. Mechanical strain and bone cell function: a review. *Osteoporosis International*, 2002. **13**(9):688–700. doi:10.1007/s001980200095. 3, 5

[20] Raggatt, L.J. and Partridge, N.C. Cellular and molecular mechanisms of bone remodeling. *Journal of Biological Chemistry*, 2010. **285**(33):25103–8. doi:10.1074/jbc.R109.041087. 3, 4, 5

[21] Blair, H.C., Robinson, L.J., Huang, C.L.H., Sun, L., Friedman, P.A., Schlesinger, P.H., and Zaidi, M. Calcium and bone disease. *Biofactors*, 2013. **37**(3):159–67. doi:10.1002/biof.143. 3

[22] Rucci, N. Molecular biology of bone remodelling. *Clinical cases in mineral and bone metabolism : the official journal of the Italian Society of Osteoporosis, Mineral Metabolism, and Skeletal Diseases*, 2008. **5**(1):49–56. 4, 5

[23] Boyce, B.F., Rosenberg, E., de Papp, A.E., and Duong, L.T. The osteoclast, bone remodelling and treatment of metabolic bone disease. *European Journal of Clinical Investigation*, 2012. **42**(12):1332–41. doi:10.1111/j.1365-2362.2012.02717.x. 4

[24] Hadjidakis, D.J. and Androulakis, I.I. Bone remodeling. *Annals of the New York Academy of Sciences*, 2006. **1092**:385–96. doi:10.1196/annals.1365.035. 4, 5

[25] Y., A., Valds-Flores, M., Orozco, L., and Velzquez-Cruz, R. Molecular aspects of bone remodeling. In *Topics in Osteoporosis*, 2013. doi:10.5772/54905. 4, 5, 6, 7

[26] Matsuo, K. and Irie, N. Osteoclast-osteoblast communication. *Archives of Biochemistry and Biophysics*, 2008. **473**(2):201–9. doi:10.1016/j.abb.2008.03.027. 5

[27] Abdelrazek, S., Szumowski, P., Rogowski, F., Kociura-Sawicka, A., Mojsak, M., and Szorc, M. Bone scan in metabolic bone diseases. review. *Nuclear medicine review. Central & Eastern Europe : journal of Bulgarian, Czech, Macedonian, Polish, Romanian, Russian, Slovak, Yugoslav societies of nuclear medicine and Ukrainian Society of Radiology*, 2012. **15**(2):124–31. doi:10.5603/NMR.2011.00022. 6, 7

[28] Feng, X. and McDonald, J.M. Disorders of bone remodeling. *Annual Review of Pathology Mechanisms of Disease*, 2011. **6**:121–45. doi:10.1146/annurev-pathol-011110-130203. 6, 7

[29] Svedbom, A., Hernlund, E., Ivergård, M., Compston, J., Cooper, C., Stenmark, J., McCloskey, E.V., Jönsson, B., and Kanis, J.A. Osteoporosis in the european union: a compendium of country-specific reports. *Archives of Osteoporosis*, 2013. **8**(1-2):137. doi: 10.1007/s11657-013-0137-0. 6

[30] Wesseling, K., Bakkaloglu, S., and Salusky, I. Chronic kidney disease mineral and bone disorder in children. *Pediatric Nephrology*, 2008. **23**(2):195–207. doi:10.1007/s00467-007-0671-3. 6

[31] Shrivats, A.R., McDermott, M.C., and Hollinger, J.O. Bone tissue engineering: state of the union. *Drug Discovery Today*, 2014. doi:10.1016/j.drudis.2014.04.010. 7, 10, 11

[32] Polo-Corrales, L., Latorre-Esteves, M., and Ramirez-Vick, J.E. Scaffold design for bone regeneration. *Journal of nanoscience and nanotechnology*, 2014. **14**(1):15–56. 7, 8, 10, 11

[33] Giannoudis, P.V., Dinopoulos, H., and Tsiridis, E. Bone substitutes: an update. *Injury-international Journal Of The Care Of The Injured*, 2005. **36 Suppl 3**:S20–7. doi:10.1016/j.injury.2005.07.029. 7

[34] Costa-Pinto, A.R., Reis, R.L., and Neves, N.M. Scaffolds based bone tissue engineering: the role of chitosan. *Tissue Eng Part B Reviews*, 2011. **17**(5):331–47. doi:10.1089/ten.teb.2010.0704. 7, 8, 10

[35] Grabowski, G. and Cornett, C.A. Bone graft and bone graft substitutes in spine surgery: current concepts and controversies. *The Journal of the American Academy of Orthopaedic Surgeons*, 2013. **21**(1):51–60. doi:10.5435/JAAOS-21-01-51. 7

[36] Frohlich, M., Grayson, W., Wan, L., Marolt, D., Drobnic, M., and Vunjak-Novakovic, G. Tissue engineered bone grafts: Biological requirements, tissue culture and clinical relevance. *Current Stem Cell Research & Therapy*, 2008. **3**(4):254. doi:10.2174/157488808786733962. 8, 9, 10, 11

[37] Malda, J., Visser, J., Melchels, F.P., Jüngst, T., Hennink, W.E., Dhert, W.J.A., Groll, J., and Hutmacher, D.W. 25th anniversary article: Engineering hydrogels for biofabrication. *Advanced Materials*, 2013. **25**(36):5011–28. doi:10.1002/adma.201302042. 8, 12

[38] O'Brien, F.J. Biomaterials & scaffolds for tissue engineering. *Materials Today*, 2011. **14**(3):88. doi:10.1016/S1369-7021(11)70058-X. 8, 9, 10, 11, 12, 21

[39] Bose, S., Roy, M., and Bandyopadhyay, A. Recent advances in bone tissue engineering scaffolds. *Trends in Biotechnology*, 2012. **30**(10):546–54. doi:10.1016/j.tibtech.2012.07.005. 8, 9, 10, 11

[40] Ma, P.X. Biomimetic materials for tissue engineering. *Advanced Drug Delivery Reviews*, 2008. **60**(2):184–98. doi:10.1016/j.addr.2007.08.041. 8, 10

[41] Rezwan, K., Chen, Q.Z., Blaker, J.J., and Boccaccini, A.R. Biodegradable and bioactive porous polymer/inorganic composite scaffolds for bone tissue engineering. *Biomaterials*, 2006. **27**(18):3413–31. doi:10.1016/j.biomaterials.2006.01.039. 8, 9, 10, 21

[42] Woodard, J.R., Hilldore, A.J., Lan, S.K., Park, C.J., Morgan, A.W., Eurell, J.A.C., Clark, S.G., Wheeler, M.B., Jamison, R.D., and Wagoner Johnson, A.J. The mechanical properties and osteoconductivity of hydroxyapatite bone scaffolds with multi-scale porosity. *Biomaterials*, 2007. **28**(1):45–54. doi:10.1016/j.biomaterials.2006.08.021. 9

[43] Holzapfel, B.M., Reichert, J.C., Schantz, J.T., Gbureck, U., Rackwitz, L., Nöth, U., Jakob, F., Rudert, M., Groll, J., and Hutmacher, D.W. How smart do biomaterials need to be? a translational science and clinical point of view. *Advanced Drug Delivery Reviews*, 2013. **65**(4):581–603. doi:10.1016/j.addr.2012.07.009. 9, 10, 11

[44] Hench, L.L. and Polak, J.M. Third-generation biomedical materials. *Science*, 2002. **295**(5557):1014–7. doi:10.1126/science.1067404. 9, 10

[45] Amini, A.R., Laurencin, C.T., and Nukavarapu, S.P. Bone tissue engineering: recent advances and challenges. *Critical Reviews in Biomedical Engineering*, 2012. **40**(5):363–408. 10

[46] Kim, H.K., Shim, W.S., Kim, S.E., Lee, K.H., Kang, E., Kim, J.H., Kim, K., Kwon, I.C., and Lee, D.S. Injectable in situ-forming ph/thermo-sensitive hydrogel for bone tissue engineering. *Tissue Engineering Part A*, 2009. **15**(4):923–33. doi:10.1089/ten.tea.2007.0407.

[47] Williams, C.G., Kim, T.K., Taboas, A., Malik, A., Manson, P., and Elisseeff, J. In vitro chondrogenesis of bone marrow-derived mesenchymal stem cells in a photopolymerizing hydrogel. *Tissue Engineering*, 2003. **9**(4):679–88. doi:10.1089/107632703768247377. 10

[48] Schieker, M., Seitz, H., Drosse, I., Seitz, S., and Mutschler, W. Biomaterials as scaffold for bone tissue engineering. *European Journal of Trauma*, 2006. **32**(2):114. doi:10.1007/s00068-006-6047-8. 10, 21

[49] Choi, D. and Kumta, P.N. Mechano-chemical synthesis and characterization of nanostructured ß-tcp powder. *Materials Science and Engineering: C*, 2007. **27**(3):377. doi:10.1016/j.msec.2006.05.035. 10, 25

[50] Karageorgiou, V. and Kaplan, D. Porosity of 3d biomaterial scaffolds and osteogenesis. *Biomaterials*, 2005. **26**(27):5474–91. doi:10.1016/j.biomaterials.2005.02.002. 10, 11

[51] Lee, H. and Kim, G. Three-dimensional plotted pcl/ß-tcp scaffolds coated with a collagen layer: preparation, physical properties and in vitro evaluation for bone tissue regeneration. *Journal of Materials Chemistry*, 2011. **21**(17):6305. doi:10.1039/c0jm03414b. 10

[52] Valente, J.F.A., Valente, T.A.M., Alves, P., Ferreira, P., Silva, A., and Correia, I.J. Alginate based scaffolds for bone tissue engineering. *Materials Science & Engineering C-Materials For Biological Applications*, 2012. **32**(8):2596–2603. doi:10.1016/j.msec.2012.08.001. 11, 17, 27

[53] Andersen, T., Strand, B.L., Formo, K., Alsberg, E., and Christensen, B.E. *Carbohydrate Chemistry: Volume 37*, volume 37, chapter 9. Alginates as biomaterials in tissue engineering, p. 227. The Royal Society of Chemistry. ISBN 978-1-84973-154-6, 2011. doi:10.1039/9781849732765-00227. 11, 15, 21, 29

[54] Augst, A.D., Kong, H.J., and Mooney, D.J. Alginate hydrogels as biomaterials. *Macromolecular Bioscience*, 2006. **6**(8):623–33. doi:10.1002/mabi.200600069. 11, 21

[55] Narayanan, R.P., Melman, G., Letourneau, N.J., Mendelson, N.L., and Melman, A. Photodegradable iron(iii) cross-linked alginate gels. *Biomacromolecules*, 2012. **13**(8):2465–71. doi:10.1021/bm300707a. 11

[56] Cai, K., Rechtenbach, A., Hao, J., Bossert, J., and Jandt, K.D. Polysaccharide-protein surface modification of titanium via a layer-by-layer technique: characterization and cell behaviour aspects. *Biomaterials*, 2005. **26**(30):5960–71. doi:10.1016/j.biomaterials.2005.03.020. 11

[57] Martínez-Vázquez, F.J., Perera, F.H., Miranda, P., Pajares, A., and Guiberteau, F. Improving the compressive strength of bioceramic robocast scaffolds by polymer infiltration. *Acta Biomaterialia*, 2010. **6**(11):4361–8. doi:10.1016/j.actbio.2010.05.024. 11, 12

[58] Suh, S.W., Shin, J.Y., Kim, J., Kim, J., Beak, C.H., Kim, D.I., Kim, H., Jeon, S.S., and Choo, I.W. Effect of different particles on cell proliferation in polymer scaffolds using a solvent-casting and particulate leaching technique. *ASAIO Journal*, 2002. **48**(5). 12

[59] Sin, D., Miao, X., Liu, G., Wei, F., Chadwick, G., Yan, C., and Friis, T. Polyurethane (pu) scaffolds prepared by solvent casting/particulate leaching (scpl) combined with centrifugation. *Materials Science and Engineering: C*, 2010. **30**(1):78. doi:10.1016/j.msec.2009.09.002. 12

[60] Duarte, A.R.C., Mano, J.F., and Reis, R.L. Dexamethasone-loaded scaffolds prepared by supercritical-assisted phase inversion. *Acta Biomaterialia*, 2009. **5**(6):2054–62. doi:10.1016/j.actbio.2009.01.047. 12

[61] Tsivintzelis, I., Pavlidou, E., and Panayiotou, C. Porous scaffolds prepared by phase inversion using supercritical co2 as antisolvent. *The Journal of Supercritical Fluids*, 2007. **40**(2):317. doi:10.1016/j.supflu.2006.06.001. 12

[62] Mikos, A.G., Bao, Y., Cima, L.G., Ingber, D.E., Vacanti, J.P., and Langer, R. Preparation of poly(glycolic acid) bonded fiber structures for cell attachment and transplantation. *Journal of Biomedical Materials Research*, 1993. **27**(2):183–9. doi:10.1002/jbm.820270207. 12

[63] Tuzlakoglu, K., Bolgen, N., Salgado, A.J., Gomes, M.E., Piskin, E., and Reis, R.L. Nano- and micro-fiber combined scaffolds: a new architecture for bone tissue engineering. *Journal of materials science. Materials in medicine*, 2005. **16**(12):1099–104. doi:10.1007/s10856-005-4713-8. 12

[64] Gomes, M., Ribeiro, A., Malafaya, P., Reis, R., and Cunha, A. A new approach based on injection moulding to produce biodegradable starch-based polymeric scaffolds: morphology, mechanical and degradation behaviour. *Biomaterials*, 2001. **22**(9):883. doi:10.1016/S0142-9612(00)00211-8. 12

[65] Mondrinos, M.J., Dembzynski, R., Lu, L., Byrapogu, V.K.C., Wootton, D.M., Lelkes, P.I., and Zhou, J. Porogen-based solid freeform fabrication of polycaprolactone-calcium phosphate scaffolds for tissue engineering. *Biomaterials*, 2006. **27**(25):4399–408. doi:10.1016/j.biomaterials.2006.03.049. 12

[66] Deville, S., Saiz, E., and Tomsia, A.P. Freeze casting of hydroxyapatite scaffolds for bone tissue engineering. *Biomaterials*, 2006. **27**(32):5480–9. doi:10.1016/j.biomaterials.2006.06.028. 12

[67] Kim, H.W., Knowles, J.C., and Kim, H.E. Hydroxyapatite and gelatin composite foams processed via novel freeze-drying and crosslinking for use as temporary hard tissue scaffolds. *Journal Of Biomedical Materials Research Part A*, 2005. **72**(2):136–45. doi:10.1002/jbm.a.30168. 12

[68] Fedorovich, N.E., Schuurman, W., Wijnberg, H.M., Prins, H.J., van Weeren, P.R., Malda, J., Alblas, J., and Dhert, W.J.A. Biofabrication of osteochondral tissue equivalents by printing topologically defined, cell-laden hydrogel scaffolds. *Tissue Eng Part C Methods*, 2012. **18**(1):33–44. doi:10.1089/ten.TEC.2011.0060. 12

[69] Hockaday, L.A., Kang, K.H., Colangelo, N.W., Cheung, P.Y.C., Duan, B., Malone, E., Wu, J., Girardi, L.N., Bonassar, L.J., Lipson, H., Chu, C.C., and Butcher, J.T. Rapid 3d printing of anatomically accurate and mechanically heterogeneous aortic valve hydrogel scaffolds. *Biofabrication*, 2012. **4**(3):035005. doi:10.1088/1758-5082/4/3/035005. 12

[70] Santos, C.F., Silva, A.P., Lopes, L., Pires, I., and Correia, I.J. Design and production of sintered ß-tricalcium phosphate 3d scaffolds for bone tissue regeneration. *Materials Science and Engineering: C*, 2012. **32**(5):1293. doi:10.1016/j.msec.2012.04.010. 12, 16, 24, 25, 28

[71] Yeong, W.Y., Chua, C.K., Leong, K.F., and Chandrasekaran, M. Rapid prototyping in tissue engineering: challenges and potential. *Trends in Biotechnology*, 2004. **22**(12):643–52. doi:10.1016/j.tibtech.2004.10.004. 12

[72] Landers, R., Hübner, U., Schmelzeisen, R., and Mülhaupt, R. Rapid prototyping of scaffolds derived from thermoreversible hydrogels and tailored for applications in tissue engineering. *Biomaterials*, 2002. **23**(23):4437. doi:10.1016/S0142-9612(02)00139-4. 12

[73] Butscher, A., Bohner, M., Doebelin, N., Hofmann, S., and Müller, R. New depowdering-friendly designs for three-dimensional printing of calcium phosphate bone substitutes. *Acta Biomaterialia*, 2013. **9**(11):9149–58. doi:10.1016/j.actbio.2013.07.019. 12

[74] Stevens, B., Yang, Y., Mohandas, A., Stucker, B., and Nguyen, K.T. A review of materials, fabrication methods, and strategies used to enhance bone regeneration in engineered bone tissues. *Journal of Biomedical Materials Research Part B: Applied Biomaterials*, 2008. **85**(2):573–82. doi:10.1002/jbm.b.30962. 12

[75] Malone, E. and Lipson, H. Fab@home: the personal desktop fabricator kit. *Rapid Prototyping Journal*, 2007. **13**(4):245. doi:10.1108/13552540710776197. 12, 13, 15

[76] Cohen, D.L., Lipton, J.I., Bonassar, L.J., and Lipson, H. Additive manufacturing for in situ repair of osteochondral defects. *Biofabrication*, 2010. **2**(3):035004. doi:10.1088/1758-5082/2/3/035004. 12

[77] Diogo, G.S., Gaspar, V.M., Serra, I.R., Fradique, R., and Correia, I.J. Manufacture of ß-tcp/alginate scaffolds through a fab@home model for application in bone tissue engineering. *Biofabrication*, 2014. **6**(2):025001. doi:10.1088/1758-5082/6/2/025001. 12, 16, 18, 21, 25, 28, 30

[78] Kang, K.H., Hockaday, L.A., and Butcher, J.T. Quantitative optimization of solid freeform deposition of aqueous hydrogels. *Biofabrication*, 2013. **5**(3):035001. doi:10.1088/1758-5082/5/3/035001. 13

[79] Yang, F., Xia, S., Tan, C., and Zhang, X. Preparation and evaluation of chitosan-calcium-gellan gum beads for controlled release of protein. *European Food Research And Technology*, 2013. **237**:467–479. doi:10.1007/s00217-013-2021-y. 16

[80] Torres, A.L., Gaspar, V.M., Serra, I.R., Diogo, G.S., Fradique, R., Silva, A.P., and Correia, I.J. Bioactive polymeric-ceramic hybrid 3d scaffold for application in bone tissue regeneration. *Materials Science and Engineering: C, Materials for Biological Applications*, 2013. **33**(7):4460–9. doi:10.1016/j.msec.2013.07.003. 17

[81] Jiankang, H., Dichen, L., Yaxiong, L., Bo, Y., Bingheng, L., and Qin, L. Fabrication and characterization of chitosan/gelatin porous scaffolds with predefined internal microstructures. *Polymer*, 2007. **48**(15):4578. doi:10.1016/j.polymer.2007.05.048. 17

[82] Jeong, S.I., Jeon, O., Krebs, M.D., Hill, M.C., and Alsberg, E. Biodegradable photocrosslinked alginate nanofibre scaffolds with tuneable physical properties, cell adhesivity and growth factor release. *European cells & materials*, 2012. **24**:331–43. 18

[83] Freed, L.E., Vunjak-Novakovic, G., Biron, R.J., Eagles, D.B., Lesnoy, D.C., Barlow, S.K., and Langer, R. Biodegradable polymer scaffolds for tissue engineering. *Bio/Technology*, 1994. **12**(7):689. doi:10.1038/nbt0794-689. 18

[84] Lee, J.T.Y. and Chow, K.L. Sem sample preparation for cells on 3d scaffolds by freeze-drying and hmds. *Scanning*, 2012. **34**(1):12–25. doi:10.1002/sca.20271. 19

[85] Lawson, M.A., Barralet, J.E., Wang, L., Shelton, R.M., and Triffitt, J.T. Adhesion and growth of bone marrow stromal cells on modified alginate hydrogels. *Tissue Engineering*, 2004. **10**(9-10):1480–91. doi:10.1089/ten.2004.10.1480. 21

[86] Dittrich, R., Tomandl, G., Despang, F., Bernhardt, A., Hanke, T., Pompe, W., and Gelinsky, M. Scaffolds for hard tissue engineering by ionotropic gelation of alginate?influence of selected preparation parameters. *Journal of the American Ceramic Society*, 2007. **90**(6):1703. doi:10.1111/j.1551-2916.2007.01598.x. 22

[87] Rassis, D., Saguy, I., and Nussinovitch, A. Collapse, shrinkage and structural changes in dried alginate gels containing fillers. *Food Hydrocolloids*, 2002. **16**(2):139. doi:10.1016/S0268-005X(01)00071-6. 22

[88] Gardin, C., Chiara, G., Ferroni, L., Letizia, F., Favero, L., Lorenzo, F., Stellini, E., Edoardo, S., Stomaci, D., Diego, S., Sivolella, S., Stefano, S., Bressan, E., Eriberto, B., Zavan, B., and Barbara, Z. Nanostructured biomaterials for tissue engineered bone tissue reconstruction. *International Journal Of Molecular Sciences*, 2012. **13**(1):737–57. doi:10.3390/ijms13010737. 23

[89] Lawrie, G., Keen, I., Drew, B., Chandler-Temple, A., Rintoul, L., Fredericks, P., and Grøndahl, L. Interactions between alginate and chitosan biopolymers characterized using ftir and xps. *Biomacromolecules*, 2007. **8**(8):2533–41. doi:10.1021/bm070014y. 24

[90] Daemi, H. and Barikani, M. Synthesis and characterization of calcium alginate nanoparticles, sodium homopolymannuronate salt and its calcium nanoparticles. *Scientia Iranica*, 2012. **19**(6):2023. doi:10.1016/j.scient.2012.10.005. 24

[91] Mansur, H.S., Sadahira, C.M., Souza, A.N., and Mansur, A.A. Ftir spectroscopy characterization of poly (vinyl alcohol) hydrogel with different hydrolysis degree and chemically crosslinked with glutaraldehyde. *Materials Science and Engineering: C*, 2008. **28**(4):539. doi:10.1016/j.msec.2007.10.088. 25

[92] Mansur, H.S. and Costa, H.S. Nanostructured poly(vinyl alcohol)/bioactive glass and poly(vinyl alcohol)/chitosan/bioactive glass hybrid scaffolds for biomedical applications. *Chemical Engineering Journal*, 2008. **137**(1):72. doi:10.1016/j.cej.2007.09.036. 26

[93] Wei, G. and Ma, P.X. Structure and properties of nano-hydroxyapatite/polymer composite scaffolds for bone tissue engineering. *Biomaterials*, 2004. **25**(19):4749–57. doi:10.1016/j.biomaterials.2003.12.005. 26, 27

[94] Román, J., Cabañas, M.V., Peña, J., Doadrio, J.C., and Vallet-Regí, M. An optimized beta-tricalcium phosphate and agarose scaffold fabrication technique. *Journal Of Biomedical Materials Research Part A*, 2008. **84**(1):99–107. doi:10.1002/jbm.a.31394. 27

[95] Islam, M.S. and Karim, M.R. Fabrication and characterization of poly(vinyl alcohol)/alginate blend nanofibers by electrospinning method. *Colloids and Surfaces A: Physicochemical and Engineering Aspects*, 2010. **366**(1-3):135. doi:10.1016/j.colsurfa.2010.05.038. 27

[96] Chhatri, A., Bajpai, J., Bajpai, A., Sandhu, S., Jain, N., and Biswas, J. Cryogenic fabrication of savlon loaded macroporous blends of alginate and polyvinyl alcohol (pva). swelling, deswelling and antibacterial behaviors. *Carbohydrate Polymers*, 2011. **83**(2):876. doi:10.1016/j.carbpol.2010.08.077. 28

[97] Weinand, C., Pomerantseva, I., Neville, C.M., Gupta, R., Weinberg, E., Madisch, I., Shapiro, F., Abukawa, H., Troulis, M.J., and Vacanti, J.P. Hydrogel-beta-tcp scaffolds and stem cells for tissue engineering bone. *Bone*, 2006. **38**(4):555–63. doi:10.1016/j.bone.2005.10.016. 29

[98] Hu, Y., Wang, J., Xing, W., Cao, L., and Liu, C. Surface-modified pliable pdlla/pcl/ß-tcp scaffolds as a promising delivery system for bone regeneration. *Journal of Applied Polymer Science*, 2014. **131**(20):n/a. doi:10.1002/app.40951. 30

[99] Yin, Y., Ye, F., Cui, J., Zhang, F., Li, X., and Yao, K. Preparation and characterization of macroporous chitosan-gelatin/beta-tricalcium phosphate composite scaffolds for bone tissue engineering. *Journal Of Biomedical Materials Research Part A*, 2003. **67**(3):844–55. doi:10.1002/jbm.a.10153. 33

Appendix

- Diogo G. S., Gaspar V. M., Serra I.R., Fradique R., Correia I.J.; Manufacture of ß-TCP/alginate scaffolds through a Fab@home model for application in bone tissue engineering. Biofabrication, 2014. 6(2):025001. doi:10.1088/1758-5082/6/2/025001

- Torres,A. L., Gaspar, V. M., Serra, I. R., Diogo, G. S., Fradique, R., Silva, A. P., Correia, I. J.; Bioactive Polymeric-Ceramic Hybrid 3D Scaffold for Application in Bone Tissue Regeneration. Materials Science and Engineering: C, Materials for Biological Applications, 2013. 33(7):4460–9. doi:10.1016/j.msec.2013.07.003

IOP Publishing Biofabrication
Biofabrication 6 (2014) 025001 (12pp) doi:10.1088/1758-5082/6/2/025001

Manufacture of β-TCP/alginate scaffolds through a Fab@home model for application in bone tissue engineering

G S Diogo, V M Gaspar, I R Serra, R Fradique and I J Correia

CICS-UBI—Health Sciences Research Centre, University of Beira Interior, Av. Infante D Henrique, 6200-506 Covilhã, Portugal

E-mail: icorreia@ubi.pt

Received 3 August 2013, revised 21 November 2013
Accepted for publication 27 November 2013
Published 21 March 2014

Abstract

The growing need to treat bone-related diseases in an elderly population compels the development of novel bone substitutes to improve patient quality of life. In this context, the advent of affordable and effective rapid prototyping equipment, such as the Fab@home plotter, has contributed to the development of novel scaffolds for bone tissue engineering. In this study, we report for the first time the use of a Fab@home plotter for the production of 3D scaffolds composed by beta-tricalcium phosphate (β-TCP)/alginate hybrid materials. β-TCP/alginate mixtures were used in a proportion of 50/50% (w/w), 30/70% (w/w) and 20/80% (w/w). The printing parameters were optimized to a nozzle diameter of 20 Gauge for the production of rigid scaffolds with pre-defined architectures. We observed that, despite using similar printing parameters, both the precision and resolution of the scaffolds were significantly affected by the blend's viscosity. In particular, we demonstrate that the higher viscosity of 50/50 scaffolds (150.0 ± 3.91 mPa s) provides a higher precision in the extrusion process. The physicochemical and biological characterization of the samples demonstrated that the 50/50 scaffolds possessed a resistance to compression comparable to that of native trabecular bone. Moreover, this particular formulation also exhibited a Young's modulus that was higher than that of trabecular bone. Scanning electron microscopy and fluorescence microscopy analysis revealed that osteoblasts were able to adhere, proliferate and also penetrate into the scaffold's architecture. Altogether, our findings suggest that the Fab@home printer can be employed in the manufacture of reproducible scaffolds, using a formulation 50/50 alginate-β-TCP that has suitable properties to be applied as bone substitutes in the future.

Keywords: rapid prototyping, bone tissue engineering, biopolymers, 3D plotter, hybrid materials

(Some figures may appear in colour only in the online journal)

1. Introduction

The rising number of bone defects in the last few decades has become a world-wide healthcare problem [1]. It is estimated that each year 2.2 million people around the world are subjected to bone grafting procedures [2]. Bone tissue engineering (BTE) has emerged as a promising solution to repair these damaged or aged bony tissues [3].

Currently, rapid prototyping (RP) technologies are gaining ever growing attention since patient-specific 3D scaffolds can be manufactured for bone tissue regeneration. This unique technique can overcome some of the limitations of conventional fabrication methods, such as solvent casting and particulate leaching, which use highly toxic solvents to produce 3D constructs with limited mechanical properties [4–6]. In addition, by using RP it is possible to have better control of porosity and pore size than in traditional methods such as fiber mesh, fiber bonding and melt molding. Another advantage of RP technology is the possibility to manufacture, on a large scale, scaffolds with reproducibility,

which differs from techniques such as phase separation which only allow a limited production [7]. These characteristics thus render RP an attractive alternative method to be used for scaffold production [4]. Furthermore, RP technologies, when combined with imaging techniques, such as computerized tomography (CT) or magnetic resonance imaging (MRI), allow the creation of an accurate 3D anatomic model of a specific bone tissue from a particular patient [3, 8, 9]. In fact, by segmenting a region of interest obtained in CT images, it is possible to visualize the skeleton architecture and then print a real model with a 3D plotter [3, 9]. This unique potential has prompted the use of RP in tissue engineering applications. The success of a 3D scaffold designed to be used in biomedical applications depends on several parameters, such as: (i) biocompatibility, (ii) biodegradability, (iii) surface characteristics, (iv) porosity, and (v) mechanical properties, in order to induce osteoinductivity and osteocondutivity of bone-progenitor cells and also allow neovascularization [1]. Such properties are dependent on the material chosen for scaffold manufacture and also on the technique used for its production.

Fab@home is an open source 3D printer developed by Lipson and collaborators in 2006 and it is one of the newest printers used for the manufacture of 3D structures [10]. This system provides a universal platform for 3D fabrication and has advantages over other equipment since it allows for the production of structures composed of various materials, such as plastics, polymer composites, ceramics and viscous solutions (like hydrogels). It also has a high degree of structural control, including pore size optimization [11]. Moreover, this new RP system is relatively simple to assemble and is inexpensive, it promotes the production of structures in a very short period of time with high reproducibility, and it ensures the creation of uniform and biologically optimal scaffolds, potentially becoming a commercially viable method of scaffold production [12].

In order to further improve and accelerate bone regeneration, scaffolds must be produced with non-toxic materials that do not elicit host immune responses [13]. Beta-tricalcium phosphate (β-TCP) is an interesting ceramic material that has been proposed to be applied in bone tissue regeneration due to its biodegradability, biocompatibility and osteocondutivity, which in turn contributes to bone formation through the induction of osteoblast differentiation [13, 14]. However, β-TCP also has some limitations, such as relative brittleness and poor resistance to fatigue [13, 15].

The combination of β-TCP with natural biopolymers like alginate can provide 3D structures with good bioactivity, adequate mechanical properties and stability [13]. Alginate is a biocompatible natural polysaccharide extracted from brown seaweeds [16, 17]. This polymer is composed of 1,4-linked β-D-mannuronic acid (M) and α-L-guluronic acid (G) residues and has the capacity to crosslink with divalent cations [16]. Previous studies have reported the successful application of alginate for BTE [16, 18].

In this study, 3D hybrid scaffolds were manufactured by RP through the use of a Fab@home printer. After optimization of the extrusion parameters, the produced scaffolds comprised a hybrid mixture of β-TCP-alginate, and presented suitable biological and mechanical properties to be applied in bone tissue regeneration.

2. Materials and methods

2.1. Preparation of β-TCP/alginate composite scaffolds by rapid prototyping

Bioactive 3D scaffolds were produced by RP. The Fab@home printing model was used for scaffold production, since it allows for the fabrication of low-cost 3D models in a short period of time and with suitable properties to become affordable commercial products in the near future.

Herein, three different types of scaffolds were produced by varying the ratios of β-TCP and alginate concentrations. β-TCP/alginate scaffolds were produced using solutions prepared with β-TCP and alginate in a proportion of 50/50% (w/w), 30/70% (w/w) and 20/80% (w/w), respectively. Initially alginate (Sigma-Aldrich, Sintra, Portugal) (Molecular weight (Mw): 120.000–190.000 Da) and β-TCP (Panreac® Barcelona, Spain) solutions were prepared. Double deionized and filtered water (milli-Q-water) was obtained using a Milli-Q Advantage A10 ultrapure Water Purification System (resistivity = 18.2 MΩ cm at 25 °C and total organic carbon (TOC): <5 parts per billion; 0.22 μm filter) [19]. Briefly, alginate was dissolved in milli-Q water at 12% (w/v) and the solution was left overnight under magnetic stirring. Subsequently, it was sonicated for 15 min (min) in order to allow for its homogenization. Then, β-TCP powder was weighed in different amounts (w/w) and added to the alginate solution. Afterwards, poly(vinyl) Alcohol (PVA) (Sigma-Aldrich) (β-TCP binder agent) was added to the polymer-bioceramic mixture in a PVA:β-TCP mass ratio of 1:10.

After the dissolution of all components, a 1% $CaCl_2$ (Sigma-Aldrich) solution was added to the polymer-bioceramic mixture in a $CaCl_2$:alginate volume ratio of 1:2. This is an important step since $CaCl_2$ crosslinks the alginate polymer chains, increasing the solution's viscosity and thus allowing better control of the extrusion process for scaffold production. The mixture's viscosities were measured by a Brookfield® DV-I Prime viscometer (3 rpm, LV-4 spindle) according to the manufacturer's instructions.

Finally, a syringe (10 cc Luer Lock) was filled with the solution for posterior extrusion. The scaffolds were then immersed in a 5% (w/v) $CaCl_2$ solution and incubated for 24 h at room temperature (RT). The cross-linked scaffolds were then frozen at −80 °C and subsequently freeze-dried for 24 h.

2.2. Optimization of 3D printing parameters

To optimize the printing parameters, 3D constructs with a rectangular shape were extruded to make a proof of concept. These structures were drawn in CAD/CAM Software (Solidworks® Premium 2011), which allows the design of 3D models with a given architecture. To initialize the scaffold's printing process, the files were converted and stored in the STL format [20]. A layer-by-layer fabrication process was used

Table 1. Printing parameters used in the Fab@home printer.

Parameters	Values
Path width (mm)	1.000
Path height (mm)	0.800
Pushout (s)	0.009
Suckback (s)	0.002
Deposition rate (mm syringe plunger motion/path length)	0.001
Path speed (mm s^{-1})	10.000
Nozzle diameter (*G*)	20.000

to produce the 3D model, with the use of Fab@home v0.23 software. During the optimization of the extrusion process, several printing parameters were tested, as previously reported by Kang and collaborators [21]. The optimized extrusion parameters are exhibited in table 1.

2.3. Fourier transform infrared spectroscopy analysis

Fourier-transform infrared (FTIR) spectroscopy was used to evaluate the physicochemical characteristics of the scaffold's materials [22]. FTIR spectra represent the average of 128 scans obtained with a spectral range between 500 and 4000 cm^{-1}, at a resolution of 4 cm^{-1}. For FTIR analysis, all of the samples were crushed and the resulting powders were placed in contact with a diamond window and the spectra were recorded on a FTIR spectrophotometer (Nicolet iS10) (Thermo Scientific, Waltham, USA). This technique was used to examine the scaffold's composition after the manufacturing process in order to confirm the presence of β-TCP and alginate in the produced scaffold.

2.4. X-ray diffraction analysis

To evaluate the characteristic phases and crystallinity of the materials that comprise the scaffolds after the production process, x-ray diffraction measurements were performed with a diffractometer (Rigaku Americas Corporation, USA). Briefly, samples were mounted in appropriate silica supports and the data were recorded over a range of 5° to 90° $2\theta^{\circ}$, with continuous scans at a rate of 1° min^{-1} with a copper ray tube operated at 30 kV and 20 mA [23].

2.5. Energy dispersive spectroscopy analysis

In order to perform the elementary characterization of the materials or, in this specific case, to evaluate the presence of calcium and phosphorus ions in the scaffold, an energy-dispersive spectroscopy (EDS) (Rontec) analysis was carried out. The samples were placed on an aluminum stub support, air-dried at RT and sputter-coated with gold [23].

2.6. Mechanical characterization of the β-TCP/alginate composite scaffolds: resistance to compression and Young's modulus

In order to study the mechanical behavior of the scaffold, compression assays were performed through an adaptation of the method previously described by Santos and collaborators, 2012 [3]. In brief, lyophilized scaffolds were cut into fragments with similar dimensions. The compression assays were performed using a Zwick® 1435 Material Prüfung (Ulm, Germany) with a crosshead speed of 0.2 mm min^{-1} and a load cell of 5 kN. Three samples from each scaffold formulation were tested and measurements were acquired in order to calculate their area. The compressive strength (Cs) of each scaffold was determined through the following equation [24],

$$Cs = \frac{F}{a \times l} \tag{1}$$

where F corresponds to the load at the time of fracture and a and l are the width and length of the scaffold, respectively. Young's modulus (YM) was obtained from the stress–strain relations calculated by applying the equation [25],

$$YM = \frac{Cs}{Hd} \tag{2}$$

where Hd is the scaffold height deformation and Cs is the scaffold compressive strength, which is determined as described above. Average values and standard deviations (s.d.) were determined for each sample ($n = 3$).

2.7. Contact angle measurements

The determination of the contact angle of the scaffold was performed by using the sessile drop technique, with water as a reference fluid. The method used was adapted from that described by Correia and collaborators [26]. The contact angle data were acquired in a Data Physics Contact Angle System OCAH 200 apparatus, operating in static mode at RT. For each sample, water drops were placed at various locations of the analyzed scaffold.

2.8. Porosity evaluation

The total porosity (P) of the scaffolds was determined by using a method adapted from Nie and collaborators, 2007 [27]. The total amount of absolute ethanol (EtOH) that the scaffolds were able to absorb in 48 h was determined by applying the following equation from Torres and collaborators [13]:

$$P(\%) = \frac{w2 - w1}{d_{\text{ethanol}} \times V_{\text{scaffold}}} \times 100 \tag{3}$$

where $W1$ and $W2$ are the weight of the dry and the wet scaffold, respectively, d_{ethanol} is the density of the ethanol at RT and V_{scaffold} is the volume of the wet scaffold, which is directly determined by immersion. For each scaffold, three replicates were analyzed and the data represent the average of each replicate.

2.9. Biological characterization of the β-TCP/alginate composite scaffolds

2.9.1. Cell culture in the presence of β-TCP/alginate scaffolds. Human osteoblasts (CRL-11372), purchased from the American Type Culture Collection (ATCC), were cultured in Dulbecco's modified Eagle medium (DMEM-F12) (Sigma-Aldrich), containing 10% heat inactivated fetal

bovine serum (FBS) (Biochrom AG), streptomycin (Sigma-Aldrich) (100 μg mL^{-1}) and gentamicin (Sigma-Aldrich) (100 μg mL^{-1}), in 75 cm^2 T-flasks (Orange Scientific). Cultures were maintained in a humidified environment at 37 °C, with 5% CO_2, until confluence was attained. The cells were then trypsinized with 0.18% trypsin (1:250) and 5 mM EDTA (Sigma-Aldrich), centrifuged at 260 rpm for 5 min and the resulting pellet was resuspended into 5 mL of complete culture medium. Prior to cell seeding, the scaffolds were cut into the desired size (10% of the well) and placed into 96-well plates for sterilization. Briefly, the scaffolds were initially sterilized in a 70% EtOH solution and then extensively washed with DMEM-F12 medium. This procedure was followed by sterilization by ultraviolet (UV) light for another 30 min. Prior to contact with the osteoblasts, the scaffolds were equilibrated with complete culture medium at 37 °C for 24 h. Then, the cells were seeded onto the scaffold's surface at a density of 10 $\times$ 10^3 cells per well in order to characterize scaffold cytotoxicity after one and seven days. The culture medium was changed every two days during the experiments.

2.9.2. Scanning electron microscopy analysis. The scaffold's morphology, pore size and cellular attachment in the presence of the scaffold were characterized by scanning electron microscopy (SEM) [13]. Samples were washed at RT with cacodylate buffer solution and fixed for 30 min with 2.5% (v/v) glutharaldehyde in 0.1 M sodium cacodylate. The samples were then washed three times with cacodylate buffer and finally incubated for 10 min in a graded series of ethanol solutions (50, 60, 70, 80, 90 and 99.9%) for dehydration. The scaffolds were then stored in absolute ethanol, at 4 °C, until being subjected to CO_2 critical point drying. Afterward, the samples were mounted onto aluminum stubs with Araldite glue and then sputter-coated with gold using an Emitech K550 sputter coater. SEM images were obtained with a Hitachi S-2700 (Tokyo, Japan) scanning electron microscope with an acceleration voltage of 20 kV, at variable magnifications.

2.9.3. Evaluation of the scaffold's cytotoxic profile. To evaluate the cytotoxic profile of the 3D scaffolds, human osteoblast (CRL-11372) cells were seeded in the presence of the materials in 96-well plates at a density of 10 $\times$ 10^3 cells per well. An 3-(4,5-dimethylthiazol-2-yl)-5-(3 carboxymethoxyphenyl) 2-(4-sulphofenyl)-2H-tetrazolium, inner salt (MTS) assay, supplied by Promega, was used to evaluate cell viability after one and seven days of the cells being seeded. After an incubation of 24 h, the metabolic activity of the cells was evaluated by quantifying the metabolic reduction of tetrazolium salt into soluble formazan [28]. Briefly, the medium of each well was removed and the cells in contact with the scaffold were incubated with a mixture of 100 μL of fresh culture medium and 20 μL of MTS/PMS solution, for 4 h at 37 °C. After incubation, the supernatant was transferred into a 96-well microplate and the fluorescence intensity was measured at 492 nm using a microplate reader (Anthos 2010, Alfagene ®).

Five replicates of each sample were used for each experimental condition. Cells cultured without materials were used as negative controls for cytotoxicity (K−)) and cells treated with EtOH (96%) were used as a positive control for cytotoxicity (K+).

2.9.4. Confocal microscopy analysis. The analysis of the distribution of osteoblasts within 3D scaffolds was visualized by confocal laser scanning microscopy (CLSM). Briefly, four days after cell seeding, the culture medium was removed and the cells were washed three times with cacodylate buffer at RT. The remaining cells were then fixed with cacodylate buffer for 30 min at RT. Afterwards, the cell nucleus was labeled with propidium iodide (1:1000) (PI) (Molecular Probes, Invitrogen, Carlsbad, MO, USA) solution, during 15 min, at RT, followed by six additional washes with cacodylate buffer. The cell-seeded scaffolds were then transferred into μ-Slide eight well Ibidi® chamber coverslips and imaged in a Zeiss LSM 710 confocal microscope (Carl Zeiss SMT Inc., USA), which was equipped with a Plan-Neofluar 10 $\times$ /NA 0.3 objective. All data were acquired in z-stack mode with a step of 4.67 μm. Z-stacks were then rendered into 3D images in the Zeiss Zen 2010 software. The depth code rendering of z-stacks was also performed in Zeiss 2010 software with the open GL and transparent rendering mode to provide visualization of cell spatial distribution within the scaffold architecture [13].

2.10. Statistical analysis

Statistical analysis of the results obtained for the different groups of scaffolds at various conditions was performed by using one-way analysis of variance (ANOVA), with the Newman–Keuls post hoc test [13]. The statistical test was used for comparison of the mean and the differences between groups [29]. A p value less than 0.05 ($p < 0.05$) was considered statistically significant.

3. Results and discussion

3.1. Printing parameters used for scaffold production

In this work, several Fab@home parameters were optimized in order to produce the 3D scaffolds. These parameters include: path width (mm), which represents the distance between adjacent paths of each layer; the distance between adjacent layers, which is named path height (mm); the pushout (s), which is the time of extrusion before the cartridge moves; the suckback (s), which is the opposite of the pushout; the deposition rate (mm syringe plunger motion/mm drawn path); the path speed (mm s^{-1}) of the cartridge; and, the nozzle diameter (mm). One of the objectives of this work was to study of the influence of solutions with different compositions in the extrusion process. For this purpose, the same Fab parameters were used for all of the ceramic-polymer blends tested.

Table 1 displays the parameters used for the extrusion of the ceramic-polymer mixture. First, through the analysis of the effect of nozzle diameter we concluded, in an initial step, that varying the nozzle diameter would affect all of the parameters studied (table 1). So, we first predetermined the diameter of the nozzle (20 Gauge) and only then optimized

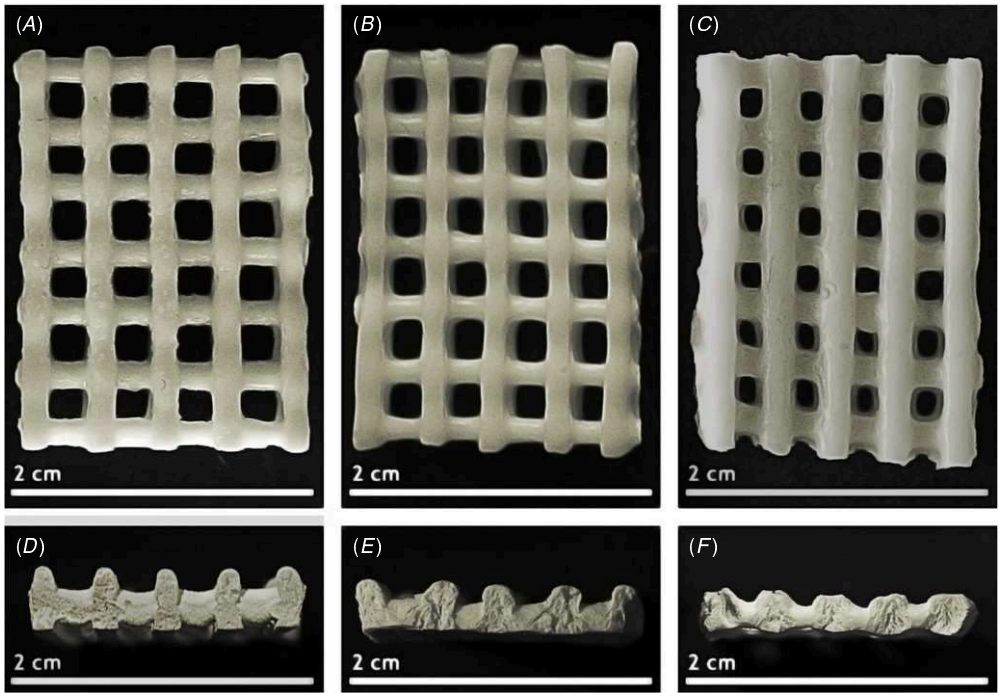

Figure 1. Representative macroscopic images of the different 50/50 (*A*), (*D*), 30/70 (*B*), (*E*) and 20/80 (*C*), (*F*) scaffolds.

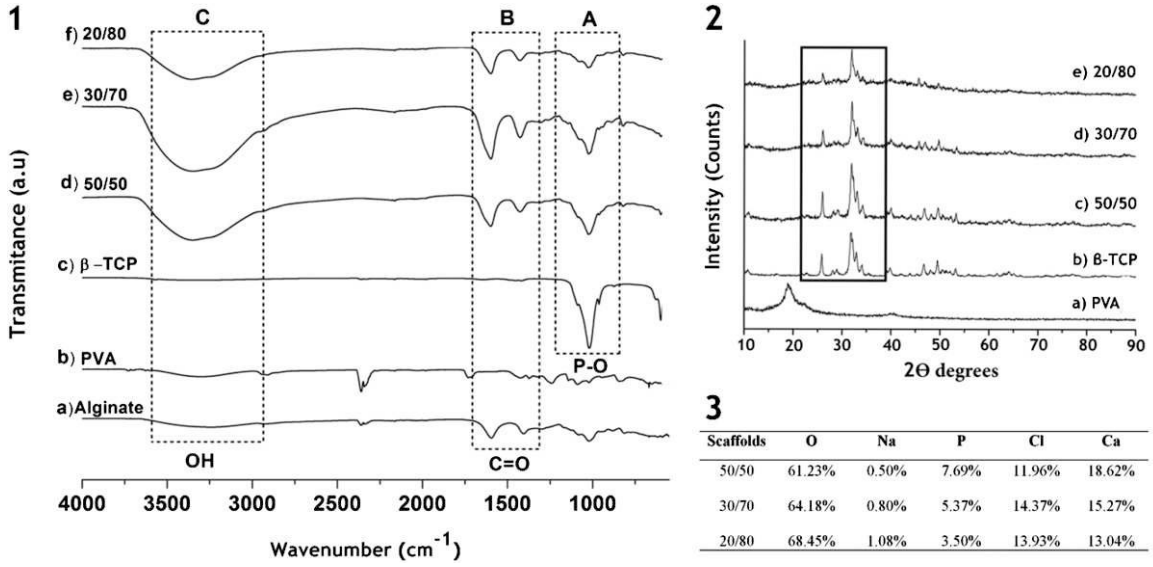

Figure 2. FTIR analysis of the powders and 3D scaffolds: (1) XRD spectra of the powders and 3D scaffolds, and (2) EDS analysis of the produced 3D scaffolds.

Table 2. Viscosities for each mixture ratio (mPa s). Data represent mean ± s.d.

Scaffolds	Values (mPa s)
50/50	150.0 ± 3.91
30/70	138.0 ± 1.00
20/80	133.0 ± 0.95

the other parameters. Taking into account that the viscosity of the different blends was not the same and is dependent on the β-TCP, as shown in table 2, we tried to approximate the parameters to obtain the best results in all of the mixtures. For the 50/50 scaffolds, which have a composition of 50:50 (w/w) of β-TCP:alginate, the resultant ceramic–polymer mixture presents a higher viscosity, making the extrusion process easier (table 2). Conversely, the extrusion process is more difficult to control for more fluid solutions, such as in the case of the 30/70 and 20/80 mixtures, where the β-TCP powder concentration is lower. This shows that the solution viscosities are dependent on β-TCP content. The chosen parameters were more suitable for the 50/50 mixture due to the higher viscosity of this ceramic–polymer solution. This initial optimization has allowed us to print scaffolds with six layers of alginate- β-TCP blends and with defined dimensions (width: 11 mm; length: 7 mm; height: 14 mm). Based on these results it was concluded that the

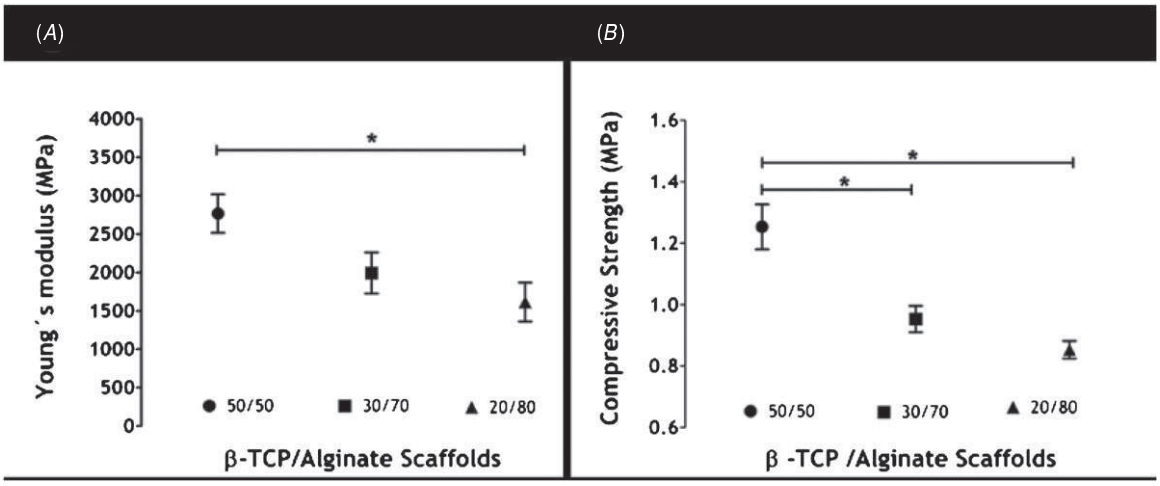

Figure 3. Characterization of the scaffolds' mechanical properties. YM (*A*) and compressive strength (*B*). Statistical analysis was performed using one-way ANOVA with a Newman–Keuls test; $^{*}p < 0.05$, $n = 3$.

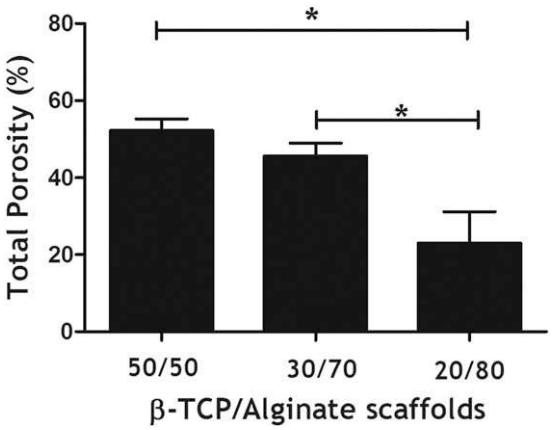

Figure 4. Analysis of scaffolds' total porosity. Statistical analysis was performed using one-way ANOVA with a Newman–Keuls test; $^{*}p < 0.05$, $n = 3$.

print accuracy/resolution depends not only on the parameters presented in table 1 but also on the flowability of the material to be extruded.

3.2. Morphology and macroscopic properties of the scaffolds

Macroscopic images were acquired in order to characterize the morphologic properties of 50/50, 30/70 and 20/80 scaffolds. It was possible to observe that, despite using the same manufacturing process and printing parameters (table 1) for all produced scaffolds, the images obtained revealed some differences between scaffolds, as can be observed in figure 1. It was also noticed that the 50/50 scaffolds (figure 1(*A*)) have a better defined structure than the 30/70 and 20/80 scaffolds (figures 1(*B*), (*C*)). The results suggest that for the 50/50, the optimized printing parameters were better. For the optimized parameters, the findings suggest that for higher viscosity solutions (table 2), the extrusion process is easier since a lower viscosity can cause spreading of the mixture, thus originating structures with less well-defined architectures.

Furthermore, such results may also be explained by the fact that the 30/70 and 20/80 scaffolds had a higher concentration of alginate. According to the descriptions in previous literature, the major disadvantage of the use of the alginate is related to its reticulation rate; that is, it is too fast and difficult to control, resulting in structures that are not always uniform, as can be observed in figure 1(*C*) [30]. The 50/50 scaffolds, which have a lower concentration of alginate and a higher concentration of β-TCP, when compared to 30/70 and 20/80 scaffolds, presented a better defined structure, as can be observed in figure 1(*A*). It is also important to emphasize that the morphological characteristics of the different scaffolds were maintained during all of the experiments, illustrating the reproducibility of the printing process used here.

3.3. Physicochemical characterization

FTIR analyses were performed to evaluate the physicochemical properties of the 50/50, 30/70 and 20/80 scaffolds produced by RP. Figure 2(1) shows the different FTIR spectra obtained for the samples. The spectra of β-TCP powder and scaffolds showed a major band at 1020 cm^{-1} (figure 2(1), area (*A*)), which is typically assigned to the P–O stretching vibration, revealing the presence of the inorganic phosphate components of β-TCP [3]. The alginate powder spectra revealed peaks at 1600 and 1400 cm^{-1} (figure 2(1), area (*B*)) which are also present in the scaffold samples, and are assigned to the $C = O$ stretching vibration of the carboxylic group of alginate, respectively [31, 32]. Moreover, both alginate alone and the scaffold's spectra presented a band between 3000–3700 cm^{-1} (figure 2, area (*C*)) belonging to the –OH stretch of water and –OH groups of the G and M units of alginate [33]. This band has a higher intensity in the scaffold's spectra, indicating the successful inclusion of alginate in the scaffold. The characteristic peak of PVA is not present in the scaffold samples due to the trace amounts that were used in their production.

Further characterization of the samples was done by XRD analysis to confirm the presence of crystalline phases of β-TCP. Figure 2(1) shows two intense peaks located at $2\theta = 25°–32°$. These peaks are characteristic of β-TCP, they can also be observed for the commercial β-TCP spectra (figures 2(3) (A) (b)) [3]. These characteristic

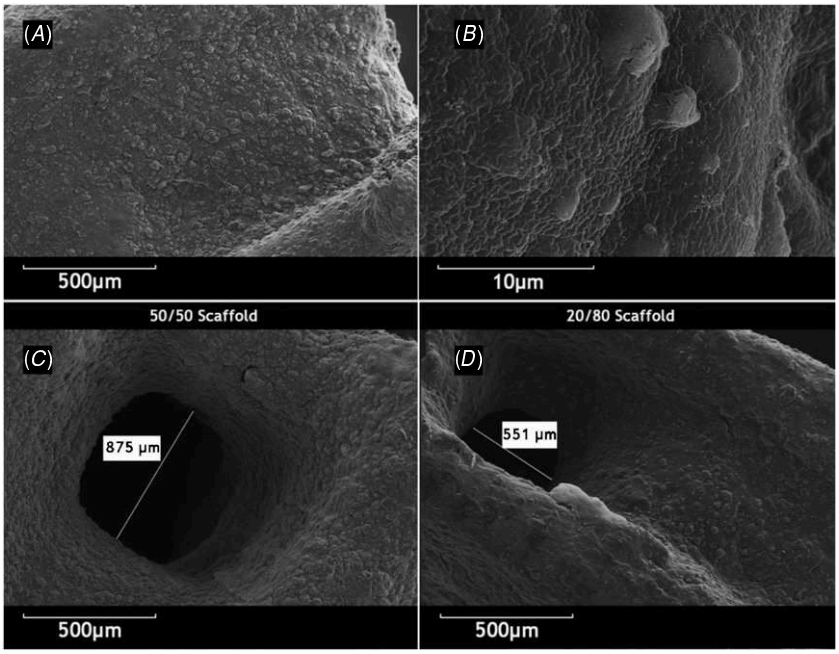

Figure 5. SEM images of the morphology and pore sizes of scaffolds. Representation of the morphology of 50/50 scaffolds at 50 × (*A*) and 3000 × (*B*) and pore sizes of the 50/50 (*C*) and 20/80 scaffolds at 50 × (*D*).

peaks of β-TCP are present in all of the manufactured scaffolds, figures 2(2) (a), (c), (d), (e). Consequently, it is important to underline that, after all of the processing and manipulation during manufacturing, the ceramic component of the scaffolds preserved its crystalline structure since no amorphous crystalline phases were identified.

Furthermore, EDS analysis of the scaffolds shows a slight increase in phosphate and calcium ions in the 50/50 scaffold, followed by 30/70 and 20/80, respectively (figure 2 (3)). These results are in agreement with those obtained for the scaffold's β-TCP composition and after the scaffold's reticulation.

3.4. Alginate/β-TCP composite scaffolds: mechanical characterization

A suitable scaffold to be used for bone regeneration must possess both flexibility and resistance to compression. The mechanical behavior of the 3D scaffolds was characterized by testing their resistance to compression and by determining the YM (figure 3). Through the analysis of figure 3, it is possible to observe that the YM and compressive strength is higher for the 50/50 scaffolds when compared to the 30/70 and 20/80 scaffolds. This shows that the increase of β-TCP concentration contributes to a YM and compressive strength increase. The results obtained for the mechanical characterization are consistent with a study previously performed by Matsuno and collaborators, where β-TCP was selected to reinforce the initial strength of an alginate hydrogel [34].

Moreover, the mechanical properties of the scaffolds are correlated with the biodegradability rate [7]. Scaffolds with improved mechanical properties have a slower degradation rate, maintaining their mechanical stability [35]. This is important because the biodegradation must be compatible with the ingrowth of bone progenitor cells and deposition of bone matrix [36]. The 50/50 scaffolds present better mechanical properties and it is expected that they will have a slower degradation rate and, consequently, a greater mechanical stability in comparison with the other formulations, thereby, maintaining the spaces required for cell ingrowth and matrix production during bone formation [7]. Furthermore, by comparing the mechanical properties of the 50/50 scaffolds with those presented by natural trabecular bone it is possible to observe that 3D scaffolds have a compressive strength comparable to that of natural trabecular bone [36, 37]. Interestingly, the produced scaffolds have a higher YM than that of trabecular bone [37]. This suggests that, in addition to having good compressive strength, the 50/50 scaffolds will also have more elasticity than natural trabecular bone, which supports its application to bone tissue regeneration.

3.5. Determination of the water contact angle

Another important physicochemical property which influences the bioactivity and regenerative capacity of a scaffold is its hydrophilic character [38]. The hydrophobic/hydrophilic character of the surface of the 3D structures was characterized by determining their contact angles [38]. According to the descriptions of several previous studies, the hydrophilic properties of the scaffolds are very important for cell attachment and nutrient diffusion, a phenomenon which is fundamental for maintaining cell viability [22]. Wei and collaborators reported that the osteoblast cell adhesion increases when the water contact angle of the material surface decreases [38]. Generally, surfaces are considered hydrophilic when the contact angle ranges between 0° and 30° and are considered as mildly hydrophilic when it is between

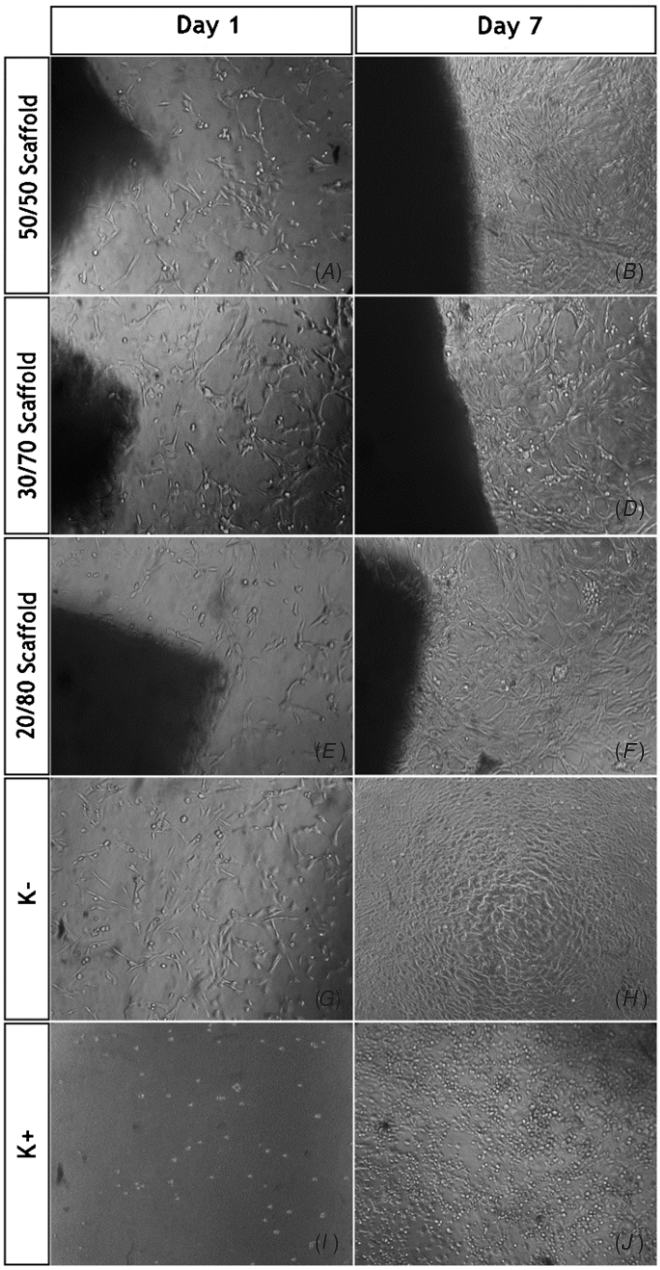

Figure 6. Macroscopic images of human osteoblast cells in the presence of scaffolds, one and seven days after seeding. 50/50 scaffolds (*A*), (*B*) 30/70 scaffolds (*C*), (*D*) 20/80 scaffolds (*E*), (*F*) negative control (K−) (*G*), (*H*) and positive control (K+) (*I*), (*J*).

31° and 90°. Surfaces that show contact angles higher than 90° are usually considered hydrophobic [39]. The results obtained (table 3) show that all samples presented a moderately hydrophilic character since the contact angle mean is around 70.4° ± 4.3 [40].

The hydrophilic character presented by the 30/70 and 20/80 scaffolds is mostly a consequence of the high number of carboxyl and hydroxyl groups present in alginate [16]. The hydrophilic properties of 50/50 scaffolds may be related to the presence of carboxyl and hydroxyl groups, although they are present in smaller percentages than those found in 30/70 and 20/80, respectively. Moreover, the roughness of their surface caused by the presence of β-TCP powders may largely affect

Table 3. Contact angles of the different scaffolds produced.

Scaffolds (β-TCP/alginate)	Water contact angle
50/50	70.7° ± 4.4°
30/70	70.3° ± 4.5°
20/80	70.3° ± 4.1°

this hydrophilic character, which is confirmed by the results of roughness of the 50/50 scaffolds presented in section 3.2. A recent study has reported that hydrophilic scaffolds allow cell adhesion and differentiation, as well as infiltration of oxygen and nutrients into the scaffolds, which have an essential role in the successful use of these 3D constructs in repairing bone defects [13].

3.6. Determination of the scaffolds' total porosity

To evaluate the total porosity of the scaffolds, the liquid displacement method using EtOH was performed [27]. One of the most important requirements for the production of scaffolds to be used in bone tissue regeneration is to achieve an equilibrium between the scaffolds' porosity and their mechanical properties [7]. The porosity influences both the mechanical and biological properties of the scaffolds [41]. In the scaffolds produced, the overall structure is similar throughout the different compositions, with the largest differences in porosity deriving from the composition itself. From the analysis of figure 4, it is possible to conclude that the 50/50 scaffolds presented the highest value of total porosity (52% ± 3.2) when compared to the 30/70 (46% ± 3.5) and 20/80 (23% ± 8.0) scaffolds. According to the previous descriptions of Santos and collaborators, these porosity results can be correlated with the density of the scaffolds [3] since porosity and density are inversely proportional. Furthermore, the particle size is known to affect the total porosity of the scaffolds [13]. Our results are in agreement with those reported by Balakrishnan and collaborators, wherein molecular dynamics simulations were carried out. They concluded that the formation of agglomerates depends on the application of forces to compact the particles [42]. The powder materials (β-TCP, mean particle size 11.64 μm) used in scaffold manufacture have microporosities which are caused by the voids formed between these particles agglomerates [3]. The 50/50 scaffolds have more β-TCP and, subsequently, a higher degree of microporosity within the printed fiber layers, resulting in a higher scaffold porosity (figure 1(*D*)). On the other hand, the 30/70 and 20/80 scaffolds have a higher amount of alginate. This polymer fills in the space gaps between β-TCP microparticles, which contributes to a reduced total porosity. In conclusion, 50/50 scaffolds present all of the characteristics to allow for better cell migration, adhesion, proliferation and also facilitate the transport of oxygen and nutrients.

3.7. Characterization of the scaffolds' biocompatibility

As previously described in the literature, cellular behavior depends largely on the material's surface properties. Surface

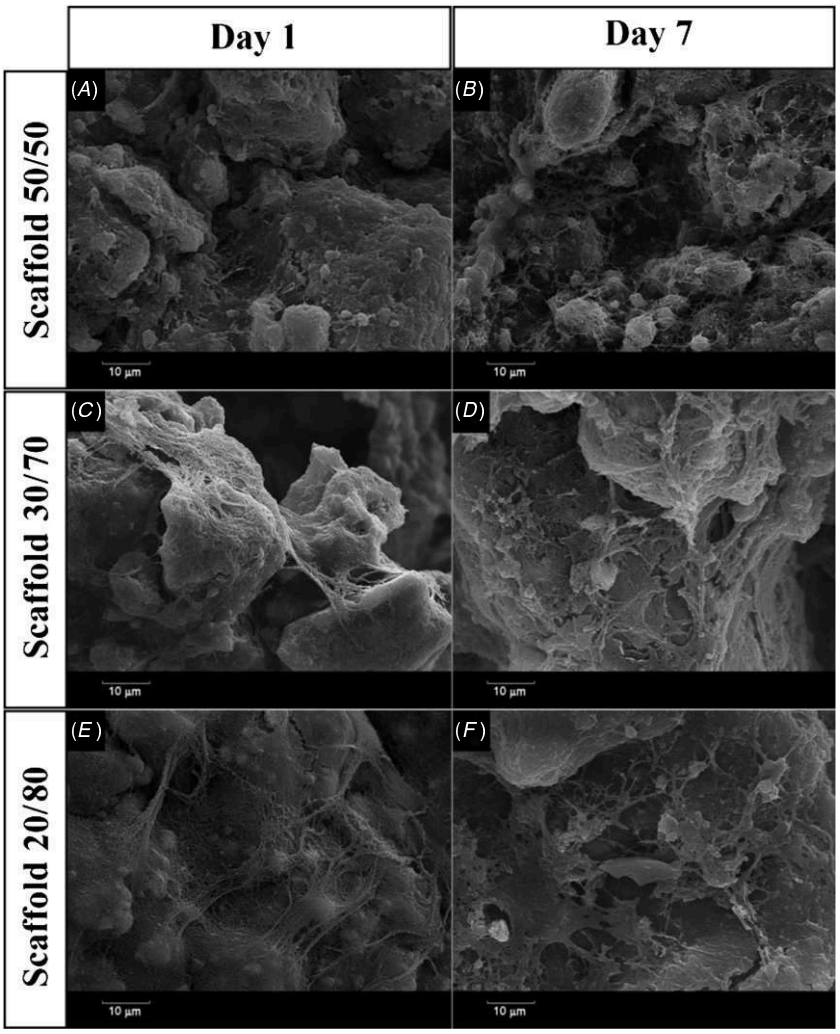

Figure 7. SEM micrographs of osteoblasts morphology in the presence of the different β-TCP/alginate formulations. 50/50 scaffolds (*A*), (*B*), 30/70 scaffolds (*C*), (*D*) and 20/80 scaffolds (*E*), (*F*)

roughness has a direct influence on cellular morphology, adhesion and proliferation [8]. Human osteoblasts attach more rapidly and produce more extracellular matrix in the presence of rough surfaces than in the presence of smoother surfaces [43].

In the results obtained in SEM images, the 50/50 scaffolds showed a slightly regular surface (figure 1(*A*)) and a high level of roughness (figure 1(*D*)), which contributes toward the osteoblasts' adhesion and proliferation within the scaffold. Cell adhesion to the surface of these scaffolds is affected by an increase in the anchoring area and spots for cell contact [44]. Furthermore, the literature describes that the contact area increases with increasing surface roughness [44].

Moreover, as previously mentioned, rough surfaces are known to affect the material wettability, influencing both the material's hydrophilic character and material–cell interactions [43, 45]. The SEM images of the 50/50 scaffolds corroborate the fact that these scaffold surfaces are rough, justifying the hydrophilicity values obtained for these 3D structures (table 3).

Subsequently, the pore diameter of the scaffolds was studied. According to the literature, the rates of alginate crosslinking can influence the scaffold's structure, shape and pore size [30]. Another factor that can affect the pore size is the crosslinker concentration [46]. The results presented in figures 5(*C*), (*D*) show that the pore diameter of the scaffolds ranged between 551 and 875 μm. The pore diameter is smaller in the 20/80 scaffolds, which can be explained by the higher percentage of alginate. This may be related to the fact that there are more calcium–alginate connections, which in turn lead to the pore's closure. These results are in agreement with those obtained for total porosity. In the 50/50 scaffolds, where alginate concentration is lower, the pore size is larger since there are fewer calcium–alginate connections to occlude the spaces between β-TCP particles.

These results are of crucial importance since pore diameters ranging from 200 to 900 μm have been shown to improve osteoblast bone deposition and proliferation while ensuring nutrient distribution [7].

To confirm the potential application of the 50/50 scaffold in bone tissue engineering, the scaffold's biological properties were thoroughly characterized. Regarding the scaffold's bioactivity, the optical microscopy images acquired at one and seven days after cell seeding show that the cells proliferated in the presence of the β-TCP/alginate scaffolds (figures 6(*A*)–(*F*)). These results are similar to those obtained for non-incubated cells (negative control) (figures 6(*G*)–(*H*)). In the

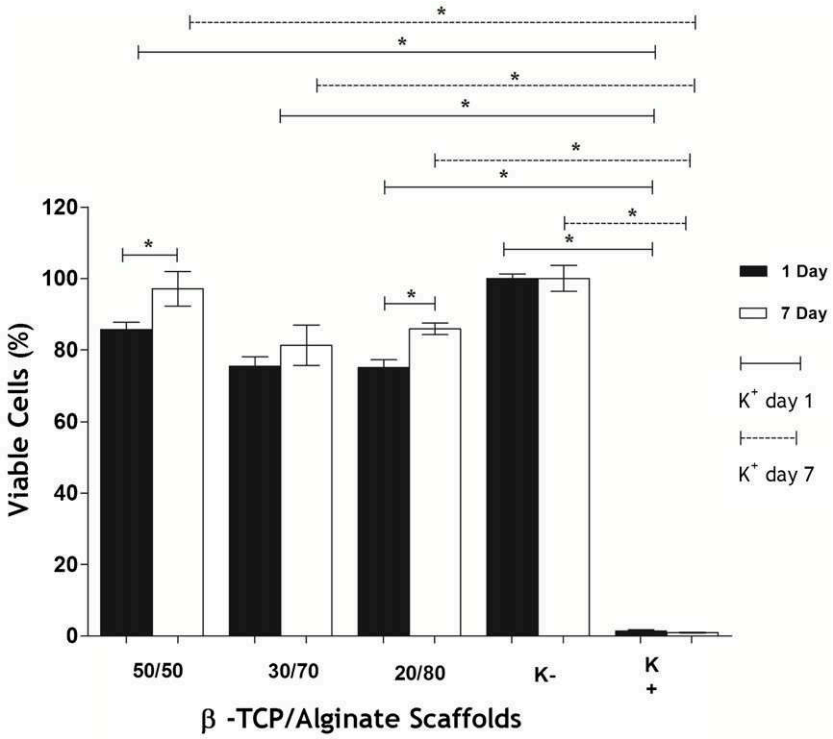

Figure 8. Evaluation of human osteoblasts cell viability when cultured in the presence of different β-TCP/alginate scaffolds. Cultures were evaluated for one and seven days. (K+) positive control and (K−) negative control indicate dead and viable cells, respectively. Statistical analysis was performed using one-way ANOVA with Newman–Keuls test.; $^{*}p < 0.05$, $n = 3$.

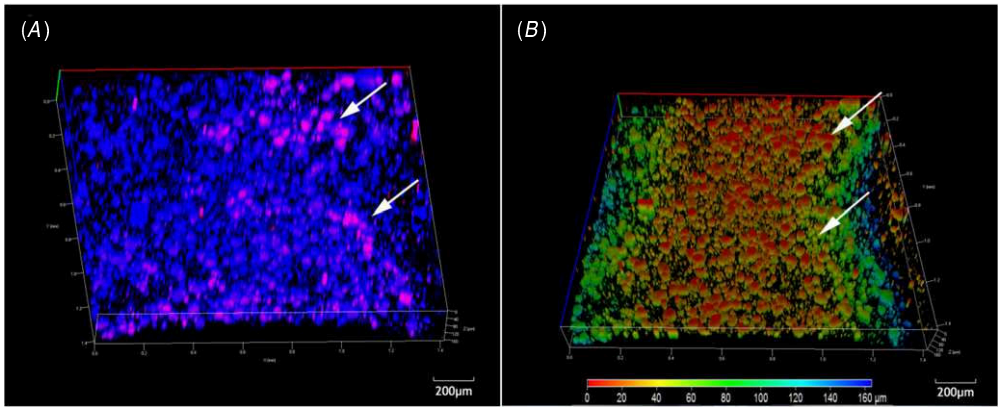

Figure 9. CSLM images of osteoblasts in contact with the 50/50 scaffold. 3D reconstruction of the 50/50 scaffold seeded with osteoblasts after four days in culture. Blue channel: 50/50 scaffold; red channel: PI stained nucleus of osteoblasts (*A*), depth coding analysis of osteoblasts distribution within the 3D volume of the scaffold (*B*).

positive control, no cell proliferation was observed. Dead cells with their typical spherical shape can be observed in figures 6(*I*) and (*J*). In addition, SEM analysis was performed to characterize cellular morphology and adhesion, both on the surface and inside the scaffolds.

SEM images of the scaffolds in the presence of cells show that cells adhered and grew within the β-TCP/alginate scaffolds after one day of being in the presence of the scaffold (see figures 7 (*A*), (*C*), (*E*)). To evaluate if the cells remained viable and proliferated with time, SEM images were also acquired after seven days. These images showed that cells were extensively attached and had spread on the surface of the β-TCP/alginate scaffolds (figures 7(*B*), (*D*), (*F*)).

The *in vitro* cytotoxicity analysis showed a significant difference between cells in the presence of β-TCP/alginate and the positive control after one and seven days of incubation, suggesting that the scaffolds did not affect cell viability (figure 8). The MTS assay also showed a significant difference in the results obtained for the 50/50 and 20/80 scaffolds between the first and seventh day. The 30/70 scaffold did not present a significant difference within this period of time.

It is also possible to observe that cell viability is higher for the 50/50 scaffolds; that is, with the increase of β-TCP, an increase in cell viability was observed (figure 8). Furthermore, these results are supported by the data obtained by Fuji and collaborators, who reported that apatite formation

through β-TCP dissolution at physiological conditions affects the osteoblasts' behavior [23]. The presence of Ca^{2+} and PO_4^{3-} resultant of β-TCP dissolution is important for the osteoconduction and osteoinduction processes, providing a favorable environment for osteoblast attachment and growth.

CLSM analysis showed that the osteoblasts are distributed within 50/50 scaffolds, further highlighting their biocompatibility and appropriate physicochemical properties for bone regenerative medicine (figure 9(*A*)). These data further corroborates the results obtained through SEM analysis.

In figure 9(*B*) it is possible to observe the 3D reconstruction and depth analysis of the 50/50 scaffold. These results show that the osteoblasts are capable of migrating and attach into deep sections of the scaffolds. Some cells were localized up to 200 μm within the scaffold's architecture (figure 9(*B*)). This is of crucial importance since the deposition of bone matrix inside the scaffold will eventually fill the bone defect while the scaffold is biodegraded, ultimately leading to the establishment of the original structure and function of the native bone.

4. Conclusions

This work has described the manufacture of β-TCP/alginate scaffolds through a rapid prototyping technology, which may be used in bone regeneration applications. The equipment used, in particular the Fab@home personal fabricator, allowed us to easily and rapidly create and optimize several different models of scaffolds, as well as to test different materials. The method used has also allowed high reproducibility between different printings. In addition, the ease of use and low maintenance costs give this equipment the potential to revolutionize scaffold manufacture at a large scale and in an economically viable way.

Furthermore, the optimal 50/50 scaffold formulation presented a well-defined morphology, with excellent biological properties for bone tissue regeneration applications. Moreover, the technology used offers the possibility of modelling the scaffold to a specific bone defect. However, despite the excellent results achieved, further studies will need to be performed to improve the properties of the scaffolds, including functionalizing their surface with molecules in order to facilitate bioadhesion and improving their mechanical properties by the use of different polymers or ceramics.

Acknowledgments

The authors would like to thank to Eng. Ana Paula for her help with the acquisition of SEM data. This work was supported by the Portuguese Foundation for Science and Technology (FCT), (PTDC/EBB-BIO/114320/2009 and PEst-C/SAU/UI0709/2011 COMPETE). VMG acknowledges a PhD fellowship from FCT (SFRH/BD/80402/2011).

References

[1] Chiara G *et al* 2012 Nanostructured biomaterials for tissue engineered bone tissue reconstruction *Int. J. Mol. Sci.* **13** 737–57

[2] Giannoudis P V, Dinopoulos H and Tsiridis E 2005 Bone substitutes: an update *Injury* **36** S20–S27

[3] Santos C F, Silva A P, Lopes L, Pires I and Correia I J 2012 Design and production of sintered β-tricalcium phosphate 3D scaffolds for bone tissue regeneration *Mater. Sci. Eng. C* **32** 1293–8

[4] Nandakumar A, Barradas A, de Boer J, Moroni L, van Blitterswijk C and Habibovic P 2013 Combining technologies to create bioactive hybrid scaffolds for bone tissue engineering *Biomatter* **3** e23705

[5] Yeong W Y, Chua C K, Leong K F and Chandrasekaran M 2004 Rapid prototyping in tissue engineering: challenges and potential *Trends Biotechnol.* **22** 643–52

[6] Rezwan K, Chen Q Z, Blaker J J and Boccaccini A R 2006 Biodegradable and bioactive porous polymer/inorganic composite scaffolds for bone tissue engineering *Biomaterials* **27** 3413–31

[7] Salgado A J, Coutinho O P and Reis R L 2004 Bone tissue engineering: state of the art and future trends *Macromol. Biosci.* **4** 743–65

[8] Lantada A D and Morgado P L 2012 Rapid prototyping for biomedical engineering: current capabilities and challenges *Annu. Rev. Biomed. Eng.* **14** 73–96

[9] Simpson R L *et al* 2008 Development of a 95/5 poly(L-lactide-co-glycolide)/hydroxylapatite and beta-tricalcium phosphate scaffold as bone replacement material via selective laser sintering *J. Biomed. Mater. Res.* B **84** 17–25

[10] Wüst S, Müller R and Hofmann S 2011 Controlled positioning of cells in biomaterials—approaches towards 3D tissue printing *J. Funct. Biomater.* **2** 119–54

[11] Malone E and Lipson H 2007 Fab@ Home: the personal desktop fabricator kit *Rapid Prototyping J.* **13** 245–55

[12] Kalejs M and von Segesser L K 2009 Rapid prototyping of compliant human aortic roots for assessment of valved stents *Interact. Cardiovasc. Thorac. Surg.* **8** 182–6

[13] Torres A L *et al* 2013 Bioactive polymeric-ceramic hybrid 3D scaffold for application in bone tissue regeneration *Mater. Sci. Eng.* C **33** 4460–9

[14] Suzuki T *et al* 1997 Surface instability of calcium phosphate ceramics in tissue culture medium and the effect on adhesion and growth of anchorage-dependent animal cells *J. Biomed. Mater. Res.* **34** 507–17

[15] Liu B and Lun D X 2012 Current application of β-tricalcium phosphate composites in orthopaedics *Orthop. Surg.* **4** 139–44

[16] Valente J, Valente T, Alves P, Ferreira P, Silva A and Correia I 2012 Alginate based scaffolds for bone tissue engineering *Mater. Sci. Eng.* C **32** 2596–603

[17] Andersen T, Strand B L, Formo K, Alsberg E and Christensena B E 2012 Alginates as biomaterials in tissue engineering *Carbohydrate Chemistry* ed A P Rauter and T Lindhorst (London: RSC) Chapter 9

[18] Lima A C, Batista P, Valente T A, Silva A S, Correia I J and Mano J F 2013 Novel methodology based on biomimetic superhydrophobic substrates to immobilize cells and proteins in hydrogel spheres for applications in bone regeneration *Tissue Eng.* A **19** 1175–87

[19] Mabic S and Kano I 2003 Impact of purified water quality on molecular biology experiments *Clin. Chem. Lab. Med.* **41** 486–91

[20] Cohen D L, Lo W, Tsavaris A, Peng D, Lipson H and Bonassar L J 2010 Increased mixing improves hydrogel

homogeneity and quality of three-dimensional printed constructs *Tissue Eng.* C **17** 239–48
[21] Kang K, Hockaday L and Butcher J 2013 Quantitative optimization of solid freeform deposition of aqueous hydrogels *Biofabrication* **5** 035001
[22] Yeo M G and Kim G H 2011 Preparation and characterization of 3D composite scaffolds based on rapid-prototyped PCL/β-TCP struts and electrospun PCL coated with collagen and HA for bone regeneration *Chem. Mater.* **24** 903–13
[23] Fuji T *et al* 2009 Octacalcium phosphate-precipitated alginate scaffold for bone regeneration *Tissue Eng.* A **15** 3525–35
[24] Wu X *et al* 2010 Preparation of aligned porous gelatin scaffolds by unidirectional freeze-drying method *Acta Biomater.* **6** 1167–77
[25] Lacroix D, Chateau A, Ginebra M-P and Planell J A 2006 Micro-finite element models of bone tissue-engineering scaffolds *Biomaterials* **27** 5326–34
[26] Correia T R *et al* 2013 A bi-layer electrospun nanofiber membrane for plasmid DNA recovery from fermentation broths *Sep. Purif. Technol.* **112** 20–25
[27] Nie H L and Zhu L M 2007 Adsorption of papain with Cibacron Blue F3GA carrying chitosan-coated nylon affinity membranes *Int. J. Biol. Macromol.* **40** 261–7
[28] Gaspar V M *et al* 2011 Nanoparticle mediated delivery of pure P53 supercoiled plasmid DNA for gene therapy *J. Control. Release* **156** 212–22
[29] Bewick V, Cheek L and Ball J 2004 Statistics review 9: one-way analysis of variance *Crit. Care* **8** 130–6
[30] Cho S H, Lim S M, Han D K, Yuk S H, Im G I and Lee J H 2009 Time-dependent alginate/polyvinyl alcohol hydrogels as injectable cell carriers *J. Biomater. Sci. Polym. Edn* **20** 863–76
[31] Pathak T S, San Kim J, Lee S-J, Baek D-J and Paeng K-J 2008 Preparation of alginic acid and metal alginate from algae and their comparative study *J. Polym. Environ.* **16** 198–204
[32] Lawrie G *et al* 2007 Interactions between alginate and chitosan biopolymers characterized using FTIR and XPS *Biomacromolecules* **8** 2533–41
[33] Lambert J B, Shurvell H F, Lightner D A and Cooks R G 1998 *Organic Structural Spectroscopy* (Upper Saddle River, NJ: Prentice Hall)
[34] Matsuno T *et al* 2008 Preparation of injectable 3D-formed BETA-tricalcium phosphate bead/alginate composite for bone tissue engineering *Dent. Mater. J.* **27** 827–34
[35] Ghanaati S *et al* 2012 The chemical composition of synthetic bone substitutes influences tissue reactions *in vivo*: histological and histomorphometrical analysis of the cellular inflammatory response to hydroxyapatite, beta-tricalcium phosphate and biphasic calcium phosphate ceramics *Biomed. Mater.* **7** 015005
[36] Hutmacher D W, Schantz J T, Lam C X F, Tan K C and Lim T C 2007 State of the art and future directions of scaffold-based bone engineering from a biomaterials perspective *J. Tissue Eng. Regenerative Med.* **1** 245–60
[37] Cordell J M, Vogl M L and Wagoner Johnson A J 2009 The influence of micropore size on the mechanical properties of bulk hydroxyapatite and hydroxyapatite scaffolds *J. Mech. Behav. Biomed. Mater.* **2** 560–70
[38] Chang H and Wang Y 2011 Cell responses to surface and architecture of tissue engineering scaffolds *Regenerative Medicine and Tissue Engineering—Cells and Biometerials* ed D Eberti (Rijeka: InTech) pp 569–88
[39] Shalumon K, Anulekha K, Chennazhi K, Tamura H, Nair S and Jayakumar R 2011 Fabrication of chitosan/poly (caprolactone) nanofibrous scaffold for bone and skin tissue engineering *Int. J. Biol. Macromol.* **48** 571–6
[40] Navarro M, Aparicio C, Charles-Harris M, Ginebra M, Engel E and Planell J 2006 Development of a biodegradable composite scaffold for bone tissue engineering: physicochemical, topographical, mechanical, degradation, and biological properties *Ordered Polymeric Nanostructures at Surfaces* vol 200 (Berlin: Springer) pp 209–31
[41] Tarafder S, Balla V K, Davies N M, Bandyopadhyay A and Bose S 2012 Microwave-sintered 3D printed tricalcium phosphate scaffolds for bone tissue engineering *J. Tissue Eng. Regenerative Med.* **7** 631–41
[42] Balakrishnan A, Pizette P, Martin C, Joshi S and Saha B 2010 Effect of particle size in aggregated and agglomerated ceramic powders *Acta Mater.* **58** 802–12
[43] Dos Santos E, Farina M, Soares G and Anselme K 2009 Chemical and topographical influence of hydroxyapatite and β-tricalcium phosphate surfaces on human osteoblastic cell behavior *J. Biomed. Mater. Res.* A **89** 510–20
[44] Yoon H, Kim G H and Koh Y H 2010 A micro-scale surface-structured PCL scaffold fabricated by a 3D plotter and a chemical blowing agent *J. Biomater. Sci. Polym. Edn* **21** 159–70
[45] Hollister S J 2005 Porous scaffold design for tissue engineering *Nature Mater.* **4** 518–24
[46] Daemi H and Barikani M 2012 Synthesis and characterization of calcium alginate nanoparticles, sodium homopolymannuronate salt and its calcium nanoparticles *Sci. Iran.* **19** 2023–8

Materials Science and Engineering C 33 (2013) 4460–4469

Contents lists available at ScienceDirect

Materials Science and Engineering C

journal homepage: www.elsevier.com/locate/msec

Bioactive polymeric–ceramic hybrid 3D scaffold for application in bone tissue regeneration

A.L. Torres [a], V.M. Gaspar [a], I.R. Serra [a], G.S. Diogo [a], R. Fradique [a], A.P. Silva [b], I.J. Correia [a,*]

[a] CICS-UBI — Health Sciences Research Centre, University of Beira Interior, Av. Infante D. Henrique, 6200-506 Covilhã, Portugal
[b] CAST-UBI — Centre for Aerospace Science and Technologies, University of Beira Interior, Calçada Fonte do Lameiro, 6201-001 Covilhã, Portugal

ARTICLE INFO

Article history:
Received 9 May 2013
Received in revised form 29 June 2013
Accepted 5 July 2013
Available online 13 July 2013

Keywords:
3D scaffolds
Bioceramics
Bone regeneration
Foam replication method
Vacuum coating

ABSTRACT

The regeneration of large bone defects remains a challenging scenario from a therapeutic point of view. In fact, the currently available bone substitutes are often limited by poor tissue integration and severe host inflammatory responses, which eventually lead to surgical removal. In an attempt to address these issues, herein we evaluated the importance of alginate incorporation in the production of improved and tunable β-tricalcium phosphate (β-TCP) and hydroxyapatite (HA) three-dimensional (3D) porous scaffolds to be used as temporary templates for bone regeneration. Different bioceramic combinations were tested in order to investigate optimal scaffold architectures. Additionally, 3D β-TCP/HA vacuum-coated with alginate, presented improved compressive strength, fracture toughness and Young's modulus, to values similar to those of native bone. The hybrid 3D polymeric–bioceramic scaffolds also supported osteoblast adhesion, maturation and proliferation, as demonstrated by fluorescence microscopy. To the best of our knowledge this is the first time that a 3D scaffold produced with this combination of biomaterials is described. Altogether, our results emphasize that this hybrid scaffold presents promising characteristics for its future application in bone regeneration.

1. Introduction

Bone is a highly vascularized and dynamic tissue, having extraordinary mechanical properties and intrinsic regenerative capacity [1]. This exceptional characteristic is however rather limited in severe bone traumatisms that involve multiple fractures, bone-associated tumors and degenerative diseases [2]. These are highly debilitating conditions that commonly require medical intervention to restore bone native properties [3].

Currently, several types of biomaterials, such as biofunctional prosthesis [4], injectable substrates [5] and hydrogels [6] are being produced for bone regeneration purposes. Among them, bioactive 3D porous scaffolds are particularly promising for clinical application due to their unique set of characteristics. Scaffolds are porous 3D matrices that act as temporary templates for cell adhesion and proliferation, while providing mechanical support until new bone tissue is formed at the affected area [7]. For this purpose these scaffolds must be produced with materials that promote proper regeneration without eliciting host immune responses or originating toxic metabolites [8]. The 3D features of the template is another critical parameter when therapeutic applications are envisioned, since its spatial architecture should be designed to have interconnected pores that simultaneously induce osteoconductivity of bone-progenitor cells and neovascularization [9]. To further improve and accelerate bone regeneration it is essential that the scaffold is bioactive, i.e., has the ability to form anchoring points with the surrounding bone and soft tissues, stimulating bone growth. Commonly these bonds are formed through an HA-like layer and are responsible for increasing osteointegration and cell growth and differentiation [10].

The desire to gather these complex characteristics into one scaffold is a challenging demand, not only in the design and manufacturing stages, but also in the translation to in vivo applications. In this context, the combination of ceramics with polymers for the synthesis of hybrid scaffolds has been widely investigated in an attempt to mimic bone tissue native structure [11,12]. β-TCP and HA are the most commonly used ceramics since their mineral compositions are similar to those found in human bone [11,13]. Although β-TCP has been extensively used for bone regeneration due to its biodegradability, biocompatibility and osteoconductivity [14,15] its applications to bone tissue regeneration are limited by its poor mechanical properties [16,17].

In different studies bioceramic-based scaffolds have been modified with polymers (as coating or interpenetrating phases) in order to reduce their brittleness and improve mechanical properties [18–21]. In the present study, β-TCP/HA scaffolds were left uncoated or coated with alginate. This polymer is comprised by 1,4′-linked β-D-mannuronic acid and α-L-guluronic acid blocks, which determines alginate physicochemical properties. This natural biomaterial has valuable characteristics, such as biocompatibility, biodegradability, hydrophilicity, low toxicity and gelling capacity with divalent cations [22–25]. In fact, its

* Corresponding author. Tel.: +351 275 329 055.
E-mail address: icorreia@ubi.pt (I.J. Correia).

0928-4931/$ – see front matter © 2013 Elsevier B.V. All rights reserved.
http://dx.doi.org/10.1016/j.msec.2013.07.003

responsiveness to calcium (Ca^{2+})-rich tissue microenvironments, renders it suitable for scaffold coating in bone tissue engineering, as previously reported by our group [26]. Importantly, the ionically cross-linked alginate mechanical strength rises with increasing divalent ion concentration, and also when these ions have high affinity for alginate [27]. Due to these valuable characteristics, this polymer has been widely used in biomedical applications, including cell encapsulation [28] and drug loading and delivery [29].

In this context, this work reports the production of β-TCP/HA scaffolds by the foam replication method (FRM), followed by their coating with alginate. The scaffold production method used is simple, cost-effective, excludes the use of organic solvents and, most importantly, allows the manufacture of reproducible structures. Three types of scaffolds with different β-TCP:HA ratios and alginate coatings were developed and their physicochemical and biological properties investigated.

2. Materials and methods

2.1. Preparation of β-TCP/HA composite scaffolds followed by alginate coating

β-TCP/HA scaffolds were produced using a polymer-based FRM, which allows the control of the dimensions, pore size and density of the 3D scaffold. Three different types of scaffolds were prepared, concerning the quantity of β-TCP (Panreac®) relatively to HA nanopowder (<200 nm particle size, Sigma-Aldrich): 80/20% (w/w), 90/10% (w/w) and 99/1% (w/w), respectively. Poly(vinyl) alcohol (PVA) (Sigma-Aldrich) (β-TCP binder agent) was added to the polymer mixture in a ratio of 1:10 (% w/w) PVA:β-TCP. Briefly, to prepare the polymer blends, PVA was dissolved in 15 mL of deionized water, under constant stirring, for 30 min, at 50 °C. Then, both β-TCP and HA powders were added in small amounts to the solution, under constant stirring at room temperature (RT). After all the powder was wetted, the mixture was sonicated for 15 min. The used polyurethane (PU) foams had similar structures to that of the human cancellous bone and were cut ($5 \times 5 \times 5$ mm^3) to be used as a sacrificial template for the FRM. All the PU foams were cleaned in a 0.1 M sodium hydroxide (NaOH) (Sigma-Aldrich) solution, followed by rinsing twice with distilled water before air-dried for 12 h. The PU foams were then repeatedly immersed in the polymer blends in order to promote polymer penetration into the PU foam pores. The PU foams impregnated with the polymer blends were then gently squeezed to remove the excess of the slurry. Homogeneous coating of the PU foams with β-TCP/HA was possible after several immersions. The coated PU foams were exposed to air, allowed to dry overnight, at RT, and then sintered. Briefly, the PU-polymer foams were step-wise heated in a furnace at 1 °C/min to 900 °C and then kept at this temperature for 240 min. Additionally, some of the 3D scaffolds were subsequently coated with a 2% sodium alginate (Sigma-Aldrich) solution, (molecular weight (Mw) 120.000–190.000 Da), under vacuum at RT, for 30 min, in order to guarantee alginate inclusion within the scaffold pores. These coated scaffolds were then immersed in a 5% calcium chloride ($CaCl_2$) solution (Sigma-Aldrich), under vacuum for 10 min, in order to cross-link alginate-coated scaffolds. The structures were maintained in the $CaCl_2$ solution for 24 h and then air dried, prior to use. From this point onwards alginate coated β-TCP/HA scaffolds are identified as: 80/20/A, 90/10/A and 99/1/A and the uncoated scaffolds as 80/20, 90/10 and 99/1.

2.2. Chemical, mechanical and morphological characterization of the β-TCP/HA composite scaffolds

2.2.1. Fourier transform infrared spectroscopy

The physicochemical characteristics of the manufactured 3D scaffolds were evaluated by Fourier transform infrared spectroscopy (FTIR) by using a Nicolet iS10 interferometer (Thermo Scientific, Waltham, MA, USA). Briefly, samples were mounted on a diamond window and compressed to improve spectrum signal to noise ratio. For each sample, 128 interferograms were acquired with a spectral width ranging from 4000 to 400 cm^{-1} and a spectral resolution of 4 cm^{-1}. The acquired data was then processed in Omnic Spectra analysis software, where baseline subtraction was performed.

2.2.2. Energy dispersive spectroscopy

Energy-dispersive X-ray spectroscopy (EDS) (Rontec) was used for the elementary characterization of both, coated and uncoated, β-TCP/HA scaffolds. Prior to all analyses, samples were placed on an aluminum stub support, air-dried at RT and sputter-coated with gold.

2.2.3. Resistance to compression, fracture toughness and Young's modulus

To characterize the mechanical behavior of the cuboid-shaped coated and uncoated scaffolds, uniaxial compression tests were performed. All the measurements were performed at RT using a Zwick® 1435 Material Prüfung (Ulm, Germany) with a crosshead speed of 0.2 mm/min and a load cell of 5 kN. Four specimens from each sample were tested and their dimensions acquired. Afterwards, compressive strength (Cs) of each type of scaffold was calculated by applying Eq. (1) [30].

$$\mathrm{Cs} = \frac{F}{a \times l} \tag{1}$$

where F is the load at the time of the fracture and a and l represent the width and length of the scaffold, respectively. The fracture toughness (FT) and Young's modulus (YM) were estimated from the stress–strain relations calculated and applying Eqs. (2) and (3), respectively [31,32].

$$\mathrm{FT} = \frac{Hd \times \mathrm{Cs}}{2} \tag{2}$$

$$YM = \frac{\mathrm{Cs}}{Hd} \tag{3}$$

where Hd is the scaffold height deformation and Cs is the scaffold compressive strength. Average values and standard deviations (s.d.) were determined for each sample as previously described in the literature [33].

2.2.4. Scanning electron microscopy

In order to assess scaffold morphology, porosity and cellular behavior in the presence of the samples, scanning electron microscopy (SEM) analysis was performed. Samples were washed at RT with phosphate buffer solution (PBS, pH 7.4) (Sigma-Aldrich) and fixed for 30 min with 2.5% (v/v) glutaraldehyde (Sigma-Aldrich) diluted in a 0.1 M sodium cacodylate solution (Sigma-Aldrich). Then, samples were washed three times with cacodylate buffer and finally incubated for 10 min in a graded series of ethanol solutions (50, 60, 70, 80, 90 and 99% v/v), for dehydration. Scaffolds were then stored in absolute ethanol, at 4 °C, until being subjected to CO_2 critical point drying, mounted onto aluminum stubs with araldite glue and sputtered-coated with gold using an Emitech K550 sputter coater (London, UK). SEM images were obtained with a scanning electron microscope Hitachi S-2700 (Tokyo, Japan) with an acceleration voltage of 20 kV at suitable magnifications.

2.2.5. Porosity evaluation

The total porosity (P) of the different types of β-TCP/HA scaffolds, was determined by following a method described elsewhere [34]. The amount of absolute ethanol that the scaffolds were able to absorb in 24 h, was determined by applying Eq. (4).

$$\mathrm{P}(\%) = \frac{W_2 - W_1}{d_{\mathrm{ethanol}} \times V_{\mathrm{scaffold}}} \times 100 \tag{4}$$

where W_1 and W_2 are the weights of the dry and the wet scaffolds, respectively, d_{ethanol} is the density of the ethanol at RT and V_{scaffold} is the

volume of the wet scaffold, directly determined by immersion. For each scaffold, three replicates were analyzed and data represents the average of each replicate.

2.2.6. Contact angle measurements

The contact angle measurements of the samples were performed using the sessile drop technique and water was used as reference fluid [35]. Contact angle data was acquired in a Data Physics Contact Angle System OCAH 200 apparatus, operating in static mode at RT. For each sample, water drops were placed at various locations of the analyzed surface.

2.3. Biological characterization of the β-TCP/HA composite scaffolds

2.3.1. Culture of human osteoblasts in the presence of the scaffolds

Human osteoblasts (CRL-11372), purchased from American Type Culture Collection, were cultured in Dulbecco Modified Eagle Medium, Nutrient Mixture F-12 (DMEM-F12) (Sigma-Aldrich), supplemented with 10% heat inactivated fetal bovine serum (FBS) (Biochrom AG), streptomycin (Sigma-Aldrich) (100 μg/mL) and gentamicin (Sigma-Aldrich) (100 μg/mL), in 75 cm^2 T-flasks (Orange Scientific). Cultures were maintained at 37 °C in a 5% CO_2 humidified atmosphere and the culture medium exchanged twice a week. Confluent cell monolayers were subcultured by initially washing them with PBS, and then detached with 0.18% trypsin (1:250) and 5 mM EDTA (Sigma-Aldrich). A Neubauer chamber was used to determine cell number using trypan blue (Sigma-Aldrich) — exclusion assay, in order to distinguish live from dead cells. Subsequently, cells were seeded in contact with 80/20, 90/10, 99/1, 80/20/A, 90/10/A and 99/1/A scaffolds at a density of 2.0×10^3 cells/well in cell culture treated polystyrene plates. Cell growth was monitored during 1, 7 and 14 days, by using an Olympus CX41 inverted light microscope (Tokyo, Japan) equipped with an Olympus SP-500 UZ digital camera.

2.3.2. Cellular metabolic activity: resazurin assay

Osteoblast cells were cultured on scaffold surfaces for 1, 7 and 14 days. A non-toxic dye, specifically, resazurin (Sigma-Aldrich) was used to assess cellular metabolic activity during this period. Resazurin is reduced to a fluorescent resorufin substrate by an intracellular enzyme, specifically oxidoreductase. At the indicated time points of culture, 400 μL of culture medium was added to the wells with 40 μL of a 10% (v/v) fluorescent dye solution and incubated for 4 h, in a humidified atmosphere, at 37 °C, 5% CO_2. Then, 80 μL of the supernatant was transferred into a 96-well plate and the fluorescence intensity measured in a SpectraMax Gemini™ XS spectrofluorometer (Molecular Devices), at $\lambda_{ex} = 545$ nm and $\lambda_{em} = 590$ nm, respectively. Cells cultured without scaffolds were used as negative control and ethanol treated cells were used as positive control.

2.3.3. Analysis of 3D scaffolds biologic properties

The analysis of osteoblast adhesion and morphology on the 3D scaffold surfaces at various days (1, 7 and 14) was visualized by fluorescence confocal laser scanning microscopy (CLSM). Briefly, at pre-determined time points the cell culture medium was removed and cells were washed three times with PBS at RT. The remaining cells were then fixed with 4% paraformaldehyde (PFA) (Sigma-Aldrich) for 30 min, at RT, and were washed once more with PBS to remove PFA. Afterwards, the cell nucleus was labeled with 2 μM propidium iodide (Molecular Probes, Invitrogen, Carlsbad, MO, USA) solution during 15 min, at RT, followed by five additional washes with PBS. Furthermore, propidium iodide stained cells were also permeabilized with 1% Triton X-100 (Sigma-Aldrich) and then blocked with blocking solution (10% FBS, 0.1% Tween (Sigma-Aldrich)) in PBS, for 10 min. Afterwards, cells were incubated with mouse anti-β-actin antibody (Molecular Probes, Invitrogen) (1:500) for 1 h at RT in a humidified chamber. Following the incubation period osteoblasts were thoroughly washed with PBS-T (0.1% Tween in PBS). The anti-mouse Alexa-488 (Molecular Probes, Invitrogen) antibody was then added to cells during 1 h, followed by the washing steps as previously described. The cell-seeded scaffolds were then transferred into μ-Slide 8 well Ibidi® chamber coverslips (Ibidi® GmbH, Germany) and imaged in a Zeiss LSM 710 confocal microscope (Carl Zeiss SMT Inc., USA) equipped with a Plan-Neofluar 10×/NA 0.3 and a Plan-Apochromat 40×/1.4 Oil DIC objectives. All data was

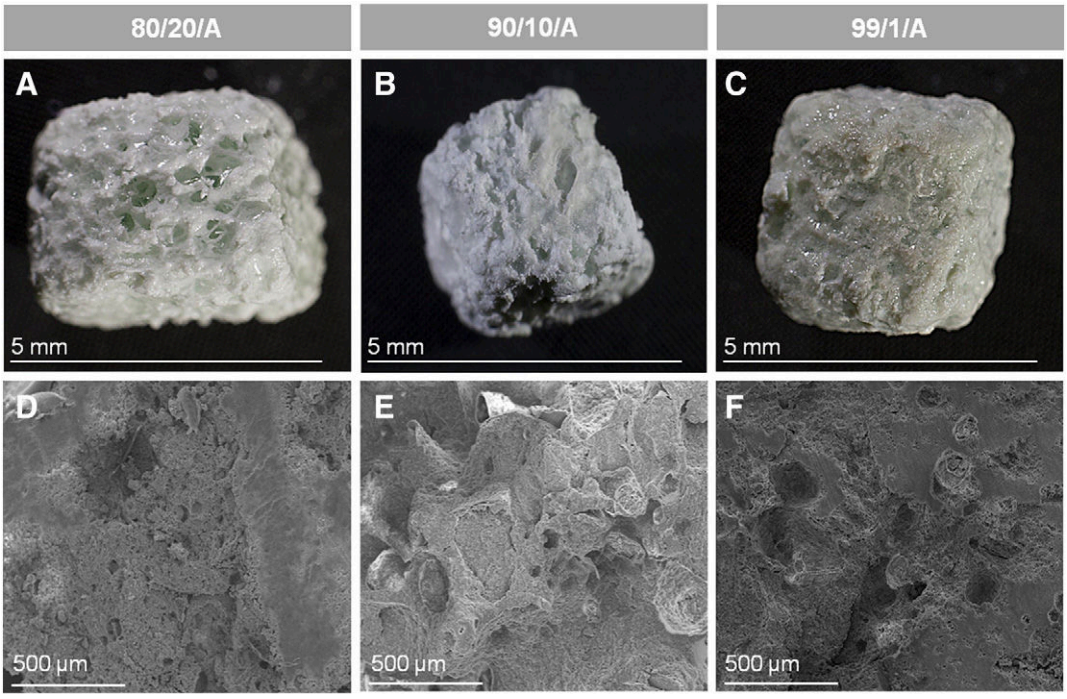

Fig. 1. Macrographs (A, B and C) and SEM images (D, E and F) of the different alginate-coated β-TCP/HA scaffold surfaces. Images show the surface characteristics and the porosity of the 80/20/A (A, D), 90/10/A (B, E) and 99/1/A (C, F) 3D scaffolds, respectively.

Table 1
Pore diameter and hydrophilic properties of the produced β-TCP/HA 3D scaffolds.

Scaffold	Pore diameter (μm)		Contact angle
	Minimum	Maximum	
80/20	80	450	[a]
80/20/A	60	250	20.6°
90/10	90	280	17.2°
90/10/A	30	160	21.6°
99/1	80	125	20.4°
99/1/A	60	115	26.6°

[a] Lower than the quantification limit.

acquired in z-stack mode with a step of 4.67 μm. Z-stacks were then rendered into 3D images in the Zeiss LSM 710 software. Depth coding rendering of z-stacks was also performed in Zeiss software with the open GL rendering mode to provide visualization of cell spatial distribution within the scaffold architecture. Additional image processing was performed in Image J (ImageJ software) [36].

2.4. Statistical analysis

Comparison of the results obtained for the different groups of scaffolds at various conditions was performed by using one-way analysis of variance (ANOVA), with the Newman–Keuls post-hoc test [37]. This statistical test is applied to compare the mean and the differences among three different groups [38]. Thus in this particular case the ANOVA test was used to evaluate the differences in the means of three samples of different scaffold formulations by using variances. This test was performed by taking into consideration that the samples are independent from each other and that the variance of the populations is equal. The addition of the post-hoc Newman–Keuls test was used to further provide a more detailed analysis of differences in the means by making a multi-pairwise comparison [39]. A p value below 0.05 ($p < 0.05$) was considered statistically significant.

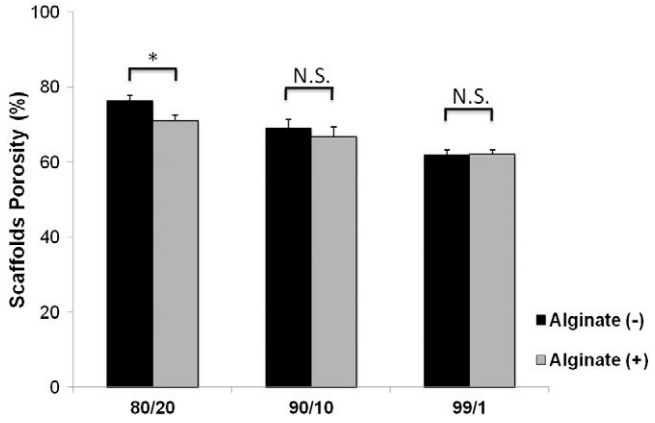

Fig. 2. Total porosity of the different β-TCP/HA scaffolds. Alginate (+) indicates coated scaffolds and alginate (−) the uncoated scaffolds. N.S.: not significant; *$p < 0.05$, $n = 3$.

3. Results and discussion

In this study the physicochemical, mechanical and biological characteristics of 3D porous scaffolds produced with two bioceramics, β-TCP and HA, were investigated. So far, two ratios of β-TCP and HA were successfully tested in humans, specifically, 50/50 and 40/60 [40,41]. Herein, the use of higher percentages of β-TCP relatively to HA was evaluated to produce scaffolds with improved mechanical properties for bone regeneration.

Furthermore, an alginate coating was added to the scaffolds to include an additional biomaterial that could mimic the extracellular matrix present in native bone cells, and also that would enhance the mechanical strength of the structure, improving its osteoconduction and osteointegration within host bone tissues [42]. Alginate was also chosen to be included in this study since its combination with β-TCP and HA forms a rigid hybrid polymer–ceramic biomimetic composite, without eliciting any immune response, or risk of contamination by allo- or xeno-proteins or viruses, unlike, for instance, collagen [43]. Furthermore, the FRM method used to produce the 3D structures allows the production of interconnected porous scaffolds with rough surfaces, with controllable pore size and porosity within the template geometry [44–46].

3.1. β-TCP/HA composite scaffold production: macroscopic, mechanical and physicochemical characterization

As previously described in the literature, scaffolds produced for bone tissue regeneration must have adequate external and internal structures, as well as desirable physicochemical characteristics that mimic the extracellular matrix of bone cells and also bone native properties. The uncoated β-TCP/HA (Supplementary Fig. 1) and alginate-coated β-TCP/HA scaffolds (Fig. 1) produced by FRM have well defined

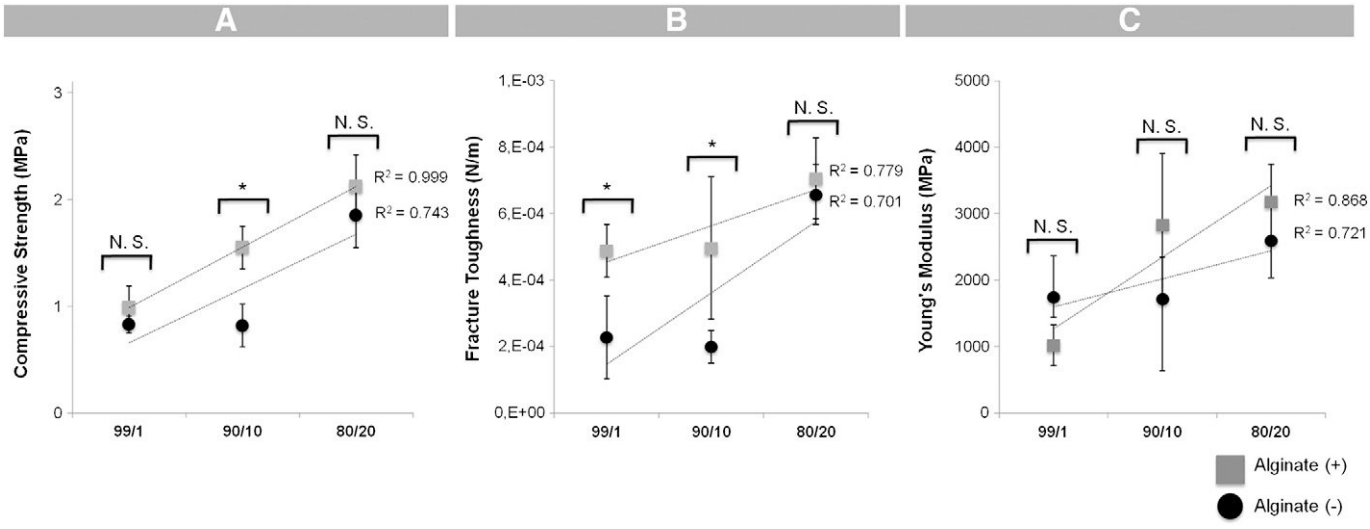

Fig. 3. Compressive strength (A), fracture toughness (B) and Young's modulus (C) of the uncoated (gray squares) and alginate-coated (black circles) 80/20, 90/10 and 99/1 scaffolds. N.S.: not significant; *$p < 0.05$, $n = 3$.

Table 2
Comparison of the mechanical properties between the 80/20/A scaffold and the human cancellous bone.

Mechanical properties	80/20/A scaffold	Human cancellous bone
Compressive strength	2.12 ± 0.30 MPa	2.00–12.00 MPa
Fracture toughness	$7.06 \times 10^{-4} \pm 1.22 \times 10^{-4}$ N/m	0.11 N/m
Young's moduli	3181.00 ± 561.93 MPa	100.00–500.00 MPa

architectures that replicate those of their sacrificial foam templates. Interestingly, although the β-TCP and HA components of bone substitutes were different among the tested scaffolds, all of them presented surfaces with some degree of roughness, even after being coated with alginate. These findings assume further importance since roughness largely influences protein adsorption and cell adhesion upon scaffold implantation [47]. In fact, as recently reported by Gittens and co-workers [48], micro- and macro-sized topographic surface roughness of bone substitutes improves osteoblast differentiation and localized growth factor production, thus enhancing scaffold osteointegration in bone defects [48]. Moreover, SEM analysis confirmed the presence of micro- and macro-porosity throughout the alginate-coated (Fig. 1) and the uncoated scaffolds (Supplementary Fig. 1).

The results presented in Table 1 revealed that the 80/20 formulation has the larger sized pores when compared to the 90/10 and 99/1 scaffolds. After performing the alginate coating, a clear decrease in the pore size was observed, in comparison with their uncoated counterparts (Table 1). Nevertheless, all the coated scaffolds maintained suitable pore diameters for use in bone regeneration, with the 80/20/A structure being the one with larger pores. Such is of crucial importance, since pore diameters ranging from 100 μm to 135 μm have shown to improve osteoblast-bone deposition and formation of rich vascular networks [49].

Furthermore, other important physicochemical properties, such as hydrophilicity and total percentage of porosity of the scaffolds, influence their bioactivity and regenerative capacity. As shown in Table 1 the measured values of the contact angles for the 90/10 and 99/1 scaffolds, indicate that these templates are highly hydrophilic. It is important to mention that the contact angle of the 80/20 scaffold could not be calculated, due to the rapid absorption of the water drop by the porous structure, suggesting that this scaffold is highly hydrophilic. However, after performing alginate inclusion, it was possible to determine the 80/20/A contact angle and it was found that this value is quite low, suggesting that, even after its coating, this scaffold remains as the most hydrophilic of the three coated scaffolds (Table 1). Although the contact angle values of the alginate-coated structures suffered a slight increase when compared to the respective uncoated ones, they remained in the range of hydrophilic associated angles, suggesting that these structures were also hydrophilic. These results indicate that cellular adhesion and migration within the 80/20/A might occur in an improved manner, since this scaffold is highly hydrophilic, and the presence of alginate may create additional biomimetic substrates between the pores, increasing the available areas within the scaffolds for cells to migrate.

The total percentage of scaffold porosity was determined by a liquid displacement method, using ethanol as the displacing liquid [50]. By analyzing Fig. 2, it is possible to observe that all the scaffolds present an internal porosity higher than 60%, a suitable value for bone regeneration, considering that the human cancellous bone bears a total porosity of 30% to 90% [51]. More importantly, the 80/20 scaffold presents the higher value of porosity (76%), when compared to the 90/10 and 99/1 scaffolds. These results corroborate the previous findings concerning the diameter of the pores and the contact angles. Such results may, at first glance, seem to be in contradiction with those previously published in the literature [52,53]. These researchers reported that porosity is inversely proportional to HA concentration. Furthermore, Muralithran and collaborators, have previously reported that by increasing the sintering temperature (from 1000 °C to 1450 °C), the relative density and linear shrinkage of HA ceramics increase and consequently the porosity decreases [54]. In this study a 900 °C temperature was used in the sintering process, which could influence the porosity results. Moreover, the increase in scaffold porosity with a higher HA (w/w) content in the scaffolds may be explained by the fact that there is a larger relative concentration of smaller sized particles in respect to those of β-TCP (HA nanoparticles < 200 nm, β-TCP mean particle size 11.64 μm). In fact, particle size has been shown to affect total porosity since as described

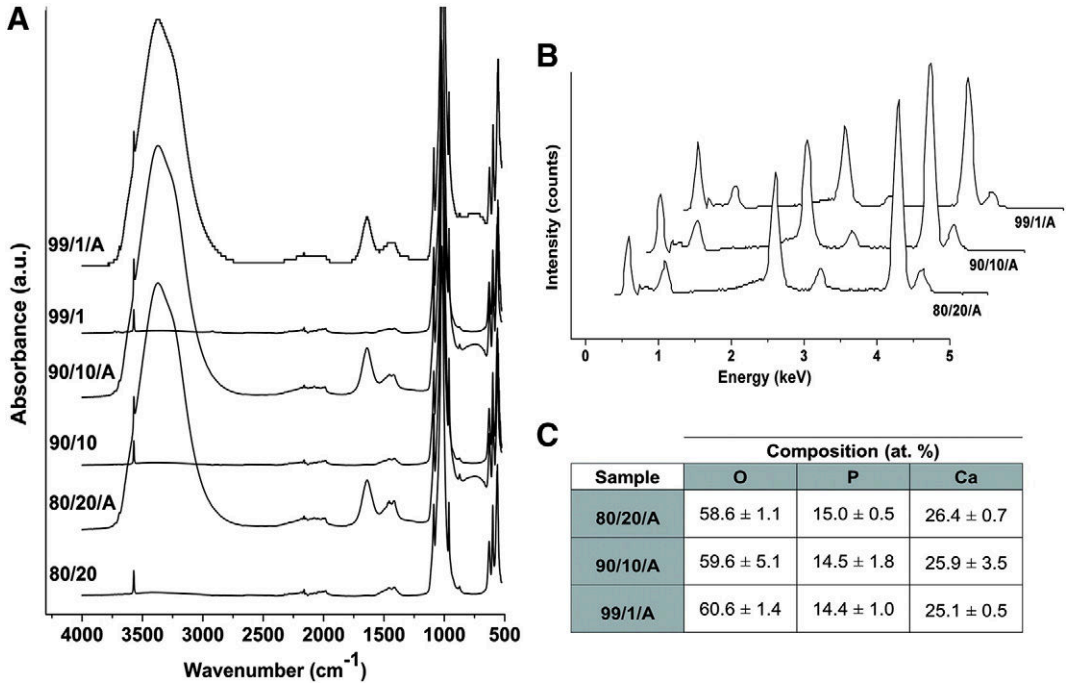

Fig. 4. Physicochemical characterization of the powders and 3D scaffolds. (A) FTIR spectra, (B) EDS spectra of the 3D scaffolds and (C) elemental analysis of the manufactured structures.

through molecular dynamics simulations performed by Balakrishnan et al. [55], the formation of agglomerates is dependent on the application of higher forces to compact nanoparticles [55]. Therefore, since no forces were applied to form compact nanoparticle aggregates the more space occupied by HA powders in 80/20 scaffolds, presents higher interfacial voids, and thus, increased total porosity. It is also important to emphasize that an increased HA concentration increases the viscosity of the slurry, a fact that will lead to highly porous materials after sintering as reported by Sopyan et al. [56]. Thus the increasing porosity in the 80/20 scaffold in comparison with the other formulations may also be correlated with the higher viscosity promoted by HA.

Regarding the scaffold porosity after the coating procedure, a slight decrease (5%) was observed for the 80/20/A template in comparison with the respective uncoated scaffold. Even though, this scaffold was also the most porous in comparison with all other coated ones (Fig. 2). The existence of pores is fundamental as it promotes nutrient intake, as well as, interactions between the β-TCP/HA template and bone cells. The establishment of this microenvironment promotes cell attachment, migration and proliferation in a 3D area [57–59]. Apart from pore size, pore interconnectivity is also a desirable characteristic due to its important influence on cell proliferation and differentiation [60]. In fact, interconnected pores facilitate the formation of vascular networks within the 3D scaffolds and provide channeling pathways for biofluids [61]. These biofluids promote the adsorption of Ca^{2+} and PO_4^{3-} ions throughout the biomaterial, creating an HA-like layer [10]. This layer establishes an interface between the implant and the 9 surrounding bone tissues and stimulates osteoblast cell activity, increasing the deposition of bone matrix in the defect area. Additionally the formation of this layer increases the osteoconductivity and osteointegration, further contributing for the bone mineralization [17].

Achieving equilibrium between scaffold porosity and adequate mechanical strength, is a demanding objective for the production of scaffolds, as it was taken into consideration in this study. The mechanical behavior of the 3D scaffolds was characterized by analyzing their resistance to compression, followed by an estimation of the values of fracture toughness and Young's modulus. Through the analysis of Fig. 3 it is possible to visualize that the compressive strength, the fracture toughness and the Young's modulus of the 80/20 scaffold are higher than the values of the 90/10 and 99/1 scaffolds. With increase of porosity (99/1 to 80/20) there is an increase in the mechanical strength by 2 times. This improvement in mechanical compression strength is due to the increasing densification of the walls due to the increase of the amount of HA. This is also corroborated by the increased material stiffness (highest Young's modulus). After coating the scaffolds with a 2% alginate solution their mechanical properties improved, with the 80/20/A maintaining better mechanical resistance to compression, resistance to fracture and elasticity modulus than the other coated 3D structures. Accordingly, it was previously described that an increase in the volume fraction of alginate from 1 to 3% results in an improvement of the compressive modulus [62]. So, it is noticeable that the most porous structures (80/20 and 80/20/A) are also those with better mechanical properties, when compared to both the uncoated and coated 90/10 or 99/1 scaffolds. These findings are likely correlated with the fact that the 80/20 and 80/20/A scaffolds have higher amounts of HA and lower quantities of β-TCP, in comparison to the other manufactured scaffolds. This is consistent with a study performed by Shiota, T. et al., that revealed that high amounts of β-TCP are responsible for a decrease in scaffold strength resistance [63]. Comparing the mechanical properties of 80/20/A scaffold with those presented by the natural cancellous bone, it is possible to observe that this scaffold is the most promising for therapeutic applications, among the scaffolds produce herein (Table 2) [64–66].

The different scaffolds produced by FRM were then characterized by FTIR spectroscopy. The stretching bands obtained between 500 and 600 cm^{-1} for the manufactured structures are characteristic of the PO_4^{-} ions present in both β-TCP and the HA powder (Fig. 4A). The stretching of the −OH groups was also observed (3571 cm^{-1} and libration mode at ≈630 cm^{-1}). This particular band intensity is higher in all the synthesized scaffolds, since it is the end result of the cumulative contribution of both HA and β-TCP (Fig. 4A). In addition, the stretching bands observed at ≈1415 and 1450 cm^{-1} are attributed to a B type apatite [67]. Furthermore, EDS analysis of the scaffolds shows that the chemical composition of all the alginate coated formulations is very similar in terms of phosphate and calcium (Fig. 4C).

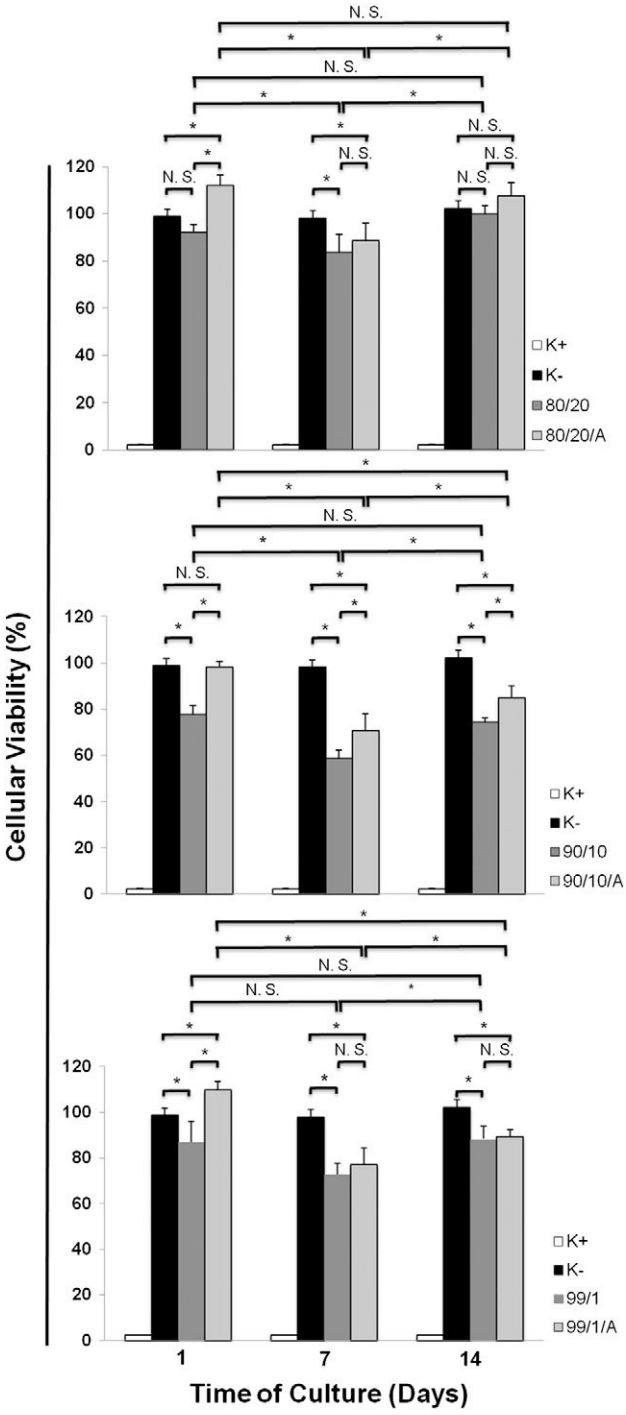

Fig. 5. Osteoblast cell metabolic activity when cultured in the presence of different β-TCP/HA scaffolds. Cultures were evaluated for 1, 7 and 14 days. K^+ and K^-, indicate dead and viable cells, representing positive control and negative control, respectively. N.S.: not significant; *$p < 0.05$, $n = 3$.

3.2. Analysis of the biological properties of the scaffolds

Subsequently, the biological performance of the porous β-TCP/HA structures was also evaluated. For this purpose, human osteoblast cells were cultured in the 3D scaffolds for up to 14 days and their metabolic activity evaluated at the indicated time points (Fig. 5). The results obtained revealed that osteoblast metabolic activity when cultured in the presence of all the scaffolds was higher than 70% during the 14 days of analysis, indicating that the 3D bioceramics are biocompatible. Among all the uncoated scaffolds, the 80/20 formulation was the one that presented higher biocompatibility along the assay and comparatively to 90/10 and 99/1 scaffolds. Cells presented higher metabolic activity in the presence of alginate coated-β-TCP/HA scaffolds than in contact with uncoated scaffolds ($p < 0.05$). The 80/20/A structure was the one for which cells presented the higher viability, being close to the value presented by the negative control for all culture days (approximately 100%).

To further characterize cellular adhesion both on the surface and inside the scaffold, SEM analysis was performed and it showed that osteoblasts were able to adhere preferably inside the pores of the bioceramic scaffolds, either coated (Fig. 6) or not (Supplementary Fig. 2) with the natural polymer. Interestingly, after the first day in contact with the scaffolds, osteoblasts were already attached and spread across the 3D structures, presenting a round shape configuration, with some cytoplasm extensions towards the substrate. At day 7, and predominantly after 14 days of culture, cells cultured in all the different structures started to present a typical osteoblastic morphology, showing a smooth arrangement with more lamellipodia connecting to surrounding osteoblast, beginning to form a continuous cell layer. For all the uncoated and coated β-TCP/HA scaffolds, the number of osteoblasts appeared to increase along time, with cells establishing connection areas between them. SEM analysis was also important to investigate whether alginate was or not occluding the pores of the coated scaffolds and if cells were still able to migrate within these scaffolds. As depicted in Fig. 6, alginate did not block the pores, but instead created additional biocompatible substrates, changed the roughness and microtopography of the scaffolds surface, which contributed to further increase osteoblast adhesion and migration. These results are further emphasized by the CLSM analysis during the various stages of osteoblast contact with the scaffolds (Fig. 7). In fact, as shown in Fig. 7, during osteoblast contact with the alginate-coated 3D scaffolds, cells were able to adhere and proliferate in all bioceramic formulations, emphasizing their biocompatibility and suitable physicochemical properties to promote osteoblast adhesion. These findings were also observed for the uncoated bioceramic scaffolds. Furthermore, at days 7 and 14 it is clear that osteoblasts migrate into the porous network during the time course of incubation. A visual analysis of the orthogonal slices of the scaffolds also clearly demonstrates that osteoblasts are spread across the entire scaffold and are also located inside the scaffold pores.

To further visualize the cytoplasmic morphology and localization of the osteoblasts that were proliferating on the 3D hybrid scaffolds an immunocytochemistry analysis of β-actin was performed. As the CLSM 3D reconstruction images demonstrate, osteoblasts present their characteristic cytoplasmic morphology for all scaffolds (Fig. 8).

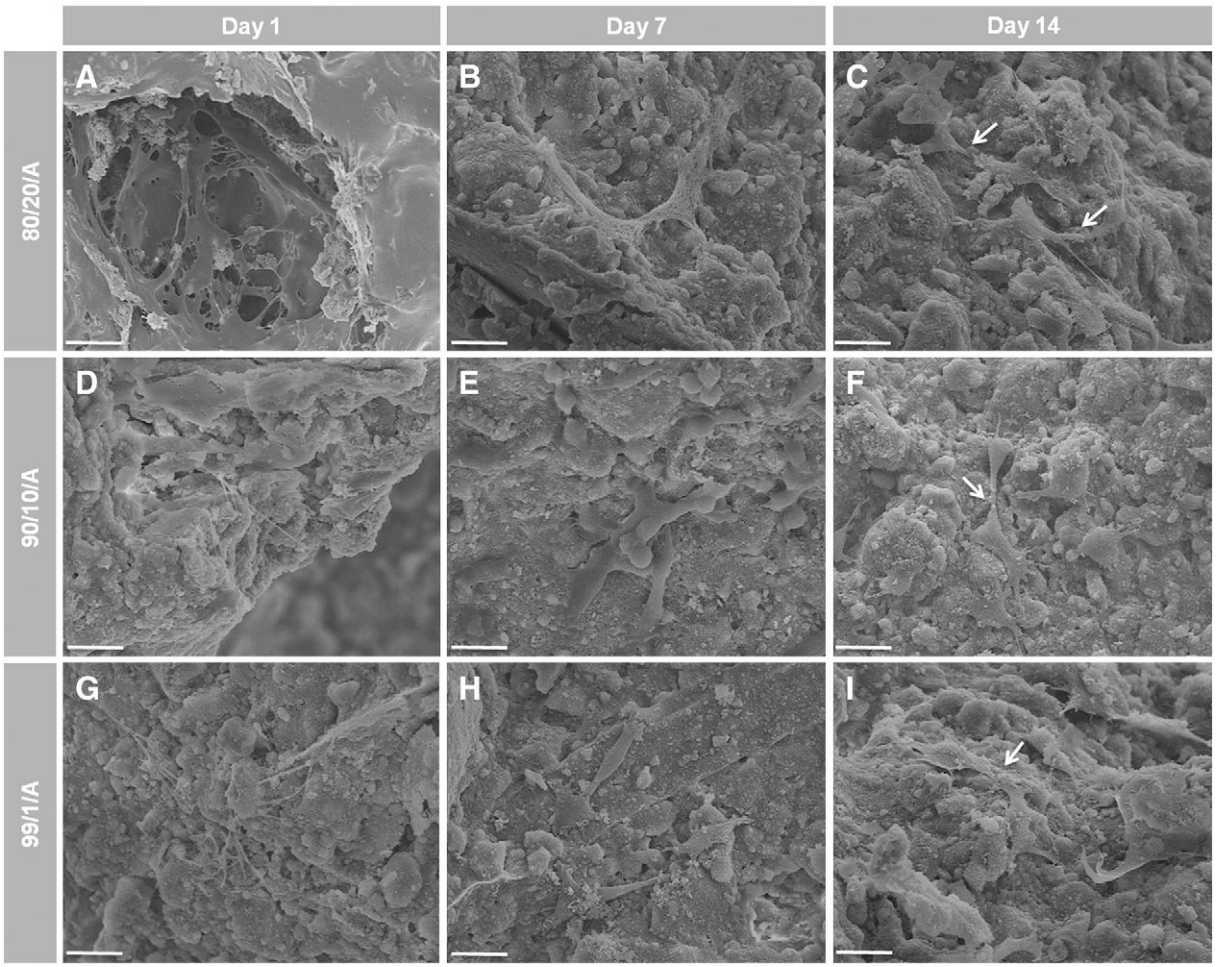

Fig. 6. SEM micrographs of osteoblast morphology in the presence of the different β-TCP/HA/alginate scaffolds. SEM images were used to visualize osteoblasts on the surface of the 80/20/A (A, B and C), 90/10/A (D, E and F) and 99/1/A (G, H and I) 3D scaffolds, at culture days 1 (A, D and G), 7 (B, E and H) and 14 (C, F and I). Scale bars correspond to 20 μm.

In addition, color coded depth analysis of the alginate coated structures clearly shows that osteoblasts are capable of migrating and attaching into deep sections of the scaffolds with some cells being localized up to 300 μm within the pores (Fig. 8). This is a relevant finding since the deposition of bone matrix inside the scaffold will eventually fill the bone defect while the scaffold is biodegraded, restoring the structure and function of the native bone.

Together, our results demonstrate that the produced β-TCP/HA structures are highly porous, hydrophilic, biocompatible and resistant to compression, improvements particularly achieved for the 80/20 structure. It was also shown that a mixture of β-TCP and HA, has the benefit of combining the bioactivity of β-TCP and the stability of HA. Moreover, higher amounts of HA increased the scaffold mechanical strength, while smaller amounts of β-TCP led to an increase of structure porosity. Besides, this study also reveals that the combination of both β-TCP and HA improves the biological and mechanical properties, in comparison with previously developed scaffolds comprised of β-TCP or HA alone [68–70]. In fact, the combination of these bioceramics originated 3D porous and bioactive structures with desirable osteoconductive and osteoinductive properties. Our novel approach involving an additional alginate coating further improves the scaffold mechanical, physicochemical and biological properties, as this natural biopolymer bridges the gap between the required material properties and bioactivity for therapeutic applications. Overall, the manipulation of bioceramic–polymer relative ratios largely influenced all the 3D scaffold properties and led to the manufacture of a particularly improved formulation with suitable characteristics for repair (Table 3, 80/20/A formulation). The role of alginate in the improvement of the mechanical properties is even more evident when comparing the scaffolds herein presented with those produced by Ebrahimi, M. et al. [31], which describes the production of β-TCP and HA scaffolds coated with collagen. An analysis of both types of scaffolds reveals the superior contribution of alginate, when compared to collagen, for the improvement of the scaffold mechanical strength and because, unlike collagen, alginate does not represent a risk of disease transmission [43]. Considering that the in vivo performance of β-TCP and HA has already been tested in humans [40,41], from this standpoint we envision that the addition of this polymer may actually improve the clinical outcome of these biomaterials.

4. Conclusions

In this work we describe the manufacture of 3D tunable porous scaffolds for bone regeneration by using a cost-effective and reproducible technique. Our results revealed that by optimizing the ratios of different bioceramic composites in the scaffolds the physicochemical and biological properties of these 3D constructs could be improved. In addition, the method employed for template production, allows the synthesis of scaffolds with rough topographies, micro- and macro-pores that are homogeneously distributed in the scaffold 3D volume. Furthermore, in order to improve the overall performance

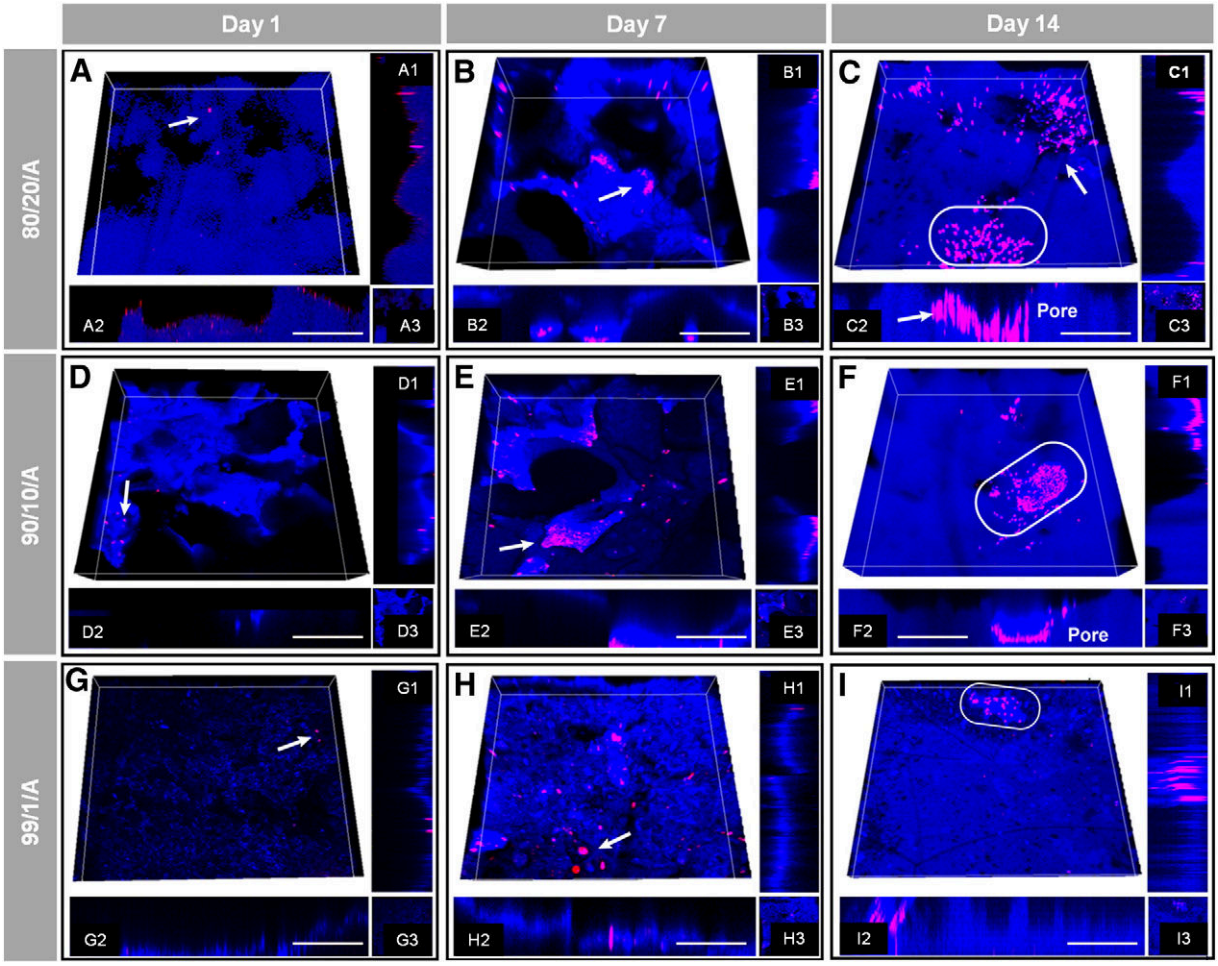

Fig. 7. Osteoblasts are able to attach to the surface of the different scaffolds. Confocal microscopy images were used to investigate osteoblast distribution on the alginate coated scaffolds at different time points. (A to I) 3D reconstruction of the hybrid scaffolds; (A1 to I1) Orthogonal slices of scaffold xx axis. (A2 to I2) Orthogonal slices of scaffold yy axis. (A3 to I3) Top view of the 3D scaffolds. Red channel: cell nucleus; blue channel: 3D scaffolds. White arrows indicate cells. White ovals indicate pores. White scale bars represent 300 μm.

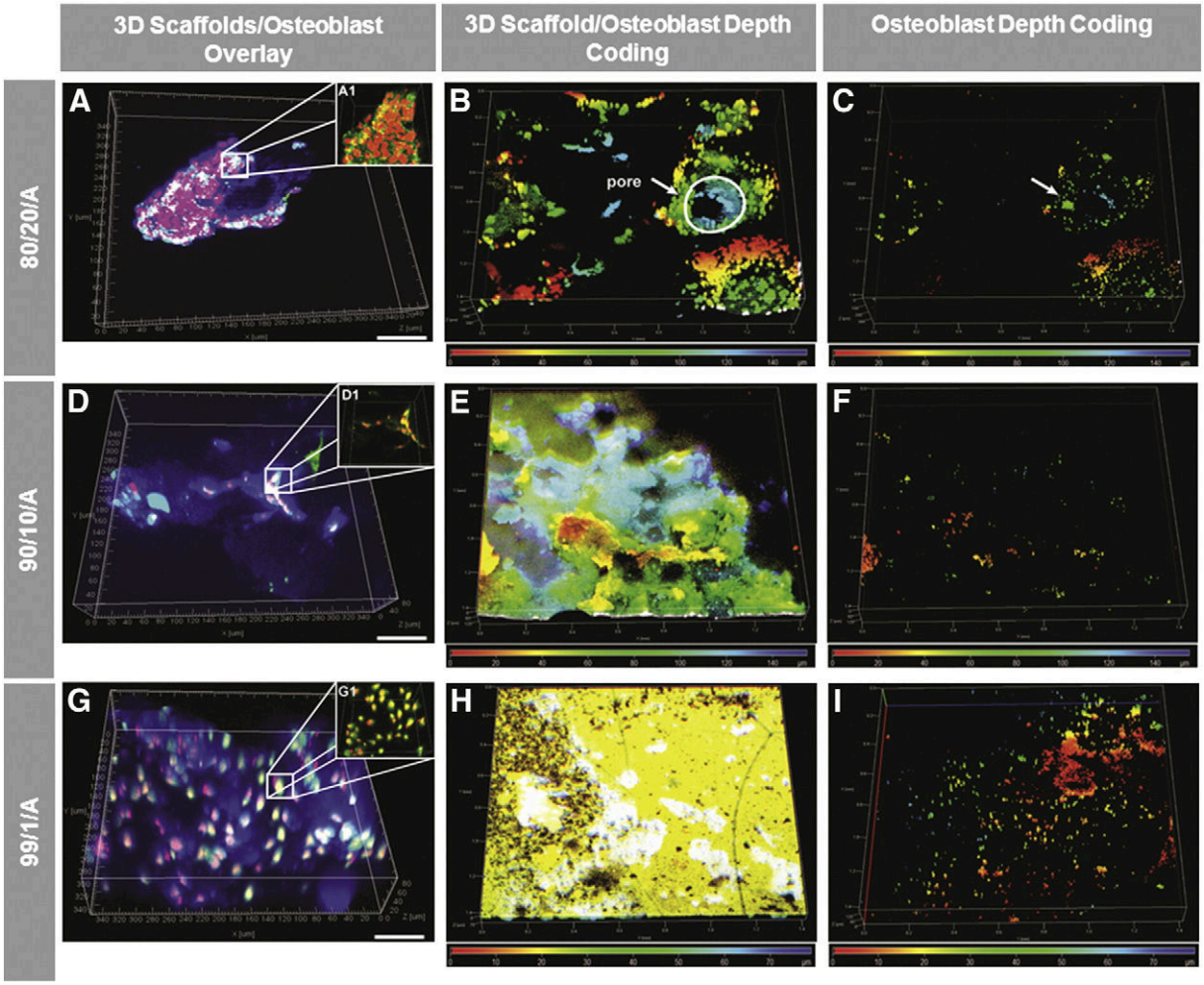

Fig. 8. 3D reconstruction and depth analysis of the different scaffolds coated with alginate. (A, D and G) Immunocytochemistry analysis of osteoblast seeded scaffolds at day 14. Green channel: β-actin; red channel: cell nucleus; blue channel: 3D hybrid scaffolds. (B, E and H) 3D depth coding of scaffolds and osteoblasts cultured on scaffold's surface. Size bar represents color-coded depth. White area represents a scaffold pore with osteoblasts inside. (C, F and I) 3D surface reconstruction of cells at the surface of the scaffold. White arrows indicate osteoblasts. Black bars indicate 300 μm.

of these structures, the bioceramics were also vacuum-coated with alginate. This inclusion greatly enhanced both the mechanical and biological properties of the scaffolds. In fact, osteoblast adhesion, migration and proliferation in contact with the coated scaffolds emphasize their suitability for regenerative medicine. To the best of our knowledge this was the first time that this combination of these biomaterials was used to manufacture 3D porous scaffolds, which resulted in unique structures with desirable biological, mechanical and physical properties that will promote bone regeneration. In a near future these hybrid bioceramic–polymeric composites will be implanted in whole animal models with small and large bone defects, in order to evaluate their bone regenerative performance.

Table 3
Summary of physicochemical and biological properties of the manufactured scaffolds.

Properties scaffold	Hydrophilicity	Porosity	Mechanical strength	Biocompatibility
80/20	+	++++++	+++++	+++++
80/20/A	++++	+++++	++++++	++++++
90/10	++	++++	+++	+
90/10/A	+++++	+++	++++	++
99/1	+++	++	++	+++
99/1/A	++++++	+	+	++++

"+" to "+++++++": symbol-based grade, indicating improvement of the scaffolds properties.

5. Acknowledgments

The authors would like to thank to Eng. Ana Paula for her help with the acquisition of SEM data. This work was supported by the Portuguese Foundation for Science and Technology (FCT) (PTDC/EME-TME/103375/2008, PTDC/EBB-BIO/114320/2009 and PEst-C/SAU/UI0709/2011 COMPETE). Vítor M. Gaspar acknowledges a PhD fellowship from FCT (SFRH/BD/80402/2011).

Appendix A. Supplementary data

Supplementary data to this article can be found online at http://dx.doi.org/10.1016/j.msec.2013.07.003.

References

[1] A.M. Martins, C.M. Alves, F.K. Kasper, A.G. Mikos, R.L. Reis, J. Mater. Chem. 20 (2010) 1638–1645.
[2] D. Fisher, J. Wong, C. Crowley, W. Khan, Curr. Stem Cell Res. Ther. 8 (2013) 243–252.
[3] T. Jiang, S.P. Nukavarapu, M. Deng, E. Jabbarzadeh, M.D. Kofron, S.B. Doty, W.I. Abdel-Fattah, C.T. Laurencin, Acta Biomater. 6 (2010) 3457–3470.

[4] A. Nekora-Azak, G. Evlioglu, M. Ozdemir-Karatas, H. Keskin, J. Oral Rehabil. 32 (2005) 693–695.
[5] M.B. Dreifke, N.A. Ebraheim, A.C. Jayasuriya, J. Biomed. Mater. Res. A (2013).
[6] A.A. Amini, L.S. Nair, Biomed. Mater. 7 (2012) 024105.
[7] J.R. Jones, L.M. Ehrenfried, L.L. Hench, Biomaterials 27 (2006) 964–973.
[8] D.F. Williams, Biomaterials 29 (2008) 2941–2953.
[9] S. Scaglione, C. Ilengo, M. Fato, R. Quarto, Tissue Eng. Part A 15 (2009) 155–163.
[10] M.G. Raucci, V. Guarino, L. Ambrosio, J. Funct. Biomater. 3 (2012) 688–705.
[11] H.S. Yu, G.Z. Jin, J.E. Won, I. Wall, H.W. Kim, J. Biomed. Mater. Res. A 100 (2012) 2431–2440.
[12] A. Abdal-hay, F.A. Sheikh, J.K. Lim, Colloids Surf. B Biointerfaces 102 (2013) 635–643.
[13] P.P. Cortez, M.A. Silva, M. Santos, P. Armada-da-Silva, A. Afonso, M.A. Lopes, J.D. Santos, A.C. Mauricio, J. Biomater. Appl. 27 (2012) 201–217.
[14] X. Lu, S. Li, J. Zhang, Z. Zhang, B. Lu, H. Bu, Y. Li, J. Cheng, Sheng Wu Yi Xue Gong Cheng Xue Za Zhi 18 (2001) 497–499.
[15] C.F.L. Santos, A.P. Silva, L. Lopes, I. Pires, I.J. Correia, Mater. Sci. Eng. C 32 (2012) 1293–1298.
[16] L.L. Hench, Biomaterials 19 (1998) 1419–1423.
[17] L.L. Hench, J. Biomed. Mater. Res. 41 (1998) 511–518.
[18] C. Wu, Y. Ramaswamy, P. Boughton, H. Zreiqat, Acta Biomater. 4 (2008) 343–353.
[19] Y. Zhang, M. Zhang, J. Biomed. Mater. Res. 61 (2002) 1–8.
[20] S.J. Florczyk, M. Leung, S. Jana, Z. Li, N. Bhattarai, J.I. Huang, R.A. Hopper, M. Zhang, J. Biomed. Mater. Res. A 100 (2012) 3408–3415.
[21] W. TheinHan, M.D. Weir, C.G. Simon, H.H. Xu, J. Tissue Eng. Regen. Med. (2012), http://dx.doi.org/10.1002/term.1466.
[22] W.R. Gombotz, S.F. Wee, Adv. Drug Deliv. Rev. 31 (1998) 267–285.
[23] J.-K. Francis Suh, H.W. Matthew, Biomaterials 21 (2000) 2589–2598.
[24] F.A. Johnson, D.Q. Craig, A.D. Mercer, J. Pharm. Pharmacol. 49 (1997) 639–643.
[25] A.D. Augst, H.J. Kong, D.J. Mooney, Macromol. Biosci. 6 (2006) 623–633.
[26] J.F.A. Valente, V.M. Gaspar, B.P. Antunes, P. Countinho, I.J. Correia, Polymer 54 (2013) 5–15.
[27] O. Smidsrød, Trends Biotechnol. 8 (1990) 71–78.
[28] A.I. Pravdyuk, Y.A. Petrenko, B.J. Fuller, A.Y. Petrenko, Cryobiology 66 (2013) 215–222.
[29] A. Schoubben, P. Blasi, S. Giovagnoli, L. Perioli, C. Rossi, M. Ricci, Eur. J. Pharm. Sci. 36 (2009) 226–234.
[30] X. Wu, Y. Liu, X. Li, P. Wen, Y. Zhang, Y. Long, X. Wang, Y. Guo, F. Xing, J. Gao, Acta Biomater. 6 (2010) 1167–1177.
[31] M. Ebrahimi, P. Pripatnanont, N. Monmaturapoj, S. Suttapreyasri, J. Biomed. Mater. Res. A 100 (2012) 2260–2268.
[32] D. Lacroix, A. Chateau, M.P. Ginebra, J.A. Planell, Biomaterials 27 (2006) 5326–5334.
[33] J. Martin Bland, D. Altman, Lancet 327 (1986) 307–310.
[34] H.L. Nie, L.M. Zhu, Int. J. Biol. Macromol. 40 (2007) 261–267.
[35] M. Rouahi, O. Gallet, E. Champion, J. Dentzer, P. Hardouin, K. Anselme, J. Biomed. Mater. Res. A 78 (2006) 222–235.
[36] T.J. Collins, Biotechniques 43 (2007) 25–30.
[37] P. Coimbra, P. Ferreira, H. De Sousa, P. Batista, M. Rodrigues, I. Correia, M. Gil, Int. J. Biol. Macromol. 48 (2011) 112–118.
[38] V. Bewick, L. Cheek, J. Ball, Crit. Care 8 (2004) 130–136.
[39] A. Hilton, R.A. Armstrong, Microbiologist 2006 (2006) 34–36.
[40] Z. Artzi, M. Weinreb, G. Carmeli, R. Lev-Dor, M. Dard, C.E. Nemcovsky, Clin. Oral. Implants Res. 19 (2008) 686–692.
[41] J.L. Rouvillain, F. Lavalle, H. Pascal-Mousselard, Y. Catonne, G. Daculsi, Knee 16 (2009) 392–397.
[42] V. Wang, G. Misra, B. Amsden, J. Mater. Sci. Mater. Med. 19 (2008) 2145–2155.
[43] M. Xie, M.O. Olderoy, J.P. Andreassen, S.M. Selbach, B.L. Strand, P. Sikorski, Acta Biomater. 6 (2010) 3665–3675.
[44] M.A.A. Muhamad Nor, L.C. Hong, Z. Arifin Ahmad, H. Md Akil, J. Mater. Process. Technol. 207 (2008) 235–239.
[45] H. Fu, Q. Fu, N. Zhou, W. Huang, M.N. Rahaman, D. Wang, X. Liu, Mater. Sci. Eng. C 29 (2009) 2275–2281.
[46] Q. Fu, M.N. Rahaman, B. Sonny Bal, R.F. Brown, D.E. Day, Acta Biomater. 4 (2008) 1854–1864.
[47] B.G. Gerberich, S.K. Bhatia, Biotechnol. J. 8 (2013) 73–84.
[48] R.A. Gittens, T. McLachlan, R. Olivares-Navarrete, Y. Cai, S. Berner, R. Tannenbaum, Z. Schwartz, K.H. Sandhage, B.D. Boyan, Biomaterials 32 (2011) 3395–3403.
[49] C.M. Murphy, M.G. Haugh, F.J. O'Brien, Biomaterials 31 (2010) 461–466.
[50] Y. Zhang, M. Zhang, J. Biomed. Mater. Res. 55 (2001) 304–312.
[51] V. Karageorgiou, D. Kaplan, Biomaterials 26 (2005) 5474–5491.
[52] A. Tampieri, G. Celotti, S. Sprio, A. Delcogliano, S. Franzese, Biomaterials 22 (2001) 1365–1370.
[53] P. Habibovic, M.C. Kruyt, M.V. Juhl, S. Clyens, R. Martinetti, L. Dolcini, N. Theilgaard, C.A. van Blitterswijk, J. Orthop. Res. 26 (2008) 1363–1370.
[54] G. Muralithran, S. Ramesh, Ceram. Int. 26 (2000) 221–230.
[55] A. Balakrishnan, P. Pizette, C. Martin, S. Joshi, B. Saha, Acta Mater. 58 (2010) 802–812.
[56] I. Sopyan, J. Kaur, Ceram. Int. 35 (2009) 3161–3168.
[57] F.C. den Boer, B.W. Wippermann, T.J. Blokhuis, P. Patka, F.C. Bakker, H.J. Haarman, J. Orthop. Res. 21 (2003) 521–528.
[58] H.W. Kim, S.Y. Shin, H.E. Kim, Y.M. Lee, C.P. Chung, H.H. Lee, I.C. Rhyu, J. Biomater. Appl. 22 (2008) 485–504.
[59] M. Okamoto, Y. Dohi, H. Ohgushi, H. Shimaoka, M. Ikeuchi, A. Matsushima, K. Yonemasu, H. Hosoi, J. Mater. Sci. Mater. Med. 17 (2006) 327–336.
[60] J.P. Gleeson, N.A. Plunkett, F.J. O'Brien, Eur. Cell Mater. 20 (2010) 218–230.
[61] Y.C. Chen, R.Z. Lin, H. Qi, Y. Yang, H. Bae, J.M. Melero-Martin, A. Khademhosseini, Adv. Funct. Mater. 22 (2012) 2027–2039.
[62] M.A. LeRoux, F. Guilak, L.A. Setton, J. Biomed. Mater. Res. 47 (1999) 46–53.
[63] T. Shiota, M. Shibata, K. Yasuda, Y. Matsuo, J. Ceram. Soc. Jpn. 116 (2008) 1002–1005.
[64] D.W. Hutmacher, J.T. Schantz, C.X. Lam, K.C. Tan, T.C. Lim, J. Tissue Eng. Regen. Med. 1 (2007) 245–260.
[65] D.N. Rockwood, E.S. Gil, S.H. Park, J.A. Kluge, W. Grayson, S. Bhumiratana, R. Rajkhowa, X. Wang, S.J. Kim, G. Vunjak-Novakovic, D.L. Kaplan, Acta Biomater. 7 (2011) 144–151.
[66] S. Kashef, A. Asgari, T.B. Hilditch, W. Yan, V.K. Goel, P.D. Hodgson, Mater. Sci. Eng., A 527 (2010) 7689–7693.
[67] A. Ślósarczyk, Z. Paszkiewicz, C. Paluszkiewicz, J. Mol. Struct. 744–747 (2005) 657–661.
[68] Z. Dong, Y. Li, Q. Zou, Appl. Surf. Sci. 255 (2009) 6087–6091.
[69] G.S. Lee, J.H. Park, U.S. Shin, H.W. Kim, Acta Biomater. 7 (2011) 3178–3186.
[70] P.H. Warnke, H. Seitz, F. Warnke, S.T. Becker, S. Sivananthan, E. Sherry, Q. Liu, J. Wiltfang, T. Douglas, J. Biomed. Mater. Res. B Appl. Biomater. 93 (2010) 212–217.